FORSCHUNGSZENTRUM ROSSENDORF

WISSENSCHAFTLICH-TECHNISCHE BERICHTE

FZR-373

Mai 2003

Annual Report 2002
Institute of Radiochemistry

Editor: Prof. Dr. F.-P. Weiß

Editorial staff: Prof. Dr. G. Bernhard
Dr. H.-J. Engelmann

Institute of Radiochemistry

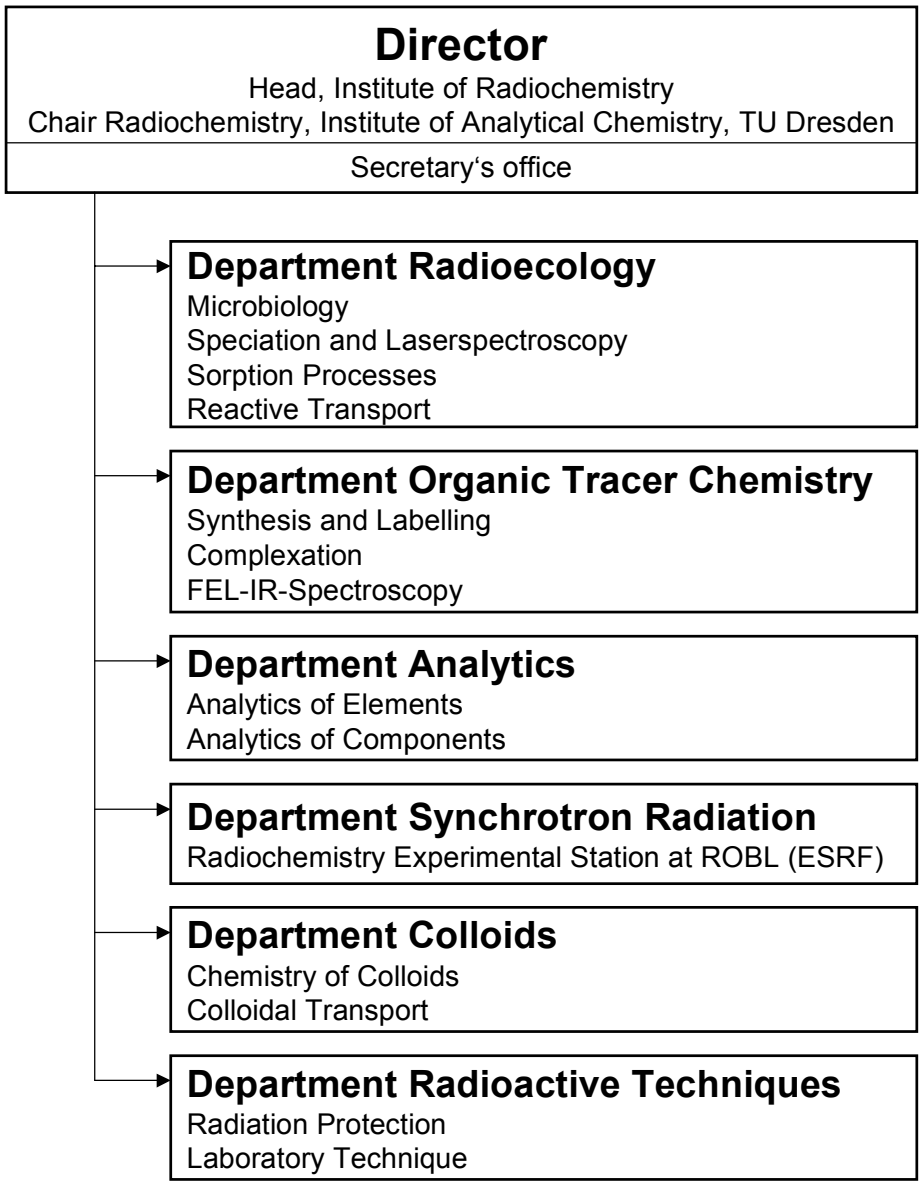

Preface

In 2002 the Institute of Radiochemistry, one of the five institutes of the Forschungszentrum Rossendorf e.V., further developed its basic and applied research in the fields of radiochemistry and radioecology.
The motivation and background of our research are environmental processes relevant for the installation of nuclear waste repositories, for the residues and remediation of uranium mining and milling sites, and for radioactive contaminations caused by nuclear accidents and fallout.

It is the main goal to improve the prediction of the behavior (speciation, migration) of actinides and other relevant long-lived radionuclides in the environment. To improve the macroscopic transport predictions a basic molecular-level understanding is required of the processes which are involved.

Current topics of our research work are:

- Aquatic chemistry of actinides / radionuclides
- Interaction of actinides / radionuclides with solid phases
- Actinides / radionuclides in biosystems
- Reactive transport of actinides / radionuclides
- Spectroscopic speciation methods

Remarkable progress was achieved in the reported period with regard to the Institute's scientific goals. The following original papers illustrate our progress. We accomplished many new scientific results but only a few can be highlighted in this preface.

Progress was achieved in understanding the structure of the Np(VII)-hydroxo complex. It was prepared by electrochemical oxidation and following ozonization. The obtained EXAFS structural parameters show that the Np (VII) forms a $NpO_4(OH)_2^{3-}$ complex.
The interaction of americium(III) and uranium(VI) with the silicate minerals smectite and kaolinite was studied by X-ray absorption spectroscopy. The mechanism of sorption was specified and the surface complexation species were detected.
To predict the transport behavior of actinides in the environment knowledge about the interaction with biosystems are needed. We found by laser spectroscopy, X-ray absorption spectroscopy, and different microscopic techniques that in dependence on the kind of bacteria uranium is bound and localized in a different dominating mode.
In the field of basic research we determined the stability constants of various uranium complexes with bioligands, like glucose and fructose phosphates, hydroxybenzoic acids and humic acids to improve the understanding of uranium binding in biological systems.

Dr. Johannes Raff was awarded the "Doktorandenpreis 2002 of Forschungszentrum Rossendorf" for his doctoral thesis "Wechselwirkung der Hüllproteine von Bakterien aus Uranabfallhalden mit Schwermetallen (Interaction of surface layer proteins of bacteria from uranium waste piles with heavy metals)"

It was a great honor for the Institute that Dr. Tobias Reich was offered a professorship in Radiochemistry at the Johannes - Gutenberg - Universität Mainz, Institute of Nuclear Chemistry. In April 2002 he started his work in Mainz. We wish him further scientific success.

This past year has also brought some changes to the Institute.
Professor Th. Fanghänel has pursued a call from Universität Heidelberg and was appointed as the new director of the Institut für Nukleare Entsorgung, Forschungszentrum Karlsruhe.
All members of the Institute would like to thank Professor Fanghänel for his successful scientific work here in Rossendorf and would like to wish him all the best for his further scientific work. We also would like to continue our close collaboration in future.

Beginning April 1, 2002 Professor Weiß, Director of the Institute of Safety Research, FZR has assumed the role as the Acting Director of the Institute of Radiochemistry.

We would like to thank the visitors for their interest in our research and would also like to thank our numerous national and international research partners and collaborators.

The Institute would like to acknowledge in particular the Executive Board of the Forschungszentrum Rossendorf, the Ministry of Science and Arts of the State of Saxony, the Federal Ministry of Education and Research, Federal Ministry of Economics and Work of Germany, the Deutsche Forschungsgemeinschaft, the European Commission and other organizations for their support.

CONTENTS

I. SCIENTIFIC CONTRIBUTIONS

Aquatic Chemistry of Actinides / Radionuclides

AN EXAFS STUDY OF THE CURIUM(III) AND AMERICIUM(III) AQUO ION

Th. Stumpf, H. Funke, C. Hennig, A. Roßberg, T. Reich, Th. Fanghänel[1]
[1]Forschungszentrum Karlsruhe, Institut für Nukleare Entsorgung, Karlsruhe, Germany

The Cm(III) and Am(III) aquo ions were investigated by X-ray absorption fine structure (XAFS) spectroscopy. The structural parameters which were found for the trivalent actinide ions in the acidic range will form the data basis for further EXAFS studies with americium and curium.

Besides plutonium, the long-lived isotopes of americium and curium play a crucial role for long-term performance assessment of nuclear waste repositories. In order to predict the mobilization and retardation of these nuclides, it is necessary to know the structures of the inorganic and organic actinide species that are involved in the process of migration. Thereby, the characterization of the Am^{3+} and Cm^{3+} aquo ions forms the base for further investigations.

In literature only few measurements can be found concerning the coordination numbers of trivalent actinides in aqueous solutions. By using UV/Vis spectroscopy, a coordination number of nine was calculated for Am^{3+} aq /1/. The complexation behavior of curium is often investigated by time-resolved laser fluorescence spectroscopy (TRLFS) /2, 3/. A coordination number of nine is assumed for Cm^{3+}aq. Extended X-ray absorption fine structure (EXAFS) spectroscopy investigations of Am^{3+} and of Cm^{3+} in 0.25 M HCl lead to coordination numbers of 10.3(0.3) and 10.2(0.3), respectively /4/.

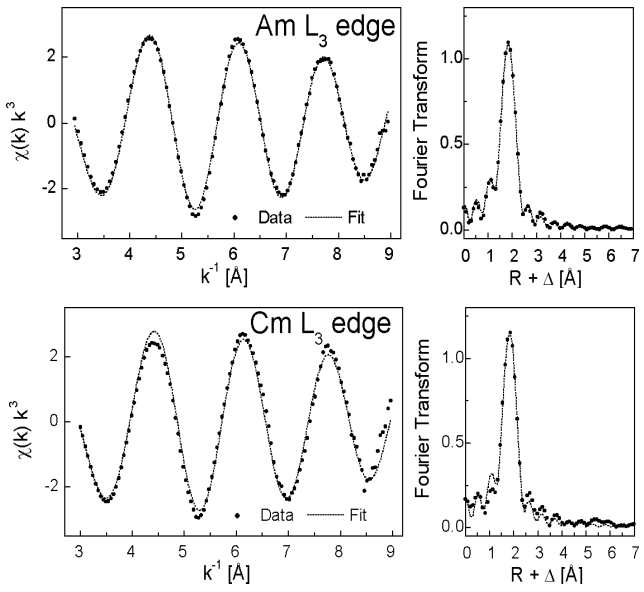

Fig. 1: Raw Am^{3+} and Cm^{3+} L_{III}-edge k^3-weighted EXAFS spectra and corresponding Fourier transforms. (Solid line - experiment; dashed line - theoretical fit.)

The EXAFS spectra and the corresponding Fourier transforms of Am^{3+} aq and Cm^{3+} aq are shown in Fig.1. In order to determine a reliable reference value for the coordination number of Cm^{3+} and Am^{3+} aquo ions, the samples used in our EXAFS measurements were prepared in non-complexing 1.0 M perchloric acid. Relatively high actinide concentrations (1 x 10^{-3} mol/L) were used in order to achieve low-noise EXAFS spectra, which enable a precise determination of bond lengths and coordination numbers of the Am^{3+} and Cm^{3+} aquo ions. EXAFS spectra were collected in transmission mode at the americium L_{III} edge at 18504 eV (E_0= 18520 eV) and at the curium L_{III}-edge at 18970 eV (E_0 = 18990 eV), respectively. Additionally a spectrum of the americium containing sample was measured in fluorescence mode. Zr and Nb metal foils were measured and the first inflection points of the X-ray absorption spectra (Zr K-edge at 17998 eV, Nb K-edge at 18986 eV) were used for energy calibration. EXAFS data treatment and fit were done using the EXAFSPAK program package. Parameters for the backscattering phase and amplitude, the mean free path, and the reduction factor were calculated using the FEFF8 code.

For comparison with EXAFS spectra of further Am(III) sorption or complexation species the americium aquo ion was measured in fluorescence (FL) and transition (TR) mode. As shown in table 1 the coordination number of Am^{3+} aq decreases from 7.8 to 7.0 when the mode changed from transition to fluorescence. This is effected by the death time correction and by the different geometry of the sample in both modes. The measured bond distances, R ± 0.03 Å, and coordination numbers, N ± 1, are the same for the Am^{3+} and Cm^{3+} aquo ions measured in transition mode and agree with the results of /4/. In the EXAFS analysis with S_0^2 = 0.9, the coordination numbers of the Am^{3+} and Cm^{3+} in 0.1 M $HClO_4$ are smaller by two atoms as compared to those in 0.25 M HCl /4/.

	R [Å]	N	σ^2 [Å^2]	ΔE [eV]	k [Å^{-1}]
Am^{3+} FL	2.494(2)	7.0(2)	0.0058(3)	-1.8	3.3-9.0
Am^{3+} TR	2.494(2)	7.8(2)	0.0075(2)	-1.8	3.3-9.0
Cm^{3+}	2.462(3)	7.9(3)	0.0070(4)	-12.5	3.3-9.0

Tab. 1: EXAFS structural parameters for the Am^{3+} and Cm^{3+} aquo ions (FL = fluorescence mode; TR = transition mode). The standard deviations as estimated by EXAFSPAK are given in parenthesis.

References

/1/ Carnall, W.T., J. Less-Common Met. **156**, 221 (1989)
/2/ Beitz, J.V., Radiochim. Acta **52/53**, 35 (1991)
/3/ Kimura, T., Choppin, G.R.J., Alloys Comp., **213/214**, 313 (1994)
/4/ Allen, P.G. et al., Inorg. Chem. **39**, 595 (2000)

COMPLEX FORMATION IN THE URANYL, EARTH ALKALINE METALS AND CARBONATE SYSTEM

S. Amayri, G. Geipel, V. Brendler, G. Bernhard

Fluorescence spectroscopy (TRLFS) was used to study the complexation of Mg^{2+}, Sr^{2+}, Ba^{2+} in the presence of uranyl and carbonate in aqueous alkaline solution. A 1:1 complexation of the type $MUO_2(CO_3)_3^{2-}$ was observed at pH 8.0. The following complexation constants were determined: $\log\beta_{Mg}{}^0{}_{113}$: 23.48 ± 0.07, $\log\beta_{Sr}{}^0{}_{113}$: 25.89 ± 0.22 and $\log\beta_{Ba}{}^0{}_{113}$: 26.00 ± 0.26.

A $Ca_2UO_2(CO_3)_3$ complex species was found in the seepage waters of various uranium mining areas /1/. The complexation constant of the related di- and tricarbonato complex was published in /2/. To complete these studies and to compare this species with others, the complexation behavior of Mg^{2+}, Sr^{2+}, Ba^{2+} and $UO_2(CO_3)_3^{4-}$ at pH 8.0 was investigated.

Determination of the complex formation constant:

Fig 1. shows, for example, a set of TRLFS spectra of aqueous solutions of $3x10^{-5}$ M UO_2^{2+}, $8x10^{-3}$ M HCO_3^- /CO_3^{2-} and magnesium varying from $1x10^{-4}$ M to $1x10^{-2}$ M at pH 8.0. As is known, the uranyl tricarbonate complex $UO_2(CO_3)_3^{4-}$ does not show any uranium fluorescence /1/.

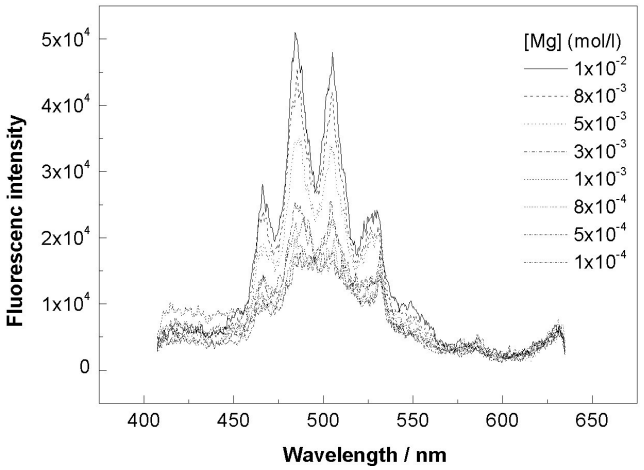

Fig.1: Fluorescence spectra of $MgUO_2(CO_3)_3^{2-}$ as a function of the Mg^{2+} concentration at pH = 8.0

The intensity of the fluorescence spectra of the magnesium species increases with increasing magnesium concentration. The main emission bands of the magnesium species were: 467.0 nm, 485.3 nm, 504.8 nm, 528.2 nm and 550.2 nm. The fluorescence life time was 13.5 ± 0.5 ns. The TRLFS spectra of the strontium and barium series show the same behavior. The fluorescence life times of the strontium and barium complex were 25.1 ± 0.6 nm and 15.2 ± 0.7 nm. The complex formation constants of these species were calculated, using linear regression (Fig. 2) as described in /3/. The slope of this fit (Fig. 2) indicates the number of Mg^{2+} ions reacting with the $UO_2(CO_3)_3^{4-}$ and the intersection value specifies the complex formation constant.

Serie	$\log\beta$ (I = 0.1)	$\log\beta^0$ (I = 0)	slope
Mg-series	0.09 ± 0.05	1.88 ± 0.05	1.17 ± 0.07
Sr-series	2.50 ± 0.22	4.29 ± 0.22	1.12 ± 0.16
Ba-series	2.61 ± 0.26	4.40 ± 0.26	1.01 ± 0.18

Tab. 1: Calculated data for the complex formation of $MUO_2(CO_3)_3^{2-}$

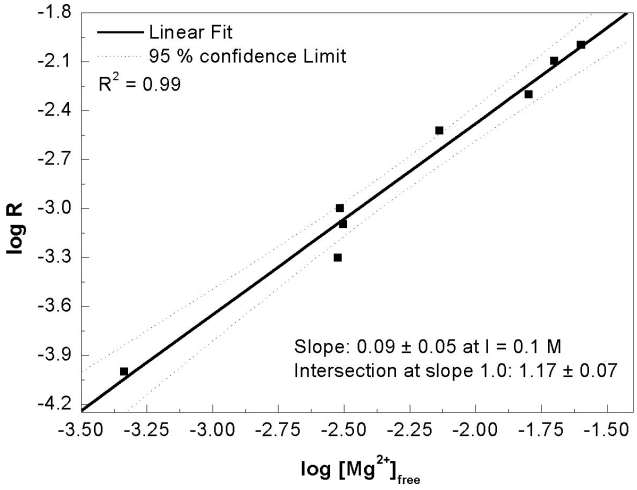

Fig. 2: Slope analysis of the complex reaction of uranyl carbonate and magnesium ions

The results in Tab. 1 show a predominant 1:1 complex formation between Mg^{2+}, Sr^{2+}, Ba^{2+} and $UO_2(CO_3)_3^{4-}$. To extrapolate the formation constant at infinite dilution, the Davies equation was used.
Using the NEA data base /4/, the constant at infinite dilution was obtained for the reaction:

$$UO_2^{2+} + 3CO_3^{2-} \Leftrightarrow UO_2(CO_3)_{3(aq)}^{4-} \qquad [1]$$

An overall brutto complex formation constant of 1:1 complex at infinite dilution was calculated as follows for the reaction [2]:

$$M^{2+} + UO_2^{2+} + 3CO_3^{2-} \Leftrightarrow MgUO_2(CO_3)_3^{2-} \qquad [2]$$

$$MgUO_2(CO_3)_3^{2-}: \log\beta_{113}^0 = 23.48 \pm 0.07;$$

$$SrUO_2(CO_3)_3^{2-}: \log\beta_{113}^0 = 25.89 \pm 0.22;$$

$$BaUO_2(CO_3)_3^{2-}: \log\beta_{113}^0 = 26.00 \pm 0.26.$$

Our results showed that the complex formation constants of uranyl tricarbonate with Mg^{2+}, Ca^{2+} ($CaUO_2(CO_3)_3^{2-}: \log\beta_{113}^0$ = 25.40 ± 0.25 /2/), Sr^{2+} and Ba^{2+} are similar in aqueous systems for 1:1 complexes within the experimental error. We can conclude that under environmental conditions (considering pH, carbonate, earth alkaline metal, and uranyl concentration) only the formation of the calcium and magnesium complex is possible. These agree well with the formation of the secondary uranium minerals bayleyite and liebigite under the same conditions.

References

/1/ Bernhard, G. et al., J. Alloys and Compounds **271-273**, 201 (1998)
/2/ Bernhard, G. et al., Radiochim. Acta **89**, 511 (2001)
/3/ Amayri, S., Dissertation, TU Dresden (2002)
/4/ Grenthe, I. et al., *Chemical thermodynamics of uranium*, 1st. ed., Els. Sci. Pub. (1992)

COMPLEX FORMATION OF U(VI) WITH GLUTATHIONE AND ITS BASIC COMPONENTS STUDIED BY X-RAY ABSORPTION SPECTROSCOPY

A. Günther, A. Roßberg, G. Bernhard

The complex formation of uranyl with the tripeptide glutathione and its basic amino acids was studied at pH4. The binding of uranyl is dominated by the carboxylic groups of the bioligands.

Introduction

Several peptides are known to bind heavy metals. We investigated the U(VI) / tripeptide glutathion model system. A 1:1 uranyl complex was found by time-resolved laser-induced fluorescence spectroscopy /1/. The purpose of this EXAFS study was the determination of the bond type between the uranyl cation and the glutathione and its basic amino acids glycine, glutamic acid and cysteine.

Experimental

The stock solutions of glutathione and of glycine, glutamic acid and cysteine were freshly prepared from pure chemicals. The uranium concentration was $1.0 \cdot 10^{-3}$ M. The concentration of the organic ligands was $2.5 \cdot 10^{-1}$ M (glycine, cysteine), $3.0 \cdot 10^{-2}$ M (glutamic acid) and $5.0 \cdot 10^{-2}$ M (glutathione). Using $NaClO_4$, the ionic strength of the complex solutions was adjusted to 0.1 M (amino acids) or 0.15 M (glutathione). The U L_{III}-edge EXAFS spectra were measured in fluorescence mode using a 4-pixel-germanium detector. The EXAFS spectra were analyzed according to standard procedures using the suite of programs EXAFSPAK /2/. The theoretical scattering phases and amplitudes were calculated with the scattering code FEFF 6 /3/ using the model compound sodium tris(acetato)dioxouranate. The minor component in the spectra was analyzed by the difference technique described in /4/.

Results and discussion

Fig.1 shows the raw U L_{III}-edge k^3-weighted EXAFS spectra and their corresponding Fourier transforms (FT) of the organic uranyl complex solutions investigated.

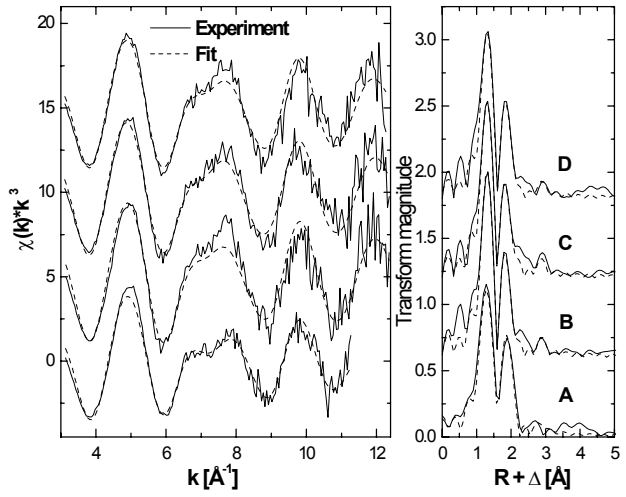

Fig. 1: Raw U L_{III}-edge k^3-weighted EXAFS spectra (left) and its corresponding Fourier transform (right) of the complex solutions at pH 4:
A: U(VI) / glutathione B :U(VI) / glycine
C: U(VI) / glutamic acid D: U(VI) / cysteine

The first and second peaks correspond to the scattering contributions of the two axial oxygen atoms (O_{ax}) of the uranium(VI) ion and of the equatorial oxygen atom (O_{eq}) (major components). The third peak in the spectra at 2.3 Å was interpreted as a backscattering carbon atom (minor component). The fit results are listed in Tab. 1.

Organic ligand	shell	N	R [Å]	$\sigma^2 \cdot 10^3$ [Å^2]
Glutathione (A)	U - O_{ax}	2	1.771(3)	4.0(3)
	U - O_{eq}	4.7(4)	2.394(5)	8.6(9)
	U - C	0.93(6)	2.955(4)	3.0
Glycine (B)	U - O_{ax}	2	1.771(3)	1.4(2)
	U - O_{eq}	6.5(9)	2.376(9)	12(2)
	U - C	1.34(7)	2.921(3)	3.0
Glutamic acid (C)	U - O_{ax}	2	1.772(3)	1.7(2)
	U - O_{eq}	6.4(8)	2.388(8)	13(2)
	U - C	1.7(1)	2.878(4)	3.0
Cysteine (D)	U - O_{ax}	2	1.776(3)	2.2(2)
	U - O_{eq}	5.4(6)	2.391(8)	11(1)
	U - C	1.19(6)	2.922(3)	3.0

The standard deviations are given in parenthesis. During the fitting procedure the coordination number of O_{ax} was held constant at N=2.

Tab. 1: EXAFS structural parameters of several complex systems U(VI)/organic ligand at pH 4.

The FT spectrum of the complex solution A differs optically from the other spectra. Note that the FT-transformed k-range for sample A is shorter than it is for the other three samples. But the structural parameters of the interaction of U(VI) with glutathione (A) are comparable with the parameters of the other complex systems (Tab. 1). We can conclude from this EXAFS study that the coordination of U(VI) to all these ligands is identical. The found equatorial distance U – O_{eq} of 2.38 to 2.39 Å indicates that uranyl is predominantly bound by the carboxylic group. Further investigations are required to determine the influence of the other functional groups NH_2 and SH.

Acknowledgment

This study was supported by DFG (BE 2234/1-2).

References

/1/ Günther, A. et al.; Report FZR-343, p. 12 (2001)
/2/ George, G.N., Pickering, I.J.: *EXAFSPAK - A Suite of Computer Programs for Analysis of X-Ray Absorption Spectra*, Stanford Synchrotron Radiation Laboratory, Stanford, CA. USA, (1995)
/3/ Zabinsky, S.I., Rehr, J.J., Ankudinov, A., Albers, R.C., Eller, M.J.: Multiple-scattering calculations of x-ray-absorption spectra, Phys. Rev. **B52**, 2995 (1995)
/4/ Teo, B.K.: *EXAFS - Basic Principles and Data Analysis* , Springer-Verlag, New York 1986

POTENTIOMETRIC INVESTIGATION OF URANIUM(VI) COMPLEXATION BY SUGAR PHOSPHATES

A. Koban, G. Bernhard

The complex formation of uranium(VI) with glucose 1-phosphate, glucose 6-phosphate, and fructose 6-phosphate was studied by potentiometric pH titration. In each case two complexes were found: the 1:1 species $UO_2(C_6H_{11}O_6PO_3)$ and the 1:2 species $UO_2(C_6H_{11}O_6PO_3)_2^{2-}$. The formation constants of these uranyl sugar phosphate complexes were determined.

Sugar phosphates are omnipresent in every living cell as intermediates of metabolism. We therefore studied their complexation behavior with uranium(VI) to obtain more information about the interaction of radionuclides with biological systems. We determined the complexation of UO_2^{2+} with glucose 1-phosphate (G1P), glucose 6-phosphate (G6P), and fructose 6-phosphate (F6P) (all $C_6H_{11}O_6PO_3^{2-}$) by potentiometric pH titration.

Potentiometric titration was carried out at an initial uranyl concentration of 10^{-4} M and ligand concentration of 10^{-3} M in a pH range from 3 to 10 and an ionic strength of 0.1 M ($NaClO_4$). The corresponding sugar phosphoric acid was synthesized *in situ via* adding 2 x 10^{-3} M $HClO_4$ to the titration solution. All solutions were prepared with carbonate free deionized water in a glove box under nitrogen. The samples were titrated with 0.01 M NaOH (Merck, Titrisol) of an ionic strength of 0.1 M. The experiments were performed by an automatic titrator (GP Titrino 736, Metrohm), using a Schott BlueLine 11 pH combination electrode with platinum diaphragm in a thermostatic vessel at 25.0±0.1 °C under nitrogen. The electrode was calibrated for each experimental run with NBS buffers at pH 4.01 and 6.87 (Schott). The titration solution was added in 0.05 ml steps. The titration method was the following: after an initialization time of 600 s NaOH was added and stirred for 60 s. After waiting for another 60 s without stirring the pH was measured and the next titration step followed. The measured potentiometric titration data were analyzed, using the Hyperquad 2000NT least squares program, version 2.1 /1/.

In order to calculate complex formation constants, the dissociation constants of the ligands have to be known. The existing literature data for the pk_a values of the two protonic ligands $C_6H_{11}O_6PO_3H_2$ vary. In addition to the discrepancies in value, they also differ in temperature, ionic strength and ionic consistency /2/. Anyhow, to be self-consistent we determined our own pk_a values for the studies (Tab. 1). In view of the pH range examined, only the second dissociation step of the ligand (Eq. 1) was relevant for calculation of the complex formation constants.

$$C_6H_{11}O_6PO_3H^- \leftrightarrow C_6H_{11}O_6PO_3^{2-} + H^+ \qquad pk_{a2} \quad (1)$$

Examination of the potentiometric measurements of the uranium(VI) sugar phosphate systems showed the formation of the 1:1 complex $UO_2(C_6H_{11}O_6PO_3)$ in the pH range between 3 and 7, which changes to a 1:2 complex $UO_2(C_6H_{11}O_6PO_3)_2^{2-}$ at higher pH values. The calculated complex formation constants are summarized in Tab. 1.

Ligand	pk_{a2}	$\log\beta_{11}$	$\log\beta_{12}$
G1P	6.15±0.03 /3/	5.40±0.25 /3/ (5.72±0.12* /3/)	8.96±0.18 /3/
G6P	6.34±0.08	5.89±0.04 (6.35±0.28* /4/)	9.45±0.08
F6P	6.17±0.02	5.72±0.21 (5.66±0.17* /4/)	9.54±0.09

* calculated from TRLFS measurements

Tab. 1: Summarized dissociation and complex formation constants at I=0.1 M.

To estimate the relevance of these complexes in biological systems with alternating conditions concerning, for instance, the concentration of CO_2, pH value, ionic composition and ionic strength, Fig. 1 shows an example of the speciation of 10^{-4} M uranium in an aqueous solution with 10^{-3} M glucose 1-phosphate, 10^{-4} M carbonate and ionic strength of 0.1 M. Both uranium sugar phosphate species dominate in the pH range between 4 and about 6.5, which is not uncommon in biosystems.

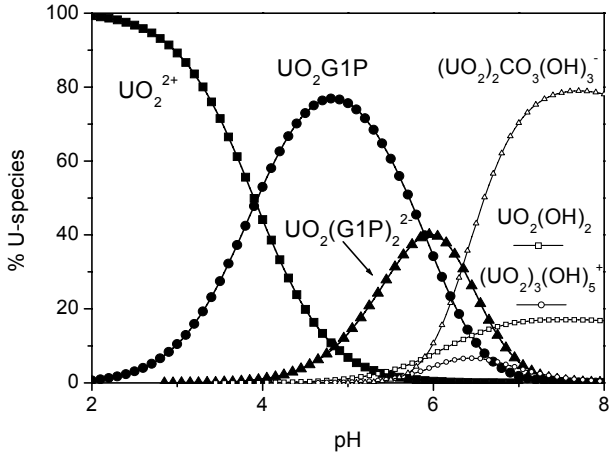

Fig. 1: Speciation of U(VI) in aqueous solution as a function of pH: 10^{-4} M UO_2^{2+}, 10^{-3} M G1P, 10^{-4} M CO_3^{2-}, I = 0.1 M.

The 1:1 complexes were also investigated by TRLFS /3,4/. The results of the two methods are in good agreement within their standard deviations (Tab. 1).

Acknowledgment

This study was supported by DFG (BE 2234/1-1, 1-2).

References

/1/ Gans, P. et al., Talanta **43**, 1739 (1996)
/2/ Martell, A.E. et al., *NIST Critically Selected Stability constants of Metal Complexes Database*, Version 5.0 (1998)
/3/ Koban, A. et al., Radiochim. Acta, in press (2003)
/4/ Koban, A. et al., Report FZR-373, p. 5, 6 (2003)

COMPLEX FORMATION OF URANIUM(VI) WITH FRUCTOSE 6-PHOSPHATE STUDIED BY TRLFS

A. Koban, G. Geipel, G. Bernhard

Fluorescence lifetimes and spectra were determined for the 1:1 complex; the formation constant of $UO_2(C_6H_{11}O_6PO_3)$ at I = 0.1 M was calculated to be log β_{11} = 5.66 ± 0.17.

For better understanding of the radionuclide speciation in biosystems we investigate the complex formation of uranium(VI) with biorelevant model compounds.

We studied the complexation of uranium(VI) with fructose 6-phosphate ($C_6H_{11}O_6PO_3^{2-}$, F6P), using TRLFS. The experiments were performed at a fixed uranyl concentration (10^{-5} M) as a function of the ligand concentrations (10^{-5} to 2 x 10^{-3} M) at different pH values between 3.0 and 4.0 and an ionic strength of 0.1 M ($NaClO_4$).

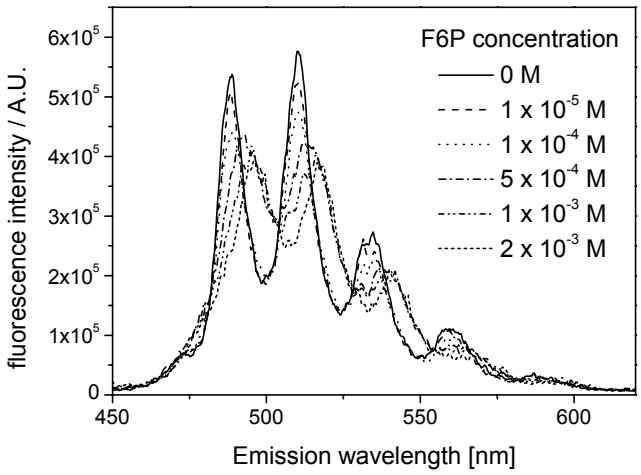

Fig. 1: TRLFS spectra of uranium(VI) (10^{-5} M) as a function of the fructose 6-phosphate concentration at pH = 4.

Fig. 1 shows the TRLFS spectra of uranium(VI) as a function of the ligand concentrations at pH = 4.0. With increasing ligand concentration we observed a small decrease in fluorescence intensity connected with a red shift of about 7 nm compared to the uranyl ion. This effect we noticed at all measurements in the pH range between 3 and 4.

The TRLFS spectra at different pH values showed triexponential decays indicating a mixture of three species. The lifetimes are (averaged about all measurements) 133 ± 50 ns, 1.3 ± 3 µs, and 9 ± 3 µs. The last one with a very low but constant intensity can be assigned to uranyl hydroxide, which is always present in small amounts under such experimental conditions. The middle one is typical for the free UO_2^{2+} ion. Its intensity decreases with increasing ligand concentration, whereas the intensity of the shortest lifetime increases. Therefore we assign it to the new complexed species UO_2F6P.

The single spectra of the different species can be determined from the composite spectrum using conventional peak deconvolution (Fig. 2). The main fluorescence emission bands of the uranium sugar phosphate complex are located at 483, 496, 518, 542, and 567 nm.

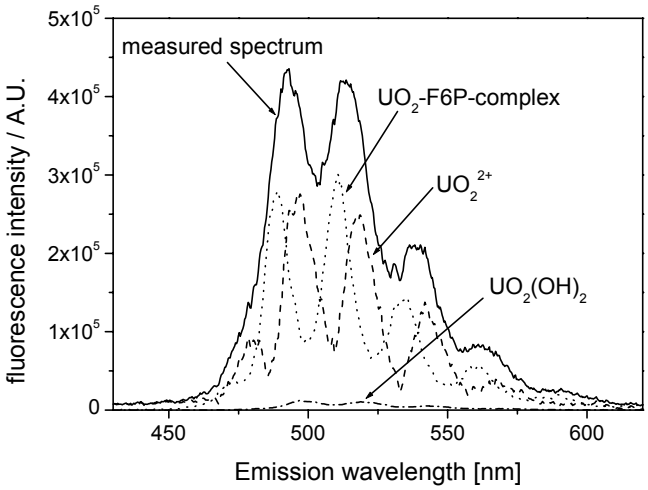

Fig. 2: Results of the peak deconvolution of the TRLFS spectrum of uranium(VI) (10^{-5} M) and F6P (5 x 10^{-4} M) at pH=4.0.

Considering similar uranium sugar phosphate systems /1, 2/ and the protolyse balance of F6P /3/ the complex formation reaction can assumed to be:

$$UO_2^{2+} + F6PH^+ \leftrightarrow UO_2(F6P) + H^+ \qquad \log k \quad (1)$$

To validate the stoichiometry of this reaction slope analyses were performed at different pH values (Tab. 1). The slopes between 0.75 and 1.05 indicate a predominant 1:1 complexation in this pH range.

pH	Slope	log k
3.0	1.05±0.08	-0.37±0.03
3.25	1.03±0.20	-0.37±0.07
3.75	0.85±0.10	-0.63±0.05
4.0	0.75±0.05	-0.77±0.05

Tab. 1: Calculated data for the complex formation of uranium(VI) with fructose 6-phosphate.

The stability constant for the complex formation reaction

$$UO_2^{2+} + C_6H_{11}O_6PO_3^{2-} \leftrightarrow UO_2(C_6H_{11}O_6PO_3) \quad \log\beta_{11} \quad (2)$$

was determined like described in /1/ to be $\log\beta_{11}$ = 5.64 ± 0.17 at an ionic strength of 0.1 M.

Acknowledgment

This study was supported by DFG under contract number BE 2234/1-1, 1-2.

References

/1/ Koban, A. et al., Radiochim. Acta, accepted (2003)
/2/ Koban, A. et al., Report FZR-373, p. 6 (2003)
/3/ Garcia, A. et al., J. Inorg. Biochem. **62**, 57 (1996)

COMPLEX FORMATION OF URANIUM(VI) WITH GLUCOSE 6-PHOSPHATE STUDIED BY TRLFS

A. Koban, G. Geipel, G. Bernhard

The obtained complex shows no fluorescence; the formation constant of $UO_2(C_6H_{11}O_6PO_3)$ at I = 0.1 M was calculated to be log β_{11} = 6.35 ± 0.28.

To identify and understand the chemical speciation of actinides in biosystems on a molecular level we investigated the complexation of uranium with selected bioligands of relevant functionality as model compounds.

We studied the complexation of uranium(VI) with glucose 6-phosphate ($C_6H_{11}O_6PO_3^{2-}$, G6P), using TRLFS. The experiments were performed at a fixed uranyl concentration (10^{-5} M) as a function of the ligand concentrations (10^{-5} to 10^{-3} M) at various pH values between 3.0 and 4.0 and an ionic strength of 0.1 M ($NaClO_4$).

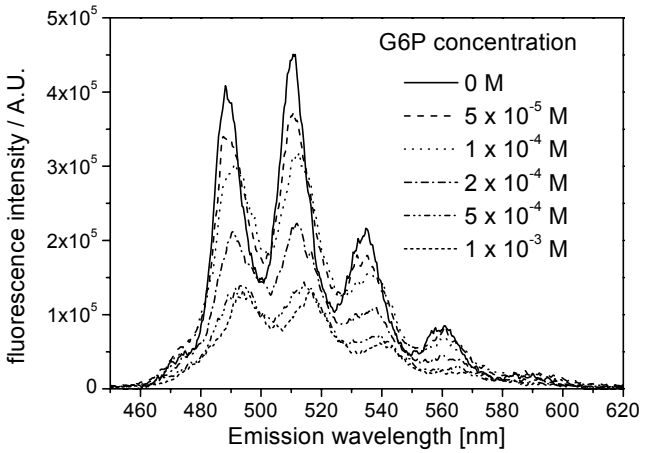

Fig. 1: TRLFS spectra of uranium(VI) (10^{-5} M) as a function of the glucose 6-phosphate concentration at pH=4.

Fig. 1 shows the TRLFS spectra of uranium(VI) as a function of the ligand concentration at pH=4.0. With increasing ligand concentration we observed a decrease in fluorescence intensity. At higher ligand concentrations only a small red shift of the emission bands caused by the dominant uranyl hydroxide species was detectable.
The TRLFS spectra indicate the presence of the free uranyl ion with a lifetime of 1.4 ± 0.3 µs and at higher pH ranges uranyl hydroxide species with a lifetime of 12 ± 4 µs. We therefore conclude that the complexed uranyl glucose phosphate species shows no fluorescence properties.
Considering the protolyse balance of the two protonic acid H_2G6P /1/ in the studied pH range the complex formation reaction can be written as:

$$UO_2^{2+} + G6PH^+ \leftrightarrow UO_2(G6P) + H^+ \qquad \log k \quad (1)$$

To estimate the stoichiometry of this reaction slope analyses were performed at different pH values (Fig. 2 and Tab. 1), using the mass action law according to eq. (1) in its linear form:

$$\log \frac{[UO_2G1P]}{[UO_2^{2+}]} = n\log[HG1P^+] + \log k + pH \qquad (2)$$

with

$$\log k + pH = \log k' \qquad (3)$$

The concentration of the free uranyl ion was determined on the basis of the measured spectra. These data were used to calculate the corresponding concentrations of the complexed uranyl species and the non complexed ligand.

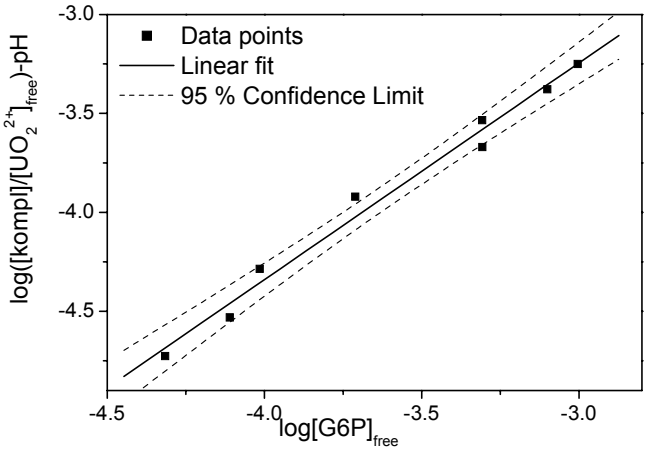

Fig. 2: Slope analysis at pH=4.

pH	Slope	log k	log k'
3.0	0.82±0.13	0.44±0.05	3.48±0.05
3.25	1.28±0.19	0.14±0.07	3.38±0.07
3.5	0.97±0.27	0.10±0.17	3.63±0.26
3.75	0.82±0.12	0.05±0.06	3.79±0.06
4.0	1.03±0.06	-0.24±0.03	3.77±0.03

Tab. 1: Calculated data for the complex formation of uranium(VI) with glucose 6-phosphate.

The slopes between 0.82 and 1.28 show clearly a 1:1 complexation in this pH range.

For the complex formation reaction

$$UO_2^{2+} + C_6H_{11}O_6PO_3^{2-} \leftrightarrow UO_2(C_6H_{11}O_6PO_3) \qquad (4)$$

we obtained a stability constant of $\log\beta_{11}$ = 6.35 ± 0.28 at an ionic strength of 0.1 M.

Acknowledgment
This study was supported by DFG under contract number BE 2234/1-1, 1-2.

References

/1/ Cowan, J., Inorg. Chem. **30**, 2740 (1991)

EXAFS INVESTIGATION OF URANIUM COMPLEXATION BY GLUCOSE 1-PHOSPHATE

A. Koban, A. Roßberg, G. Bernhard

The U(VI) glucose 1-phosphate system (U-G1P) shows a monodentate complexation of the uranium via the phosphate group.

To get further information about the binding properties and the structure of actinides in biological systems we investigate selected bioligands with relevant funtionalities like sugar phosphates as model compounds.

The EXAFS-measurements were carried out on solutions containing 10^{-3} M UO_2^{2+}, and 5 x 10^{-2} M sugar phosphate (I = 0.15 M) at pH = 4.0 in polyethylene tubes of 13 mm diameter. Measurements were performed on the Rossendorf Beamline (ROBL) at the European Synchrotron Radiation Facility (ESRF) in Grenoble. The U L_{III}-edge spectra were measured in fluorescence modus. The EXAFS spectra were analyzed using the suite of programs EXAFSPAK. The theoretical scattering phase and amplitude functions used in data analysis for U-G1P were calculated for the model compound $Ca(UO_2)_2(PO_4)_2$ x 6 H_2O /1/ using the FEFF8 program.
The raw U L_{III}-edge k^3-weighted EXAFS spectra and the corresponding Fourier transform (FT) for the uranium solution containing glucose 1-phosphate (U-G1P) are shown in Fig. 1 and the fit results are listed in Tab. 1.

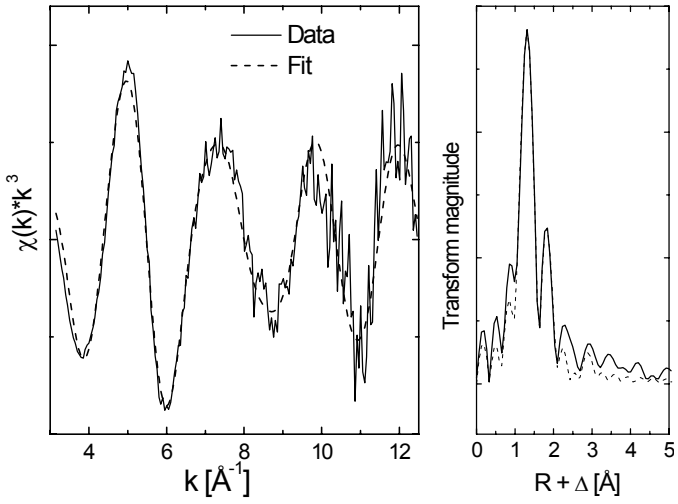

Fig. 1: Raw U L_{III}-edge k^3-weighted EXAFS spectra (left) and the corresponding Fourier transform (FT) (right).

In the FT from the sample U-G1P four peaks are visible. The first and the second peak correspond to the scattering contribution of the two axial oxygen atoms (O_{ax}) of the uranyl ion and the scattering contribution of the equatorial oxygen atoms ($O_{eq(1)}$), respectively. The third peak is probably due to backscattering from a light element like carbon or oxygen. Because of the respectable possibilities in this molecule, we assumed an oxygen shell ($O_{eq(2)}$) in our fit. The fourth peak we interpret as a scattering contribution of phosphorus, which overlap with the multiple scattering path along the uranyl chain (U-O_{ax1}-U-O_{ax2}).

The main contributions to the total EXAFS amplitude are caused by the axial and the equatorial oxygen atoms. In comparison, the contributions of the $O_{eq(2)}$ and P coordination shells are very small. Therefore, we consider the O_{ax} and $O_{eq(1)}$ shells as major and the $O_{eq(2)}$ and P shells as minor components in the EXAFS spectra, respectively. To increase the precision in determination of the EXAFS structural parameters for the minor components, we use the difference technique as described in /2/. The best fit of the EXAFS spectra of the major components were subtracted from the raw k^3-weighted U L_{III}-edge EXAFS spectra. The obtained residuals contain only the signal of the minor components and some experimental noise. After Fourier transformation of the residual EXAFS spectra, the region of the minor components was Fourier filtered and back transformed into k-space. Furthermore the twofold degenerated 3-legged MS path U-$O_{eq(1)}$-P (MS2) had to be considered because its intensity is similarly to the backscattering of P.
The spectra and structural parameters are in good agreement with those of m-autunite /1/. In m-autunite each U(VI) ion is coordinated monodentate by four phosphate groups. Therefore we assume that the sugar phosphate coordinates the U(VI) via the monodentate binding phosphate group.

Sample	Shell	N	R [Å]	σ^2 [Å^2]
U-G1P	U-O_{ax}	2	1.771(3)	0.0019(2)
	U-$O_{eq(1)}$	4.3(5)	2.336(7)	0.008(1)
	U-$O_{eq(2)}$	0.82(6)	2.864(5)	0.003
	U-P	N_P=2.4(6)	3.587(9)	0.0030(7)
	MS2	2xN_P	3.71(1)	0.0014(8)

Standard deviations of variable parameters are given in parenthesis; N - coordination number; R – Radial distance; σ^2 – Debye-Waller factor

Tab. 1: Summary of the EXAFS structural parameters.

The complexation of uranium with glucose 1-phosphate was also studied by TRLFS and potentiometric titration /3/. These studies show the formation of two different complexes, the 1:1 complex UO_2G1P and the 1:2 complex $UO_2(G1P)_2^{2-}$. According to the speciation both complexes are existing on the current conditions of the EXAFS experiments. Further studies will determine both complexes separate on the appropriate experimental conditions.

References

/1/ Makarov, E.S. et al., Doklady Akademii Nauk SSSR **132**, 673 (1960)
/2/ Teo, B. K.: *EXAFS: Basic Principles and Data Analysis*, Springer Verlag New York (1986)
/3/ Koban, A. et al., Radiochim. Acta, in press (2003)

COMPLEX FORMATION OF URANIUM WITH 2,3-DIHYDROXYBENZOIC ACID – FLUORESCENCE STUDY OF URANIUM

G. Geipel

We studied the complex formation of uranium with 2,3-dihydroxybenzoic acid using the fluorescence properties of uranium. In agreement with former studies /1/ of the fluorescence of the ligand a 1 to 1 complex formation occurred; combined with the release of two protons from the ligand. The formation constant was assigned to be log K = -3.99 ± 0.44.

The complex formation of uranium and 2,3-dihydroxybenzoic acid was studied, using the fluorescence properties of uranium. Fig. 1 shows a set of fluorescence spectra as a function of the concentration of the 2,3-dihydroxybenzoic acid (2,3-DHBA) added.

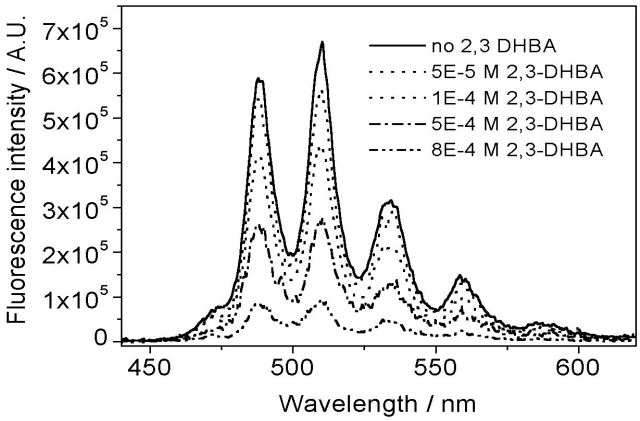

Fig. 1: Fluorescence spectra of uranium as function of the 2,3-DHBA concentration at pH 3.5

No shift in the fluorescence emission maxima was observed. This was expected, as the complex formed does not show any fluorescence emission. In this case the complex formation constant can be derived from the static quench effect. However, the fluorescence lifetime of the non-complexed uranium is influenced by the free ligand. A decrease in the fluorescence lifetime (and also in the fluorescence intensity) occurs due to dynamic quench processes. When calculating the complex formation this dynamic quench process has to be taken into consideration. Fig. 2. shows the Stern-Volmer plots at various pH values.

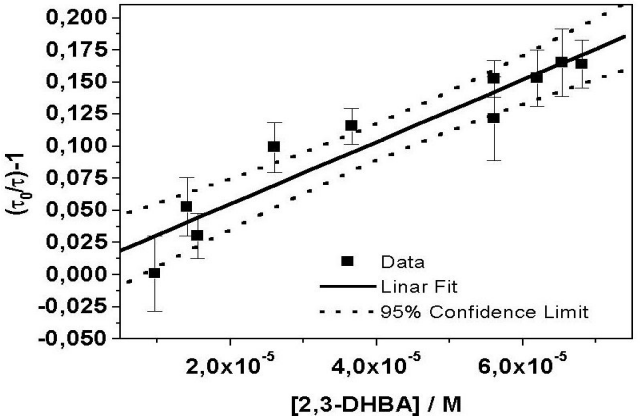

Fig. 2: Stern-Volmer Plot for the dynamic quench effect

From these data we obtain an equation expressing the pH dependence of the dynamic quench process:

$$K_{sv} = (22000 \pm 160) + (4644 \pm 42)\cdot\log[H^+] \quad (1)$$

The increase of the dynamic quench constant with increasing proton concentration allows the conclusion that only the protonated 2,3-DHBA contributes to the dynamic quench process. Using this equation, we can correct the measured intensities for the dynamic quench effect to obtain the intensities of the free uranyl ion only influenced by the static quench effect from complex formation. The corrected intensity values were used for calculation of the complex formation constant. Fig. 3 shows the validation of complex formation at pH 4.0, for example. The slope was found to be 1.02 ± 0.1, indicating a 1 to 1 complex formation.

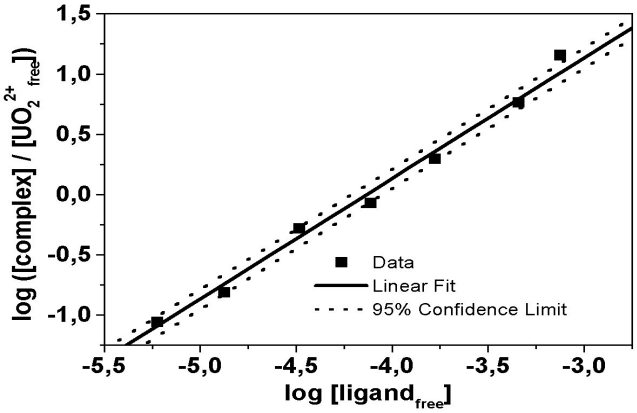

Fig. 3: Validation of the complex formation of uranium with 2,3-DHBA at pH 4.0

As the deprotonation of 2,3-DHBA was not taken into account in this validation step, the formation constant obtained should be dependent on pH. In Fig. 4 this behavior is shown. The slope of the fit was fixed to be –1.95 ± 0.45. From this it was concluded that two protons were released. This was also the result obtained in the study of the fluorescence properties of the ligand.

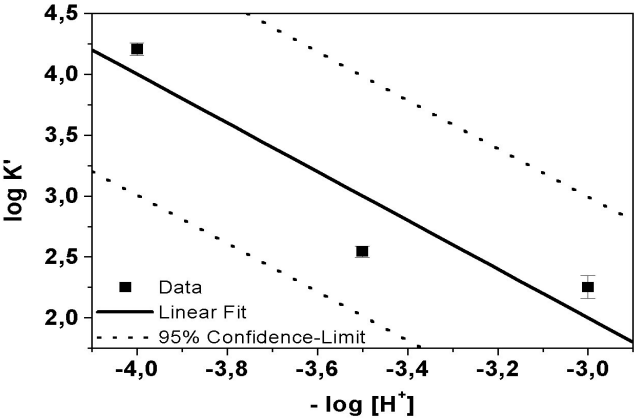

Fig. 4: Determination of the formation constant

However, the complex formation constant was determined to be log K = -3.99 ± 0.44. This constant is smaller than the constant derived from the fluorescence study of the ligand by an order of magnitude of about 0.8. This can be explained by excited state proton transfer reactions. These excited state reactions have to be included in the calculation to obtain the correct complex formation constant from the spectroscopic properties of the ligand.

COMPLEX FORMATION OF URANIUM WITH 2,5-DIHYDROXYBENZOIC ACID

G. Geipel, S. Nagasaki[1]
[1] University of Tokyo, Institute of Environmental Studies, Tokyo, Japan

We studied the complex formation of uranium with 2,5-dihydroxybenzoic acid. Due to the somewhat longer fluorescence lifetime of this acid a dynamic fluorescence quenching occurs. Therefore the fluorescence intensities must be corrected due to this effect. We found a 1 to 1 complex formation. The formation constant is assigned to be log K = 0.76 ± 0.36.

To study of the complex formation of dihydroxybenzoic acids we recorded the spectra of 2,5-dihydroxybenzoic acid (2,5DHBA) as function of pH and concentration of uranium. As example in Fig. 1 the spectrum of 5E-05 M 2,5DHBA at pH 3.0 with 8E-04 M uranium is shown. The intensity of the spectra changes with pH and uranium concentration.

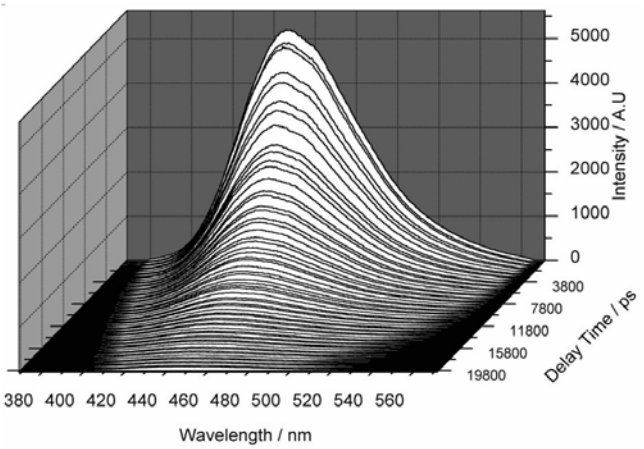

Fig. 1: TRLIF spectrum of 2,5-Dihydroxybenzoic Acid

Also a change in the fluorescence lifetime could be obtained. The fluorescence lifetimes were found to be in the range from 1.8 ns to 5.7 ns. Due to this and despite the static quenching caused by complex formation a dynamic quench process occur. As a first step for the calculation of formation constants we have therefore to determine the dynamic quench constant. Unfortunately besides the 2,5DHBA also the uranium quenches the fluorescence of the 2,5DHBA. The dynamic quench constants were found to be K_{SV} = 216 ± 4 for the ligand itself and K_{SV} = 45 ± 1 for uranium.

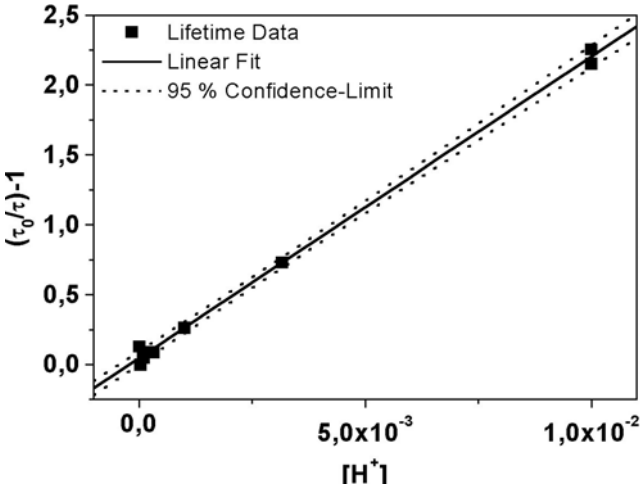

Fig. 2: Stern-Volmer Plot for the dynamic quench effect of the ligand

Both have to been taken into consideration for the estimation of the complex formation constant. As an example Fig. 3 shows the validation plot for the formation constant at pH 3.5.

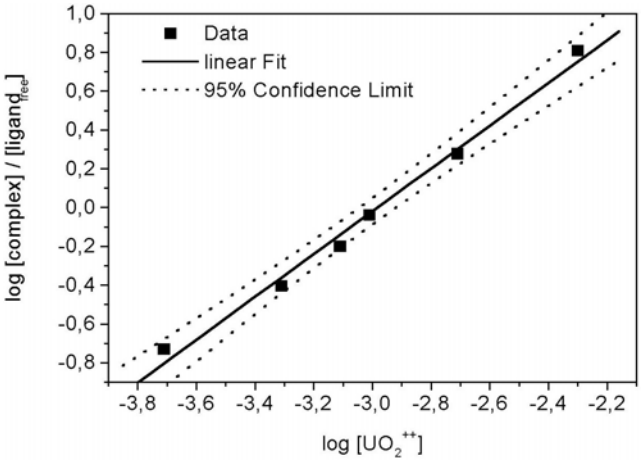

Fig. 3: Validation plot for the complex formation at pH 3.5

Form the validation plot we obtain a slope of 1.1 ± 0.12. In the pH range 2.0 to 4.0 slopes between 0.91 and 1.39 were found. We conclude therefore a one to one complex formation between uranium and 2,5DHBA.

In a second step we have to validate the dependence of the formation constants at the several pH values as function of pH in order to determine the number on protons involved in the complex formation and to assign the formation constant. Fig. 4 shows this plot.

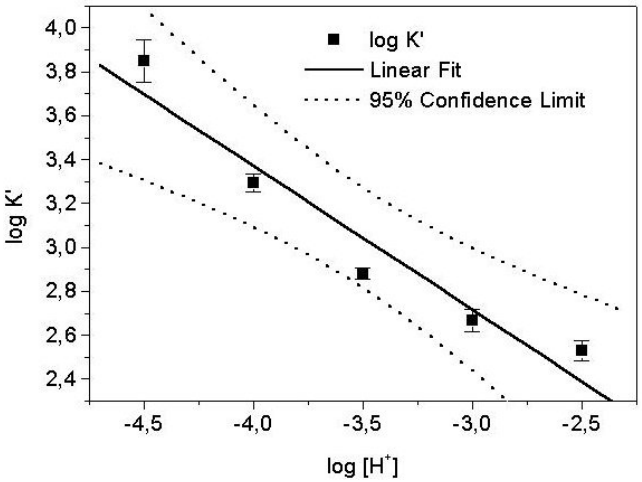

Fig. 4: Validation of the complex formation of uranium with 2,4 DHBA

The complex formation constant was assigned to be log K = 0.76 ± 0.36. Form the slope -0.65 ± 0.1 we conclude that maximum one proton is involved in this complex formation. This means that in the main only the carboxylic group is involved in the complex formation.

As uranium shows also fluorescence properties the complex formation will be confirmed by a study form the uranium fluorescence.

COMPLEX FORMATION OF URANIUM(VI) WITH ORGANIC LIGANDS STUDIED BY FS-TRLFS PART III: 3-HYDROXYBENZOIC ACID

D. Vulpius, G. Geipel, L. Baraniak, G. Bernhard

The first dissociation constant of 3-hydroxybenzoic acid and the formation constant of the corresponding 1:1 uranyl complex was determined by fs-TRLFS at I = 0.1 M and 25 °C to be pK_a = 4.09 ± 0.02 and log K_1 = 3.14 ± 0.05, respectively.

Introduction

In previous contributions we reported on the determination of dissociation constants and complex formation constants by time-resolved laser-induced fluorescence spectroscopy with ultra-short laser pulses (fs-TRLFS) /1/. We asserted that the formation constant of the 1:1 uranyl vanillate complex could not be determined by fs-TRLFS due to the self-absorption of the vanillic acid fluorescence by the uranium(VI). Now we found arguments which maybe give us an understanding of this problem.

Results and Discussion

The observed excessive fluorescence quenching of vanillic acid as function of the uranium(VI) concentration is not caused by self-absorption but by a temporal shift of the fluorescence decay curves. The quantitative extent of this effect depends on the actual working time of the laser. Shifts up to 625 ps were measured. The cause of this malfunction is not well-known yet. This effect is the smaller the longer the laser works, and has the smallest influence on chemical systems with long fluorescence lifetimes such as 3-hydroxybenzoic acid (Fig. 1)

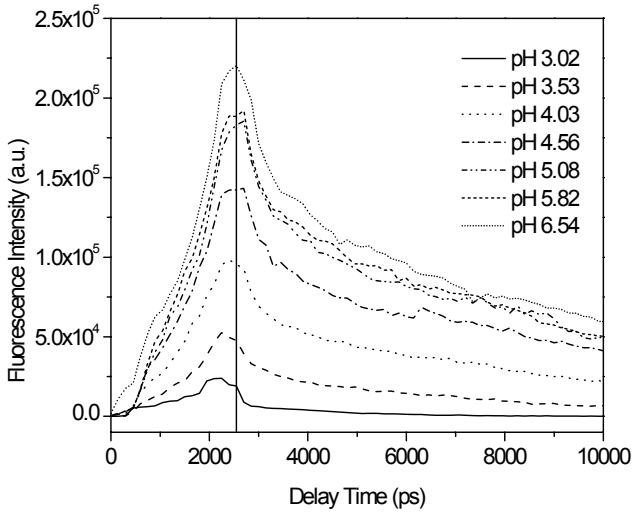

Fig. 1: Fluorescence decay of 3-hydroxybenzoic acid at various pH values

3-Hydroxybenzoic acid has two lifetimes within the entire pH range: a longer one of 8400 ± 500 ps and a shorter one of 470 ± 180 ps (all indicated uncertainties correspond to 1.96*s*). The longer lifetime is associated with the emission maxima at 423 nm (Fig. 2). This peak probably results from the single and the double negatively charged anion in the acidic and the basic region, respectively. The arrow in Fig. 2 points at the spectral section of the shorter lifetime. The emission maxima at 344 nm is not shown due to the limited measuring range of our spectrograph. The highest fluorescence intensity of this species is situated in the neutral pH range.

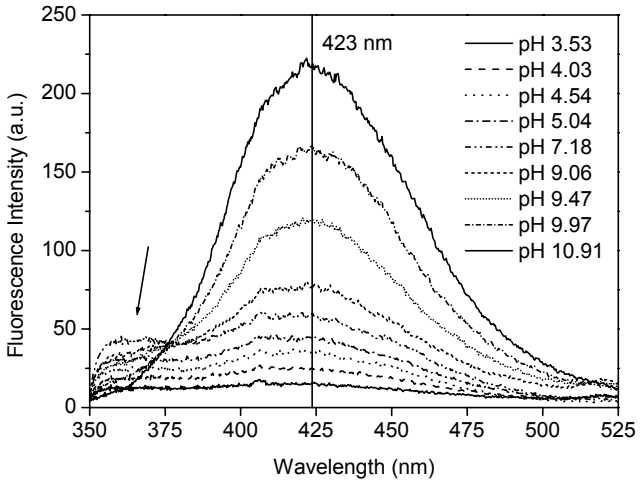

Fig. 2: Fluorescence spectra of 3-hydroxybenzoic acid as a function of pH

It is well-known that many aromatic molecules are subject to a proton transfer in the excited state. That means that their acid-base properties in the excited state differ significantly from those in the ground state /2/. It is possible that the fluorescence with the short lifetime comes from a species which resulted from excited-state proton transfer:

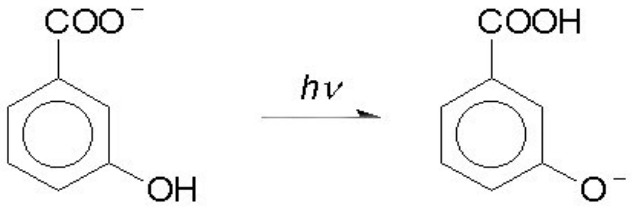

This new reaction must be considered in the calculations. At present we work on this problem. Our preliminary results are given in Tab. 1.

Reference	pK_a	log K_1
NIST /3/	3.99 ± 0.03	not available
this work	4.09 ± 0.02	3.14 ± 0.05

Tab. 1: First dissociation constant of 3-hydroxybenzoic acid and formation constant of the corresponding 1:1 uranyl complex at *I* = 0.1 M and 25 °C

Acknowledgment

This study was supported by the DFG under Contract No. BE 2234/3-1 and BE 2234/3-2.

References

/1/ Vulpius, D. et al., Report FZR-343, p. 9, 10 (2002)
/2/ Ireland, J. F. et al., Adv. Phys. Org. Chem. **12**, 131 (1976)
/3/ Martell, A. E. et al., *NIST Critically Selected Stability Constants of Metal Complexes Database*, 1998

SYNTHESIS AND CHARACTERIZATION OF HUMIC ACIDS WITH DISTINCT REDOX PROPERTIES: COMPARISON OF DIFFERENT PRECURSOR SUBSTANCES

S. Sachs, K.H. Heise, G. Bernhard

Different syntheses for humic acid-like model substances based on the oxidation of hydroquinone, catechol and vanillic acid were studied in order to obtain synthetic humic acids with distinct redox properties.

Introduction

The actinide speciation determines the mobility of these pollutants in the environment. It depends, amongst others, on the oxidation states of actinides that can be influenced by humic acids (HA). Therefore, the description of the impact of HA on the mobility of actinides in the environment requires, besides the knowledge of the actinide complexation by HA, the understanding of the effects of HA on the oxidation states of actinide ions. In order to study the redox properties of HA and the redox stability of actinide humate complexes in detail, we started to develop HA model substances with distinct redox properties. In /1/ we described syntheses of humic acid-like model substances with distinct redox capacities based on the oxidation of hydroquinone in the presence and absence of amino acids. In continuation of these studies we synthesized humic acid-like substances starting from different phenolic compounds (catechol, vanillic acid). Exemplary we determined the influence of the applied precursor substances on the redox properties of the resulting synthetic HA.

Experimental

The syntheses are based on the oxidation of catechol or vanillic acid in alkaline solution at 60 °C in the presence or absence of glycine or glutamic acid. Potassium peroxodisulfate is used as oxidizing agent /2,3/. The humic acid-like fractions of the reaction products are separated by precipitation with HCl and subsequent centrifugation, dialyzed, and lyophilized. The synthetic products were characterized for their elemental, functional and structural properties. By way of examples we will discuss HA type R4 (synthetic product of catechol and glycine) and type R5 (synthetic product of vanillic acid and glycine). For both HA we additionally determined the Fe(III) redox capacities (RC) at pH 3 as explained in /4/ ($[Fe(III)]_0$: 8.6 ± 0.2 mmol/L, [HA]: 0.12 g/L, 0.1 M KCl). The RC were compared to those of natural HA from Aldrich (AHA) and synthetic HA type R17 (synthetic product of hydroquinone and glycine /1/).

Results

Tab. 1 summarizes functional characteristics of HA type R4 and R5 compared to HA type R17 and AHA.

Humic acid	*COOH (meq/g)*	*Phenol./acidic OH (meq/g)*
Type R4	4.16 ± 0.04	6.6 ± 0.7
Type R5	5.74 ± 0.08	3.3 ± 1.3
Type R17	4.38 ± 0.11	6.0 ± 0.3
AHA	4.49 ± 0.14	3.1 ± 0.1

Tab. 1: Functional group contents of HA

As expected, the synthetic product of vanillic acid and glycine (R5) shows the highest carboxyl group content but the lowest phenolic/acidic OH group content compared to the products from glycine and catechol (R4) or hydroquinone (R17). Its amount on phenolic/acidic OH groups is similar to that of HA AHA. By contrast, HA type R4 shows a significant higher amount of phenolic/acidic OH groups and a similar carboxyl group content compared to that of AHA. Fig. 1 shows the RC of HA type R4 and R5 as a function of time in comparison to that of HA type R17 and AHA.

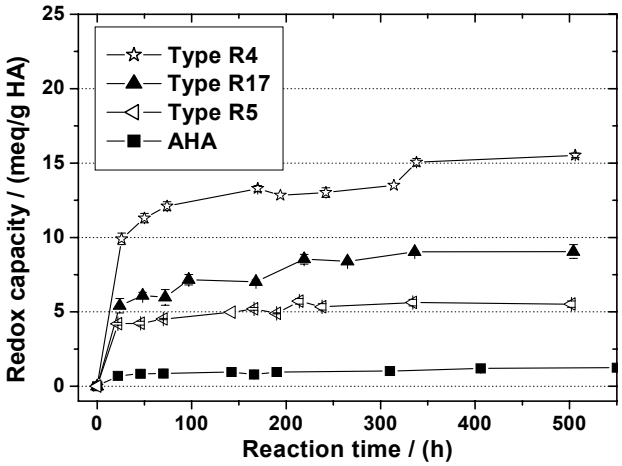

Fig. 1: Fe(III) redox capacities of synthetic HA based on the oxidation of phenolic compounds in comparison to HA AHA.

Although synthetic HA type R5 has a phenolic/acidic OH group content that is comparable to AHA, all synthetic HA show significant higher RC than AHA. The differences in the RC of HA AHA and type R5 points to structural differences of both HA which influence their redox behavior.

Compared to the synthetic products of diphenols and glycine (HA type R4 and R17), HA type R5 has the lowest RC which can be attributed to its lower phenolic/acidic OH group content. In contrast to that, HA type R4 shows the highest phenolic/acidic OH group content and also the highest Fe(III) RC. These results point to a correlation between the phenolic/acidic OH group content of the humic acid-like products of different phenolic compounds and their Fe(III) RC. It can be concluded, that it is possible to synthesize HA model substances with distinct RC based on the oxidation of phenolic compounds. The RC can be varied by specific variations of the precursor substances.

Acknowledgment

This work was supported by BMWA (No. 02E9299).

References

/1/ Sachs, S. et al., Report FZR-343 (2002) p. 13
/2/ Eller, W., Koch, K., Ber. Dt. Chem. Ges. **53**, 1469 (1920)
/3/ Adhikari, M. et al., Proc. Indian Natn. Sci. Acad. **51A**, 876 (1985)
/4/ Mack, B. et al., Report FZR-285 (2000) p. 40

STUDY OF THE REDOX PROPERTIES OF HUMIC ACIDS USING HUMIC ACID MODEL SUBSTANCES WITH SPECIFIC FUNCTIONALITIES

S. Sachs, K.H. Heise, G. Bernhard

The redox properties of humic acids (HA) at pH 9.2 were studied applying synthetic HA with specific functionalities. This study verifies that HA phenolic/acidic OH groups play a major role in the reduction of ferricyanide by HA.

Introduction

The redox activity of humic acids (HA) can be ascribed to the system hydroquinone-quinone and to the oxidation of phenols. In order to verify the dominating role of phenolic/acidic OH groups in the redox behavior of HA we studied the reduction of ferricyanide by different HA with specific functionalities.

Experimental

We determined the redox capacities (RC) of synthetic HA type R17 and R18 (HA-like products from hydroquinone and glycine or glutamic acid, respectively) which are characterized by distinct redox functionalities /1/, chemically modified HA type R18 with blocked phenolic/acidic OH groups (R18-PB) and synthetic HA type M42 (HA-like melanoidin from xylose and glutamic acid) in comparison to that of natural HA from Aldrich (AHA). We studied solutions of potassium ferricyanide and HA under N_2 atmosphere and exclusion of light ($K_3[Fe(CN)_6]$: 0.5 mmol/L, HA: 5 mg/L, 0.1 M KCl, borate buffer pH 9.2). The decrease of the ferricyanide concentration due to the reduction process by HA was determined by spectrophotometry /2/.

Results

Fig. 1 shows the RC of the investigated HA as a function of time. In Fig. 2 the RC after about three weeks equilibration time are compared to the phenolic/acidic OH group contents of the HA.

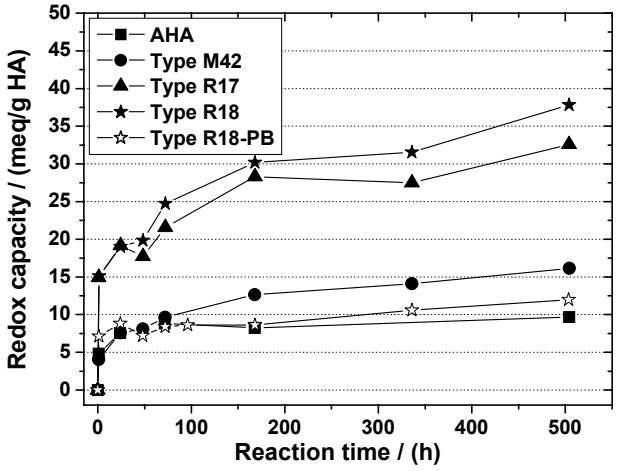

Fig. 1: Redox capacities of different HA at pH 9.2.

At pH 9.2, all unmodified synthetic HA show higher RC than AHA. The significant higher RC of HA type R17 and R18 with distinct redox functionalities can be attributed to their higher phenolic/acidic OH group content compared to HA type M42 and AHA (cf. Fig. 2). The RC that were determined for the unmodified HA are higher than their phenolic/acidic OH group contents. From that we conclude that there are other functional groups than phenolic/acidic OH groups or other processes than the single oxidation of phenolic OH groups contributing to the ferricyanide reduction.

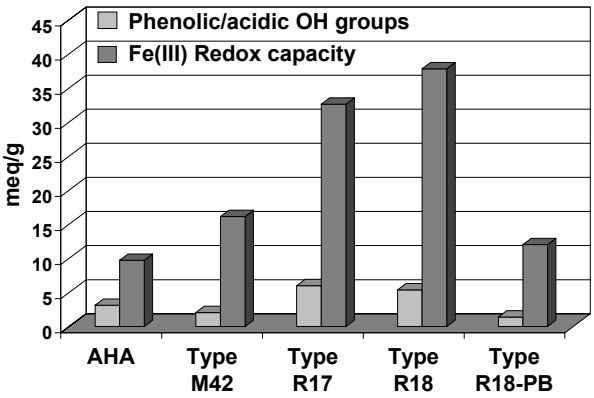

Fig. 2: RC of different HA in comparison to their phenolic/acidic OH group contents.

Due to the blocking of 76 % of the initial HA phenolic/acidic OH groups, the RC of HA type R18-PB is 64 % lower than that of HA type R18. This result points to a dominating role of phenolic/acidic OH groups in the studied redox process. However, the RC of HA type R18-PB is higher than its amount on residual, unmodified phenolic/acidic OH groups. Again, this supports the assumption that there are other processes than the simple oxidation of phenolic OH groups contributing to the reduction of ferricyanide.

The oxidation of phenols by ferricyanide proceeds via intermediate radicals and results in various, often complex products, e.g., complex phenolic compounds /3/. Subsequently, these phenolic reaction products could be additionally involved in the redox process, causing RC that are higher than those which would be expected under consideration of the phenolic OH group content of the starting compound and assuming that only phenolic OH groups contribute to the reduction of ferricyanide. HA show a very heterogeneous and complicated structure. Therefore, such secondary reactions with phenolic structural elements formed during the redox process between HA and ferricyanide could be possible. This would be a justification for the observed RC that are higher than the HA amount of phenolic/acidic OH groups. However, there is still the possibility for the involvement of other HA functional groups in the studied redox process.

Acknowledgment

This work was supported by the BMWA (No. 02E9299) and the EC Commission (No. FIKW-CT-2001-00128).

References

/1/ Sachs, S. et al., Report FZR-343 (2002) p. 13
/2/ Matthiessen, A., Vom Wasser **84**, 229 (1995)
/3/ Stewart, R., *Oxidation Mechanisms. Applications to Organic Chemistry*. W.A. Benjamin, Inc., NY, 1964, p. 84

CHARACTERIZATION OF 2-AMINOBENZENETHIOL AND ITS Re(VI) COMPLEX BY LASER-INDUCED FLUORESCENCE SPECTROSCOPY

H. Stephan[1], H. Spies[1], G. Geipel, G. Bernhard
[1] Institut für Bioanorganische und Radiopharmazeutische Chemie

The complex formation of rhenium the was studied by time-resolved laser-induced fluorescence spectroscopy of the ligand. The encapsulation of rhenium can be detected by changes in the fluorescence emission and lifetime.

Introduction

On the way to develop stable rhenium complexes with fine-tuned solubility behaviour one promising approach seems to be the dendritic encapsulation (Fig. 1) /1/.

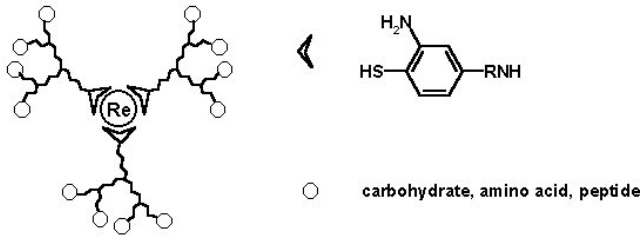

Fig. 1: Conceptual sketch of dendritic encapsulation

2-aminobenzenethiol (H_2abt) is of special interest as chelating unit in view of this synthetic procedure. The formation of a stable 3:1 complex of H_2abt with rhenium(VI) having a pre-organized globular structure /2/ give the reason for that.
Different spectroscopic methods are mainly applied for the evaluation of shielding effects caused by the dendritic encapsulation /3/. To the best of our knowledge, time-resolved laser-induced fluorescence spectroscopy (TRLFS) has not yet been used for this purpose. Due to the short fluorescence lifetime of the organic ligand spectra were recorded using a fs-laser system as excitation source and an intensified CCD-camera with a time resolution up to 25 ps /4/. We want to report on the characterization of H_2abt and $Re(abt)_3$ by TRLFS.

Results and Discussion

H_2abt was purchased from Merck-Schuchardt. $Re(abt)_3$ was prepared according to the procedure described by Danapoulus /5/.

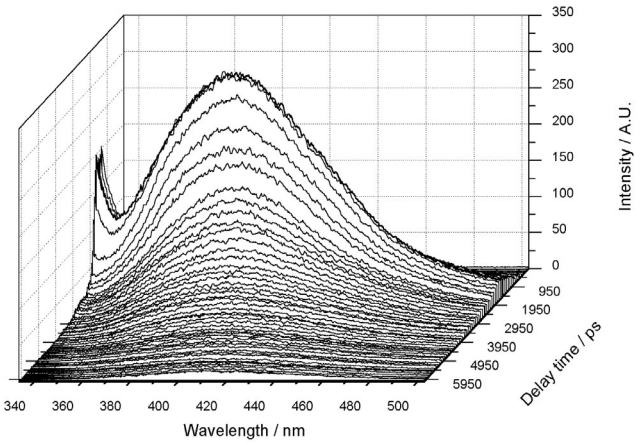

Fig. 2: Time resolved fluorescence spectrum of the H_2abt in ethanol

Fig. 2 shows the TRLFS-spectrum of the pure ligand H_2abt in ethanol. The excitation wavelength was set to be 320 nm. The fluorescence lifetime was determined to be 990 ± 20 ps and the deconvolution of the spectra results in maxima at 379 and 409 nm, respectively. The fluorescence spectra of $Re(abt)_3$ complex were recorded under the same conditions. The fluorescence lifetime increases slightly to 1485 ± 15 ps. Also a shift of the two emission maxima to 384 nm and 416 nm was observed.

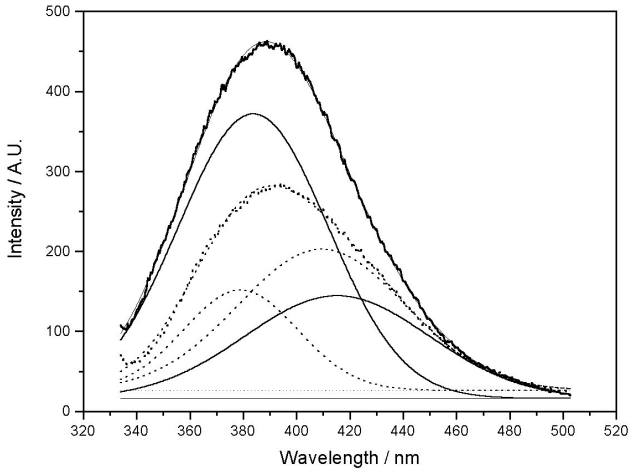

Fig. 3: Comparison of the fluorescence spectra of H_2abt and $Re(abt)_3$ in ethanol

Fig. 3 shows the overlaid spectra at 1.8 ns. The changes in the emission maxima and also in the distribution of the fluorescence intensity can be clearly detected. The higher fluorescence intensity (Fig. 3) and fluorescence lifetime of the complex leads to the conclusion that Re stabilizes the excited state.

References

/1/ Stephan, H. et al., in *„Technetium, Rhenium and other Metals in Chemistry and Nuclear Medicine“*, M. Nicolini, U. Mazzi (Eds.), SGE Editoriali, Padova, Italy, 6, 2002, 267-269
/2/ Kirmse, R. et. al., Inorg. Chim. Acta **45,** L251-L253 (1980)
/3/ Hecht, S., Frechet, J. M. J., Angew. Chem. **113,** 77-94 (2001)
/4/ Geipel, G., Report FZR-343 (2002) p.7
/5/ Danopoulos, A.A. et al., J. Chem. Soc. Dalton Trans. (1990) 315-331

EXAFS STUDIES OF TECHNETIUM AND RHENIUM COMPLEXES WITH THE METAL AT OXIDATION STATES III AND I

J.-U. Kuenstler[1], S. Seifert[1], H.-J. Pietzsch[1], C. Hennig, A. Roßberg, B. Johannsen[1]
[1] Institut für Bioanorganische und Radiopharmazeutische Chemie

Structural parameters of Tc(III) complexes and of the tricarbonyl Tc(I) and Re(I) aqua ions which are available only in solution were determined by EXAFS.

Introduction

EXAFS studies were performed at Tc(III) /1/ and Tc(I)/Re(I) /2/ complexes. Studies of EXAFS analyses at **Tc1** and **Tc2** as prototypic representatives of a novel class of Tc(III) compounds will be compared with results of single-crystal X-ray diffraction analyses. The detection of non-coordinated carbon atoms of the chelate ligand should be studied.
Structural parameters of the metal(I) precursor complexes **Tc3** and **Re1** which are available only in aqueous solution were determined by EXAFS measurements.

Results and Discussion

The studies were carried out using ^{99}Tc and $^{185/187}$Re compounds (Fig. 1) at the Rossendorf Beamline, ESRF, France /3/. We applied Tc K-edge (21.044 keV) and Re L_{III}-edge (10.535 keV) EXAFS measurements (transmission mode, room temperature, two or three scans averaged; **Tc1**, **Tc2**: solid, each sample contained 4 mg metal pressed into Teflon powder; **Tc3**, **Re1**: concentration = 0.01 to 0.02 M, 2 cm sample thickness). The data were evaluated using the EXAFSPAK software. Effective scattering amplitude and wave phase-shift functions were calculated using FEFF6. To get a satisfactory evaluation of the EXAFS spectra, multiple-scattering paths along the isocyanide and the carbon monoxide group were taken into account.

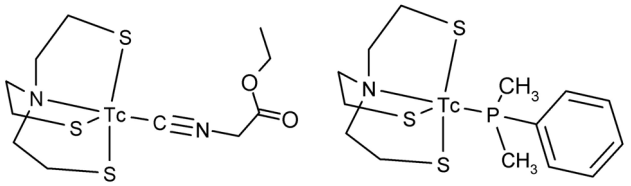

Tc1

Tc2

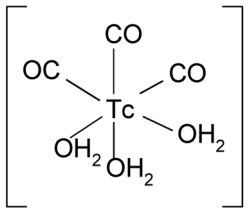

Tc3

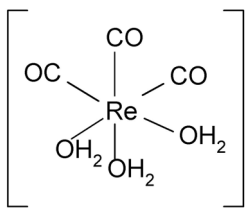

Re1

Fig. 1: Complexes studied by EXAFS

For **Tc1** atomic distances of 2.22 Å (averaged distances for Tc-N and Tc-S), 1.94 Å (Tc-C_{CN}) and 3.13 Å (Tc-N_{CN}) were estimated. For the six carbon atoms included in the chelate system a Tc-C distance of 3.12 Å and a coordination number of 5.3 with a high standard deviation of ± 1.7 was obtained. For **Tc2** atomic distances of 2.24 Å (averaged distances for Tc-N and Tc-S), 2.31 Å (Tc-P) and 3.19 Å (Tc-C, averaged value for six carbon atoms of the chelate system and two carbon atoms bound to phosphorous) were estimated. For the carbon coordination shell a coordination number of 7.4 was obtained but also with a high standard deviation of ± 1.6. The estimated distances and coordination numbers for **Tc1** and **Tc2** are consistent with the data from X-ray crystal-structure analyses. The difference between the bond distances Tc-N and Tc-S obtained from X-ray crystal-structure data is distinct smaller than the expected resolution in distance of the EXAFS analysis, therefore only an averaged value was obtained.
The estimated atomic distances for **Tc3** are 1.89 Å (Tc-C), 2.21 Å (Tc-O_{aq}) and 3.05 Å (Tc-O_{CO}) and for **Re1** 1.91 Å (Tc-C), 2.19 Å (Tc-O_{aq}) and 3.07 Å (Tc-O_{CO}). Thus no differences between the atomic distances of the analogous complexes were observed assuming an uncertainty of ± 0.02 Å. The estimated coordination numbers agree with the expected values.

Structural parameters were successfully determined by EXAFS but also limitations of the EXAFS analysis were shown.

References

/1/ Pietzsch, H.-J. et al., Bioconj. Chem. **12**, 538-544 (2001)
/2/ Alberto, R. et al., Coord. Chem. Rev. **190-192**, 901-919 (1999)
/3/ Matz, W. et al., J. Synchrotron Rad. **6**, 1076-1085 (1999)

Interaction of Actinides / Radionuclides with Solid Phases

DETECTION OF ADSORBED U(VI) SURFACE SPECIES ON MUSCOVITE WITH TRLFS

T. Arnold, G. Geipel, V. Brendler, G. Bernhard

Spectroscopic evidence for two adsorbed uranium(VI) surface species on edge surfaces of a muscovite platelet were obtained by Time resolved Laser induced Fluorescence Spectroscopy (TRLFS). In contrast, no fluorescence signal was obtained on the basal plane surfaces clearly indicating that U(VI) sorption on muscovite predominantly takes place at the edge surfaces.

Experimental

TRLFS was used to study the sorption of U(VI) on the sheet silicate muscovite. Muscovite platelets were used as sample specimens to simultaneously investigate the uranium(VI) sorption on basal plane surfaces as well as on edge surfaces. For this purpose, muscovite platelets of approximately 1 cm^2 and 5 mm height were immersed in 0.1 N $NaClO_4$ solution, and a pH of about 6,3 was adjusted. The sorption experiment was then conducted as described in /1/. The pH was readjusted every day until it was stable. Then a certain amount uranyl(VI) was added to set the total uranium(VI) concentration in solution to 1×10^{-5} M. A contact time of 60 h to ensure complete uranium(VI) sorption was applied. Then the final pH was measured and the uranium concentration in solution was determined by ICP-MS. The results are given in Tab.1.

sample	final pH	U adsorbed on muscovite platelet [%]
Muscovite platelet in contact with 1×10^{-5} M U(VI)	6,33	72,56

Tab. 1: Uranium(VI) sorption on muscovite platelet in contact with 1×10^{-5} M U(VI)

TRLFS measurements, shown in Fig. 1, in solution, on basal plane surfaces, and on edge surfaces of the muscovite platelets were carried out.

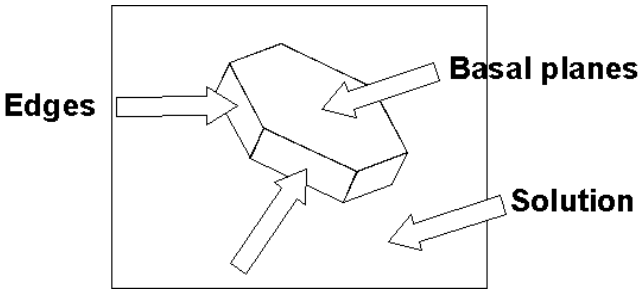

Fig. 1: TRLFS measurements were conducted in the surrounding solution, on the basal plane surfaces, and on the edge surfaces of muscovite platelets.

Results and Discussion

TRLFS Spectra of the solution, in which the platelets were immersed, showed a spectra which is typical for the remaining U(VI) concentration in solution, confirming the results from the ICP-MS analyses.
The spectra of the basal plane surfaces showed no U(VI) fluorescence signal at all, clearly indicating that U(VI) does not adsorb on the basal plane surfaces of muscovite. However, Uranium(VI) adsorbs on the edge surfaces of the muscovite platelets. The TRLFS spectrum of the adsorbed U(VI) surface species on muscovite edge surfaces is shown in Fig. 2.

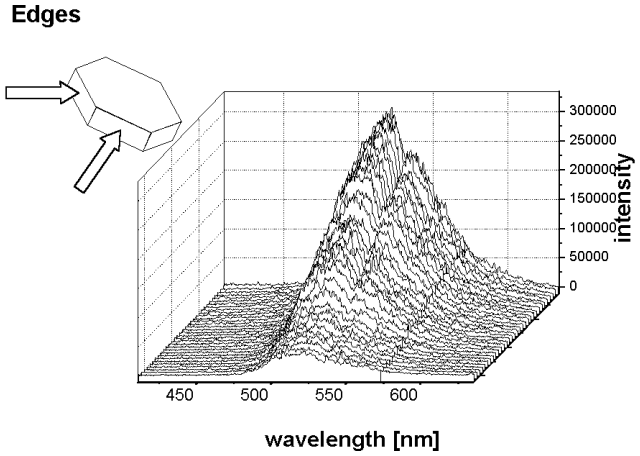

Fig. 2: TRLFS of U(VI) sorbed on the edge surfaces of muscovite platelets.

The spectrum was deconvoluted. It is best described with two surface species with different fluorescence life times. Specie 1 has a fluorescence life time of 1,15 µs and species 2 a distinctively greater one of 9,65 µs. The emission bands and lifetimes of the fluorescence signal of the adsorbed U(VI) edge surface species are shown in Tab. 2.

Species	lifetimes [ns]	peak center				
1	1150±20	502,87	522,1	545,39	569,18	596,37
2	9650±50	502,13	521,65	545,24	569,81	599,39

Tab. 2: Life times and emissions bands of the two U(VI) surface species detected on the edge surfaces of muscovite platelets.

Since the positions of emission peaks are very similar it can be concluded that the two U(VI) edge surface species on muscovite are quite similar in their chemical environment. They are probably only distinguished by their number of surrounding water molecules. Our findings show that, in respect to U(VI) sorption reactions on muscovite, the edge surfaces are by far more reactive than the basal plane surfaces. This is in agreement with the growth and dissolution behavior of muscovite.

Acknowledgements

C. Berger is thanked for sample preparation and U. Schaefer for ICP-MS analyses.

References

/1/ Arnold, T. et al., Journal of Contaminant Hydrology **47**, 219-231 (2001)

SORPTION OF U(VI) AND CALCULATION OF SURFACE SITES ON DISSOLVING CHLORITE DURING THE MIXED-FLOW EXPERIMENTS

E. Krawczyk-Bärsch, T. Arnold, N. Schmeißer[1], G. Bernhard
[1] Experimental Facilities and Information Technology

In mixed-flow experiments the sorption of U(VI) on a dissolving chlorite can be described by two different sorption sites. The first site is attributed to a surface site on the chlorite which is occupied after 138 hours of our experiment. The continuously retardation of U(VI) indicates an additional process, which can be refer to newly formed ferrihydrite as a second sorption site.

Introduction

During the dissolution of an iron-rich chlorite the major cations Al, Fe, Mg and Si are released into the aqueous solution leaving an altered chlorite mineral which eventually transformed to vermiculite. Depending on the pH of the solution new Fe-minerals, in particular ferrihydrite, precipitate from solution at pH > 5. Ferrihydrite forms coatings on the chlorite edges as well as colloids in the aqueous solution /1/. It is an important sorbent for U(VI) due to its very high specific surface area and its high affinity to bind heavy metals.

During sorption experiments of U(VI) on dissolving chlorite U(VI) is fixed to both chlorite and newly forming ferrihydrite. In this study, mixed-flow experiments with U(VI) are carried out to determine the sorption capacity and the number of occupied sorption sites on the dissolving chlorite.

Experimental

The iron-rich chlorite we used for the experiments was a ripidolite chlorite (CCa-2) from Flagstaff Hill (El Dorado County, California, USA), which we obtained from the Source Clays Repository of the Clay Minerals Society. The chemical formula of the chlorite can be described as follow /2/:

$$(Mg_{5.5}Al_{2.48}Fe^{2+}_{3.02}Fe^{3+}_{0.94})[(Si5.33Al_{2.66})O_{20}](OH)_{16}$$

Half a gram of the chlorite (63-200 µm grain size) was kept between two membrane filters in the mixed-flow reactor, while a $NaClO_4$-solution with an initial U(VI)-concentration of $1 \cdot 10^{-6}$ M was pumped through the reactor at 0.35 ml per minute. The experiments were performed at room temperature, and under oxic condition. An ionic strength of 0.1 M was used to approximate natural weathering conditions. The reacted solution samples were analyzed for U using ICP/MS and AAS, and a final pH of 6.5 was measured.

Results and discussion

Based on the specific surface area for chlorite, which we determined as 1,1 m^2/g, and the surface site density of 1,45 sites/nm^2 /3/ the available reactive sites on chlorite were determined to be $1{,}324 \cdot 10^{-6}$ M. According to EXAFS investigations U(VI) is sorbed on chlorite as a bidentate surface complex /4/. For this case two moles sorption sites bind one mol U(VI). That means 0.5 g chlorite should adsorb $6{,}617 \cdot 10^{-7}$ M U(VI).

In mixed-flow experiments we achieved the experimental data of the sorbed U(VI) on chlorite during the experiment, which are shown in Fig. 1 together with the fitted sorption curve. Our calculation revealed that $7{,}48 \cdot 10^{-7}$ moles of U(VI) were sorbed on the chlorite during the whole experiment. In Fig. 1 this sorption process is described as "sorption site I" during the first 138 hours. Although the available reactive sites of chlorite are occupied U(VI) is continuously sorbed in our experiment. This indicates that an additional process must have taken place, which created additional U(VI) sorption sites during the dissolution of chlorite.

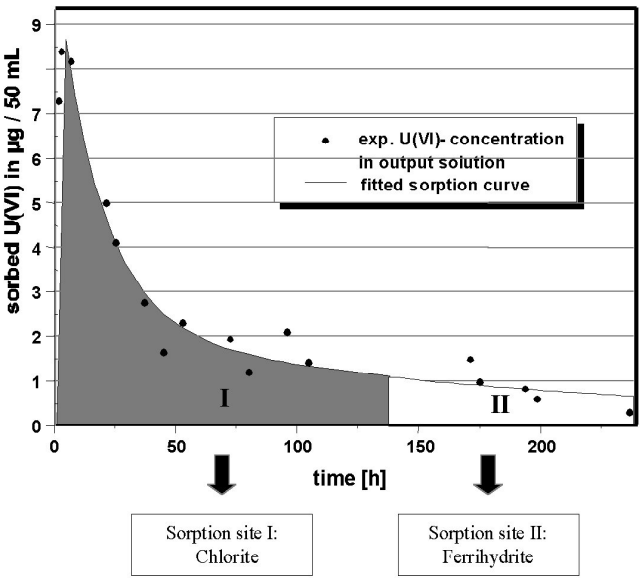

Fig. 1: Sorption of U(VI) during mixed-flow experiments with chlorite (CCa-2) in a 0.1 M $NaClO_4$-solution and an initial U(VI) concentration of $1 \cdot 10^{-6}$ M

Due to previous studies /1/, where the formation of ferrihydrite was determined, we conclude that the additional process refers to ferrihydrite particles, which are forming during the dissolution of chlorite. U(VI) is sorbed on ferrihydrite in our experiment as described in Fig. 1 as "sorption site II".

Acknowledgment

This work was supported by DFG (BE 2234/4-2).

References

/1/ Krawczyk-Bärsch et al., Applied Geochemistry (submitted, 2003)
/2/ Brandt, F. et al., Geochimica et Cosmo-chimica Acta (accepted for publication, 2003)
/3/ Arnold, T. et al., J. Contam. Hydrol. **47**, 219-231 (2001)
/4/ Arnold, T. et al. (in preparation)

SORPTION OF URANIUM(VI) ON FERROUS CHLORITE - EXAFS INVESTIGATIONS

M. Walter, E. Krawczyk-Bärsch, T. Arnold, G. Bernhard

Under oxidizing conditions uranium(VI) sorbs on ferrous chlorite as U(VI) inner–sphere surface complex. There are no spectral information, which would indicate a preferred uranium(VI) adsorption on specific chlorite of ferrihydrite surface sites.

Ferrous chlorite minerals are major constituents of phyllite rocks, a main component of uranium tailings in Saxony/Thuringia. Weathering of ferrous chlorite leads to a release of iron, followed by precipitation as ferrihydrite /1/. The aim of this study was to obtain structural information about the influence of ferric iron precipitates on the sorption mechanism of uranium(VI) in the chlorite system.

Experimental

Samples for EXAFS analyses were prepared under air using 200 mg of ferrous chlorite (grain size 2-6.3 µm, $(Mg_{5.5}Al_{2.48}Fe^{2+}_{3.02}Fe^{3+}_{0.94})[(Si_{5.33}Al_{2.66})O_{20}(OH)_{16}]$) /2/ from Flagstaff Hill, California, dispersed in 1000 ml of 0.01 N $NaClO_4$ solution. The initial U(VI) concentrations were set to $1x10^{-5}$ M at pH 6.5. The U(VI) was added to one sample immediately, and furthermore, two samples were altered 2 and 5 months in 0.01 N $NaClO_4$ solutions before U(VI) sorption occurred. In addition, one chlorite sample was altered 5 months under N_2 –atmosphere in the presence of $1x10^{-5}$ M U(VI). Uranium L_{III}–edge XAS spectra were recorded at room temperature in fluorescence mode at the Rossendorf beamline (ROBL) at the ESRF in Grenoble. The EXAFS oscillations were extracted and fitted using EXAFSPAK procedure. The theoretical phase shifts and backscattering amplitudes were calculated with FEFF8. Multiple scattering effects along the uranyl unit were included into the fit.

Results

Two axial oxygen's were found at a distance of 1.79 Å to the uranium atom. In addition, the XANES spectra of uranium sorbed on chlorite are very similar compared with the XANES spectrum of U(VI) sorbed on ferrihydrite. This indicates, that surface–catalyzed U(VI) reduction to U(IV) by the ferrous iron oxidation /3/ is *not* the dominant sorption mechanism. The uranium(VI) reduction may be prevented by preparation conditions (air, 0.01 N $NaClO_4$ solution). The low mean distance of the equatorial oxygen's of 2.34 to 2.35 Å and the high Debye-Waller factors are typical for an inner-sphere surface complexation of uranium(VI) /4/. An iron backscatterer at a distance of 3.43 Å, which is typical for a bidentate inner–sphere surface complexation /4/, is clearly found for uranium(VI) sorbed on ferrihydrite. For uranium sorbed on chlorite a uranium–iron distance of approx. 3.47 Å was observed, but the iron shell contributes less than 5 % to the EXAFS and correlates with the multiple scattering path. However, there are no unambiguously spectral information, which would suggest the uranium(VI) surface complexation on Mg, Al, Si or Fe polyhedra. On the basis of these results it was not possible to attribute the adsorbed uranium to different crystallographic sites (edges versus basal plane sites) including secondary iron sites.

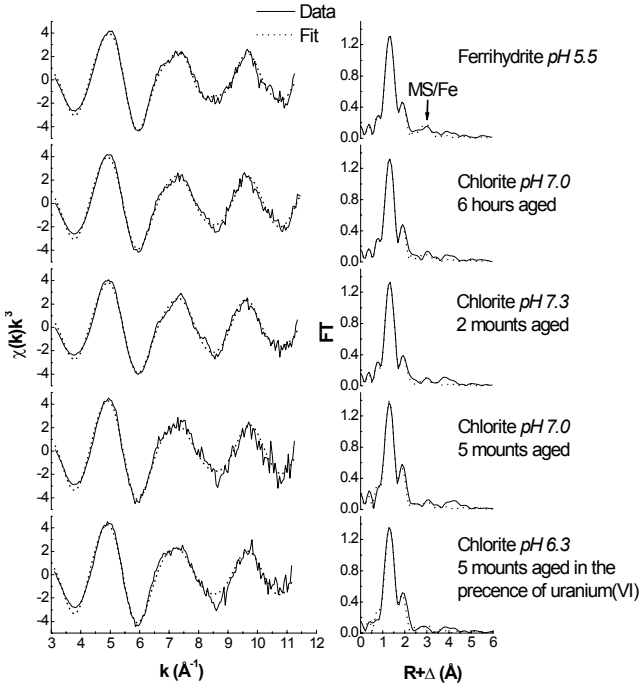

Fig. 1: $U–L_{III}$ edge EXAFS spectra and Fourier transforms of the uranium(VI) sorption samples.

U(VI) – sample	Shell	N	R (Å)	σ^2 (Å^2)	ΔE_0
Ferrihydrite *pH 5.5*	O_{ax}	2.3	1.79	0.0037	2.2
(0.1 N $NaNO_3$)	O_{eq}	4.2	2.35	0.015	
	Fe	0.8	3.43	0.010[f]	
Chlorite *pH 7.0*	O_{ax}	2.1	1.79	0.0028	0.0
6 hours aged	O_{eq}	5.3	2.34	0.018	
Chlorite *pH 7.3*	O_{ax}	1.9	1.78	0.0019	-0.6
2 months aged	O_{eq1}	2.1	2.26	0.005	
	O_{eq2}	2.3	2.44	0.005	
Chlorite *pH 7.0*	O_{ax}	2.2	1.78	0.0032	-0.7
5 months aged	O_{eq}	5.8	2.34	0.017	
Chlorite *pH 6.3*	O_{ax}	2.4	1.79	0.0042	0.5
5 months aged[*]	O_{eq}	5.3	2.35	0.017	

[f] parameter was fixed during fit

[*] 5 months aged in the presence of uranium(VI)

$\Delta N = \pm 25$ %, $\Delta R = \pm 0.02$ Å, ΔE_0 is given in eV

Tab. 1: Structural parameters of sorbed uranium(VI) surface species on ferrihydrite and chlorite.

References

/1/ Krawczyk-Bärsch, E. et al., Chem. Geol. (submitted)

/2/ Brandt, F. et al., Geochim. Cosmochim. Acta (submitted)

/3/ Liger, E. et al., Geochim. Cosmochim. Acta **63**, 2939-2955 (1999)

/4/ Reich, T. et al., J. Electron Spectros. Related Phenom. **96**, 237- 234 (1998)

IDENTIFICATION OF METAL BACKSCATTERERS IN THE EXAFS SPECTRA OF URANIUM(VI) SORBED ON FERROUS CHLORITE

M. Walter

EXAFS spectra of U(VI) sorbed on ferrous chlorite were evaluated to identify U(VI)–substrate interactions. The information concerning metal backscatterers is limited because of destructive interference effects of single scattering paths.

EXAFS spectroscopy is a well-established method to obtain structural information for a better mechanistic understanding of trace metal sorption reactions /1/. The aim of the present study was to evaluate the uranium–substrate interactions and the corresponding EXAFS information on the U(VI)–chlorite–Fe(II/III) system. Detailed experimental information are listed in /2/, this report.

Results

Three structural models were tested to fit the EXAFS spectra of uranium(VI) sorbed on ferrous chlorite. Model **A** only comprises the axial (O_{ax}) and one equatorial (O_{eq}) oxygen shell, whereas model **B** consists of O_{ax} and two equatorial (O_{eq1}, O_{eq2}) oxygen shells. In addition, model **C** comprises O_{ax}, O_{eq} and a silicon shell at approximately 2.7 Å. The Debye-Waller factor σ^2 for the silicon shell was held constant at 0.0040 Å^2 /3/. The EXAFS spectrum of uranium(VI) sorbed at pH 7.3 on two months altered chlorite as well as the fitted models **A**–**C** are shown in Fig 1.

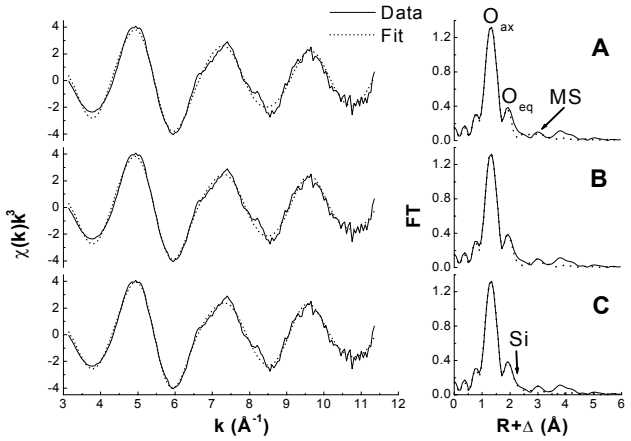

Fig. 1: U–L_{III} edge EXAFS spectra and FT of U(VI) sorbed at pH 7.3 on chlorite (two months altered before U(VI) addition).

Model	Shell	N	R (Å)	σ^2 (Å^2)	ΔE_0	Res.[1]
A	O_{ax}	2.2	1.79	0.0031	-0.6	**0.125**
	O_{eq}	5.8	2.32	0.023		
B	O_{ax}	1.9	1.78	0.0019	-0.6	**0.103**
	O_{eq1}	2.1	2.26	0.005		
	O_{eq2}	2.3	2.44	0.005		
C	O_{ax}	2.2	1.79	0.0029	-1.5	**0.082**
	O_{eq}	4.0	2.29	0.017		
	Si	0.6	2.69	0.004		

[1] residuals are given as the normalized fit error

$$\frac{\sum\left(\chi_{fit}(k)k^3-\chi_{data}(k)k^3\right)^2}{P-F}$$

P number of data points
F number of variables

$\Delta N = \pm 25$ %, $\Delta R = \pm 0.02$ Å, ΔE_0 is given in eV

Tab. 1: Structural parameters of uranium(VI) sorbed at pH 7.3 on chlorite (two months altered before U(VI) addition).

The corresponding structural parameters are listed in Tab. 1.

Model **C** gave the fit with the lowest residuals (Tab. 1), but compared with the results of model **A** both the coordination number and the distance of the equatorial oxygen shell decreased. The strong correlation of O_{eq} and Si shells can be explained by the high static disorder of the equatorial oxygen shell, which is not exactly fitted assuming a Gaussian distribution of the backscatterer. This was verified as the difference EXAFS after subtracting model **B** shows no significant features at 2.2 Å (R+Δ). Because the fitted silicon shell may include spectral information of the disordered equatorial oxygen shell, model **C** was discarded. As expected, model **B** shows lower residuals than model **A**. However, the trueness of model **B** is limited by the fit resolution of 0.19 Å.

With the exception of the multiple scattering path of the uranyl unit, no significant backscattering was observed at approx. 2.9 Å (R+Δ). Such distances would indicate a bidentate, inner–sphere surface complexation of U(VI) on metal (≡$Me(O)_2$=UO_2; Me: Mg, Al, Fe) octahedra. Assuming that U(VI) adsorbs in a bidentate coordination on Al–octahedra (50 %) as well as on Fe–octahedra (50 %), the interference of the U(VI)–Al and U(VI)–Fe single scattering paths was simulated (Fig. 2). For both single scattering paths following structural parameters were used (N_{Me}=0.5; $R_{U(VI)-Me}$=3.43 Å; $\sigma^2_{U(VI)-Me}$=0.01 Å^2; ΔE_0=0 eV) to calculate the EXAFS spectra.

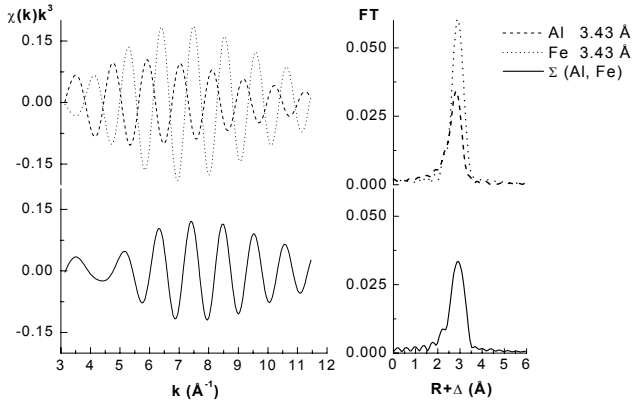

Fig. 2: Destructive interference of U(VI)–Al and U(VI)–Fe single scattering paths.

Fig. 2 shows clearly that the individual EXAFS spectra results in a *destructive* interference, which is caused by the different phase shift of U(VI)–Al and U(VI)–Fe backscattering. This allows the conclusion, that in the presence of both ≡$Al(O)_2$=UO_2 and ≡$Fe(O)_2$=UO_2 surface species the detection of the U(VI)–Me backscattering may be prevented by the decrease in amplitude.

References

/1/ Manceau, A. et al., Appl. Clay Sci. **7**, 201 (1992)
/2/ Walter, M. et al., Report FZR-373, p.17 (2003)
/3/ Reich, T. et al., Radiochim. Acta **74**, 219 (1996)

THORIUM SORPTION ONTO QUARTZ IN THE ABSENCE AND PRESENCE OF HUMIC ACID

A. Krepelová, S. Sachs, K. H. Heise, G. Bernhard

In the present work the influence of humic acid on thorium(IV) sorption onto quartz was investigated in batch experiments as a function of the pH. The results obtained were to improve the understanding of the geochemical interaction of tetravalent actinides in the environment.

Introduction

Understanding the sorption behavior of tetravalent actinides on geological materials is essential for a reliable safety assessment of nuclear waste disposal sites. The sorption behavior of actinides may be strongly influenced by HA. We investigated the influence of HA on Th sorption onto quartz as a function of the pH.

Experimental

The sorption experiments were performed under inert gas conditions (N_2), applying ^{14}C-labelled synthetic HA type M42 with a specific activity of 2.38 MBq/g. The final concentrations of Th and HA were 1.2×10^{-8}M and 20 or 60 mg/l, respectively. The solid solution ratio was 50 mg of quartz (63-200 μm grain size)/10 ml 0.1M $NaClO_4$. The pH values were in the range from pH 3 to pH 7.5. Th and HA were simultaneously added to the preconditioned mineral. The contact time was 96 hours. The samples were analyzed by LSC for the final HA concentration and by ICP-MS for the final Th concentration.

Results and discussion

Sorption of Th onto the vial walls:

Depending on the pH, Th is significantly sorbed onto polypropylene (PP) tubes. The amount of Th sorbed onto the vial walls increases with the pH to a maximum of 75% at pH 7, then it decreases. The results show that Th sorption on PP tubes competes with sorption on quartz. In this case wall sorption is higher than sorption on quartz. The presence of HA influences Th sorption on the walls. The percentage of Th sorbed onto the vial walls decreases to the amount of 15%.

Sorption of HA onto quartz:

The HA sorption onto quartz depends on the pH (Fig. 1). With increasing pH value, the sorption decreases. These results correspond to the properties of quartz and HA. Quartz has a low point of zero charge so that the surface species in the pH range studied are generally negatively charged. HA sorption behavior can be characterized by cation-like sorption at low pH values (high sorption) and anion-like behavior at higher pH values. The sorption of negatively charged HA species is thus blocked due to electrostatic repulsion.

Sorption of Th onto quartz:

The Th sorption onto quartz is affected by HA (Fig. 2). The sorption curve can be divided into two parts. In the first pH region between pH 3 and pH 4.5 Th sorption in the system with HA is higher than in the HA-free system. This enhancement is a result of the overcompensation of the number of mineral binding sites blocked by sorbed HA. Additional binding site for thorium ions thus stem from HA itself. The Th uptake decreases with increasing pH value.

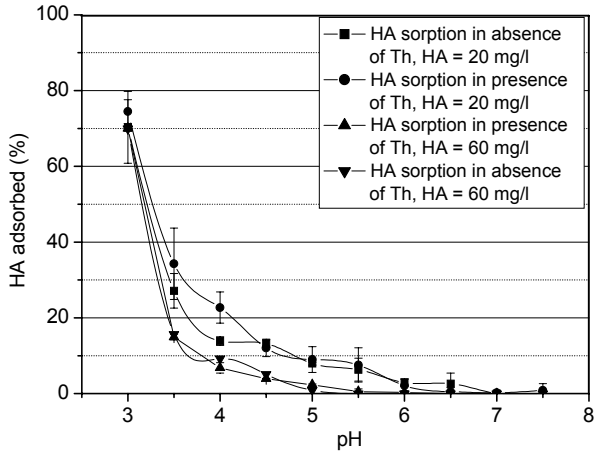

Fig. 1: HA uptake by quartz

This could be caused either by the progressive desorption of HA from the quartz surface, leading to the complexation of Th in solution, or by an increase in the complexing strength of HA. In the second pH region between pH 4.5 and pH 7.5 Th sorption in the HA-free system is very low. The reason for that is the above-mentioned high Th sorption onto the vial walls at alkaline pH values. Contrary to expectations Th sorption in the binary system is lower than in the system with HA, which can also be explained by the high wall sorption of Th in the absence of HA.

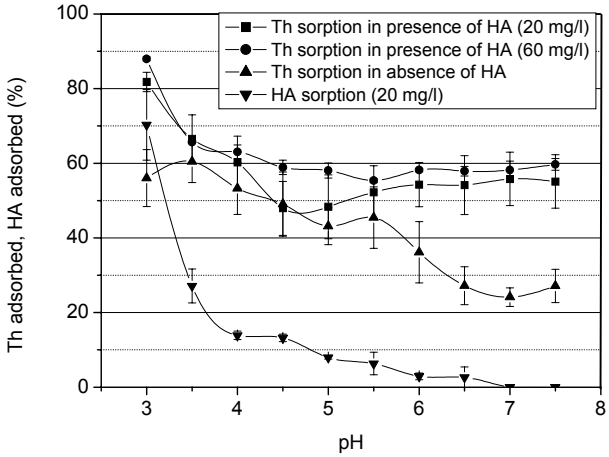

Fig. 2: Thorium uptake by quartz

Acknowledgment

This work was supported by BMWA (No. 02E9299).

References

/1/ Schmeide, K. et al., Radiochim. Acta **88**, 723 (2000)

/2/ Reiler, P. et al., 2nd Technical Progress Report, FZKA – 6324, Karlsruhe, p. 82 (1999)

/3/ Reiler, P. et al., 3rd Technical Progress Report, FZKA – 6524, Karlsruhe, p. 133 (2000)

/4/ Murphy, R.J. et al., Colloids and Surfaces **A 157**, 47 (1997)

AN EXAFS STUDY OF THE SORPTION OF AMERICIUM(III) ONTO SMECTITE AND KAOLINITE

Th. Stumpf, C. Hennig, A. Bauer[1], Th. Fanghänel[1]
[1]Forschungszentrum Karlsruhe, Institut für Nukleare Entsorgung, Karlsruhe, Germany

The surface sorption process of Am(III) onto smectite and kaolinite at different pH was investigated by X-ray absorption fine structure (XAFS) spectroscopy. At low pH Am(III) is sorbed onto smectite as an outer-sphere complex and retains its complete primary hydration sphere. With increasing pH, inner-sphere adsorption onto kaolinite and smectite occurs.

Sorption to mineral surfaces is a major process controlling the concentration, mobility and bioavailability of radionuclides in nature. Oxides and clay minerals are the main constituents in the groundwater and soil systems and therefore they are responsible for metal ion sorption. In nuclear waste repositories clays are used as backfill material (technical barrier). Consequently it is essential for the long-term performance assessment of nuclear waste repositories to know about the interactions of actinide ions with clay minerals. Therefore it is necessary to identify the surface species that are formed during the sorption process. For this purpose, the sorption process of a trivalent actinide ion onto smectite and kaolinite was studied by X-ray absorption fine structure (XAFS) spectroscopy, as a function of pH.

Previous time-resolved fluorescence spectroscopy studies with Cm(III) showed that at pH values < 5 Cm(III) is sorbed onto smectite as an outer-sphere complex. At higher pH (> 5) Cm(III) inner-sphere surface complexation onto smectite, kaolinite and γ-alumina occurs via the aluminol sites. Cm^{3+} is hydrated by 9 water molecules whereas the Cm(III)/clay inner-sphere complexes above pH 5 have five water molecules in the first coordination shell /1/.

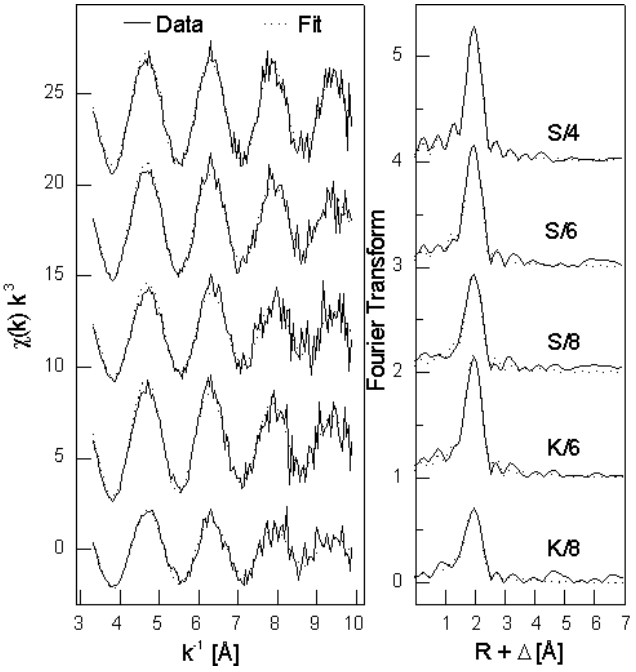

Fig. 1: Am(III) sorbed onto smectite (S) and kaolinite (K) at different pH; L_{III}-edge k^3-weighted EXAFS spectra and corresponding Fourier transforms. (Solid line - experiment; dashed line - theoretical fit.).

The EXAFS spectra and the corresponding Fourier transforms of Am(III) sorbed onto smectite and kaolinite at different pH are shown in Fig. 1. In all Fourier transformed spectra one peak dominates which can be attributed to an average Am/O distance composed out of Am/water and out of Am/O-mineral surface distances. Neither a further signal that could be an indication for an Am/Am distance as a consequence of Am precipitation was obtained nor a signal that could be attributed to an Am/Al distance. For the back scattering effect of the mineral surface, as it is documented by Am(III) sorption onto iron oxides /2/, aluminum seems to be too small. The EXAFS parameter derived from the spectra of Am sorbed onto the clay surfaces together with values found for the Am aquo ion are listed in table 1. As expected the accordance between the parameter found for the Am^{3+} aquo ion and obtained for the Am/smectite outer-sphere complex at pH 4 (S/4) is very high. As a consequence of Am/clay inner-sphere complex formation at higher pH (6, 8) a slight shortening of the Am-O distance is obtained. The small effect on the bond length indicates that only one mono- or bi-dentate bond to the mineral surface is formed. The influence of this shorter bond length on the Am-O signal is reduced by the relatively large number of water molecules in the first Am(III) coordination sphere.

With increasing pH the coordination number of the Am(III) sorbed onto kaolinite and smectite decreases. Grenthe et al. showed that the $U\text{-}O_{eq}$ coordination number is reduced from 5 to 4 with the formation of uranyl-hydroxo species. The reduction of the Am(III) coordination number with pH might be an indication for the formation of a ternary OH-/Am/clay surface complex.

1	R [Å]	N	σ^2 [Å^2]	Δ E [eV]
Am^{3+}	2.494(2)	7.0(2)	0.0058(3)	-1.8
S/4	2.486(4)	6.7(4)	0.0047(6)	-2.1
S/6	2.480(5)	7.5(4)	0.0074(6)	-2.5
S/8	2.475(7)	6.3(5)	0.008(1)	-2.0
K/6	2.487(5)	7.8(5)	0.0077(7)	-2.0
K/8	2.479(6)	5.5(4)	0.0097(9)	-1.7

Tab. 1: EXAFS parameter of the Am(III) aquo ion and the Am(III)/clay sorption samples.

References

/1/ Stumpf, T. et al., Environ. Sci. Technol., **35**, 3691 (2001)
/2/ Stumpf, S. et al., Radiochim. Acta submitted
/3/ Moll, H. et al., Radiochim. Acta **88,** 411 (2000)

UPTAKE OF TRIVALENT ACTINIDES (CM(III)) BY CALCIUM SILICATE HYDRATES: A TIME-RESOLVED LASER FLUORESCENCE SPECTROSCOPY (TRLFS) STUDY

Th. Stumpf, J. Tits[1], Th. Fanghänel[2]
[1]Paul Scherrer Institute, Waste Management Laboratory, Villigen, Switzerland
[2]Forschungszentrum Karlsruhe, Institut für Nukleare Entsorgung, Karlsruhe, Germany

The interaction of Cm(III) with calcium silicate hydrates (CSH phases) at pH 13.3 has been investigated by TRLFS. Two different types of sorbed Cm(III) species have been identified. A structural model for Cm(III) incorporation in CSH phases is proposed based on the substitution for Ca(II) at two different types of sites in the CSH structure /1/.

Cementitious materials are commonly used worldwide in immobilization strategies for radioactive waste. In a repository for radioactive waste, the immobilization of radionuclides by cementitious materials takes place both in the waste containers and in the construction materials, such as backfill, liners etc. A mechanistic understanding of the chemical processes by which radionuclides are immobilized in cement-based matrices is important for long-term predictions of the performance of disposal sites for hazardous waste and repositories for radioactive waste. Calcium silicate hydrates (CSH phases) are considered to be among the most important cement phases governing immobilization processes, because of their abundance and appropriate structures for cation and anion binding.

Selected fluorescence emission spectra of Cm(III) ($1x10^{-7}$ M) in CSH suspension ($5.0 \cdot 10^{-5}$ kg L^{-1}) measured at different contact times are shown in Fig. 1. Three different peak maxima at 606.0 nm, 618.9 nm and at 620.9 nm appear in the spectra.

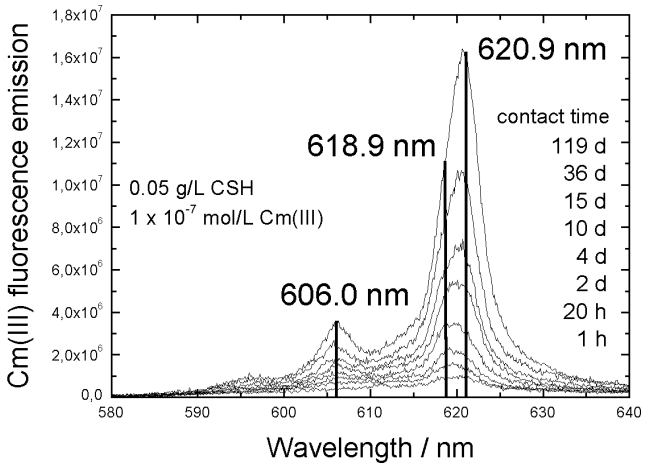

Fig. 1: Fluorescence emission spectra of 10^{-7} M Cm(III) in CSH suspension (0.05 g L^{-1}) measured at different Cm(III)/CSH contact times

A Cm(III) emission spectrum of a system containing Cm(III) and CSH was recorded at a temperature of 20 K and compared with spectra of the same system obtained at 298 K. The peak at 606.0 nm was not detected in the spectrum at 20 K. Hence, this peak is the result of visible transitions of thermally populated states at room temperature and has no chemical relevance. From all measured spectra (obtained after different equilibration times and different S:L ratios) the contributions of the pure components were calculated using an eigenvector analysis /2/. From this, two different fluorescing Cm(III) species sorbed onto CSH were identified with peak maxima at 618.9 nm (F1) and 620.9 nm (F2). The lifetimes of F1 and F2 were determined to be $\tau = 289 \pm 11$ µs and $\tau = 1482 \pm 200$ µs, respectively. According to the correlation of the fluorescence emission lifetime with the number of water molecules in the first Cm(III) coordination sphere which was found by Kimura et al. /3/ a lifetime of 298 ± 11 µs corresponds to 1.4 water molecules in the first coordination shell of the Cm(III) F1 complex, whereas a lifetime of 1482 ± 200 µs indicates the total loss of the hydration sphere of the Cm(III) F2 complex.

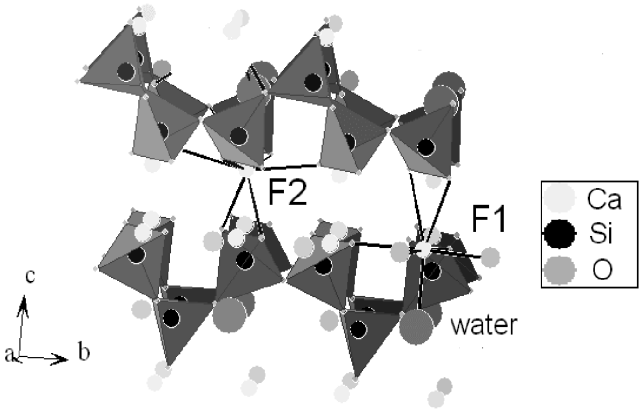

Fig. 2: A three dimensional view of the tobermorite structure. Cm(III) substitute for two types of Ca(II) with different coordination

A structural model for Cm(III) incorporation into CSH phases was developed based on a defect 11 Å Tobermorite structure. It consists of layers of Ca octahedral linked by non-bridging oxygens to chains of silicate tetrahedral on either side, forming Ca-silicate layers. Thus, the Tobermorite structure contains Ca atoms at two different types of sites: In the first type Ca is coordinated by 6 oxygen atoms from Si tetraedra and one oxygen from H_2O, in the second type of sites Ca is coordinated by 7 oxygen atoms originating from Si tetraedra. The fluorescing Cm(III) species F1 corresponds to Cm(III) substituting Ca bound in the type 1 sites of the Ca octahedral layers, whereas the fluorescing Cm(III) species, F2, can be interpreted as being a Cm(III) substituting for Ca in the type 2 sites of the Ca octahedral layers.

References

/1/ Stumpf, T. et al., Environ. Sci. Technol. submitted
/2/ Roßberg, A., Ph.D. Thesis, TU Dresden (2002)
/3/ Kimura, T. et al., J. Alloys Comp. **213/214**, 313-317 (1994)

THE SORPTION OF AM(III) ONTO FERRIHYDRITE AND ONTO ITS ALTERATION PRODUCTS: INVESTIGATIONS BY EXAFS

S. Stumpf[1], Th. Stumpf, C. Hennig, Th. Fanghänel[1], J.I. Kim[1]
[1]Forschungszentrum Karlsruhe, Institut für Nukleare Entsorgung, Karlsruhe, Germany

The sorption of americium onto ferrihydrite was investigated by EXAFS measurements at pH 5.5 and 8. The fourier transforms of the EXAFS spectra show two peaks that can be attributed to Am-O and Am-Fe shells. The found distances indicate an inner sphere, bidentate coordination of Am(III) onto ferrihydrite also after heating the samples and transformation of ferrihydrite to goethite.

Hydrous iron oxides (ferrihydrite) are of great importance in the environment. Ferrihydrite is able to dominate the retardation of radionuclides in particular the actinides in the near-field as well as in the far-field of a nuclear waste repository /1/. Upon heating pure ferrihydrite converts to crystalline goethite and hematite. This EXAFS study deals with the question if Am(III) can be immobilized by sorption onto ferrihydrite. Furthermore the interaction of Am(III) with the mineral surface after a thermal treatment is studied.

Fig. 1 shows the EXAFS spectra of Am(III) sorbed onto ferrihydrite and the appropriate fourier transform at pH 5.5 and pH 8 (Am2-1, Am2-2). The first peak can be attributed to a Am-O distance of 2.48 Å and agrees with the value cited in literature /2/. This distance is comparable to the bond length that can be found for the Am^{3+} aquo ion determined either in transmission (Am1-6) or fluorescence (Am2-7) (Tab.1). Moreover there is no significant change in the coordination number. Obviously the number of coordinating water overbalances the coordination by the substrate. The second peak can be attributed to a Am-Fe distance of 3.78 Å. This bond length indicates an inner sphere, bidentate coordination of Am(III) onto ferrihydrite. There is no peak that can be attributed to a Am-Am distance. Therefore Am(III) did not precipitate.

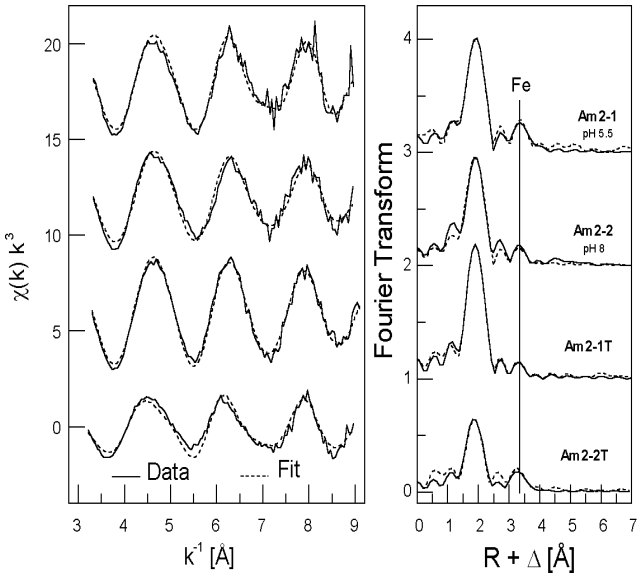

Fig. 1: k^3- weighted EXAFS spectra and the according fourier transformed spectra of the Am / ferrihydrite sorption samples before (Am2-1/2) and after the transformation (Am2-1T/2T) at pH 5.5 and 8.

The EXAFS samples were heated in a water bath at 85°C for 67 days. The transformation product goethite was characterized by TEM (Fig.2) and IR.

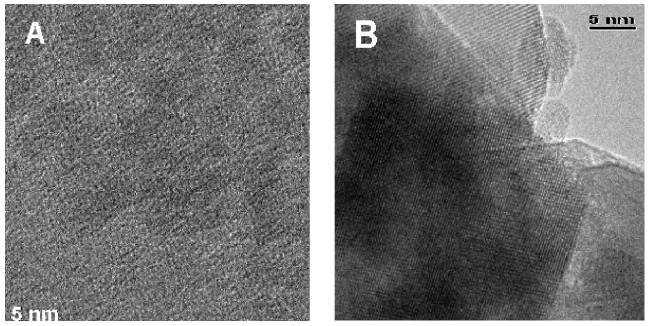

Fig. 2: TEM spectra of A) not altered and B) altered ferrihydrite samples at pH 8

The fourier transform of the EXAFS spectra at pH 5.5 and pH 8 are also shown in Fig. 1 (Am2-1T, Am2-2T). There is no increase of the Am-Fe peak intensity. Therefore we can conclude that Am is not incorporated after transformation but still surface coordinated.

Sample	Shell	R [Å][a]	N[b]	σ^2 [Å^2][c]
Am1-6	Am-O	2.494(2)	7.8(2)	0.0075(2)
Am2-7	Am-O	2.494(2)	7.0(2)	0.0058(3)
Am2-1	Am-O	2.489(6)	6.2(4)	0.0077(8)
	Am-Fe	3.78(3)	1	0.004(2)
Am2-2	Am-O	2.480(5)	6.0(4)	0.0080(7)
	Am-Fe	3.79(2)	1	0.010(2)
Am2-1T	Am-O	2.486(2)	6.7(2)	0.0063(4)
	Am-Fe	3.80(5)	0.5(2)	0.008
Am2-2T	Am-O	2.477(6)	3.5(2)	0.0053(8)
	Am-Fe	3.74(3)	1.2(2)	0.008

Tab. 1: EXAFS parameter of the Am(III) aquo ion (Am1-6, Am2-7) and the Am(III)/ferrihydrite sorption samples

References

/1/ Jambor, J.L., Dutrizac, J.E., Chem. Rev. **98**, 2549-2585 (1998)
/2/ Allen, P.G. et al,. Inorg.Chem. **2000**, 595

TIME-RESOLVED LASER FLUORESCENCE SPECTROSCOPY (TRLFS): INVESTIGATIONS OF THE SORPTION OF CM(III) ONTO FELDSPARS

S. Stumpf[1], Th. Stumpf, T. Arnold, Th. Fanghänel[1], J.I. Kim[1]
[1]Forschungszentrum Karlsruhe, Institut für Nukleare Entsorgung, Karlsruhe, Germany

The sorption of curium onto feldspars (albite, orthoklas) was investigated by TRLFS in the trace concentration range. Two sorption species, that are identical for both feldspars, were found. The correlating lifetimes indicate a coordination of five water molecules for the sorbed Cm(III).

For the long-term performance assessment of nuclear waste repositories, knowledge concerning the interactions of actinide ions with mineral surfaces is imperative. The mobility of released radionuclides is strongly dependent on the sorption/desorption processes at mineral surfaces. Therefore, it is necessary to characterize the surface species formed and to elucidate the reaction mechanisms involved. Insight into the sorption mechanisms and identification of surface species is of cardinal importance for a reliable predictive modeling of sorption reactions. Silicates are a relevant sorption surface in the geo-sphere. Time-resolved laser fluorescence spectroscopy (TRLFS) allows due to its high fluorescence yield speciation studies of Cm(III) in the nanomolar concentration range. In this study the sorption of curium onto two different feldspars (albite= Na-feldspar; orthoklas= K-feldspar) was investigated by TRLFS measurements.
Fig. 1 shows the emission spectra of 2.5×10^{-7} mol/L Cm(III) in the presence of 0.2 g/L albite (grain size <5μm) in the pH range 3.44 to 9.42. Similar spectra are obtained for the sorption onto orthoklas.

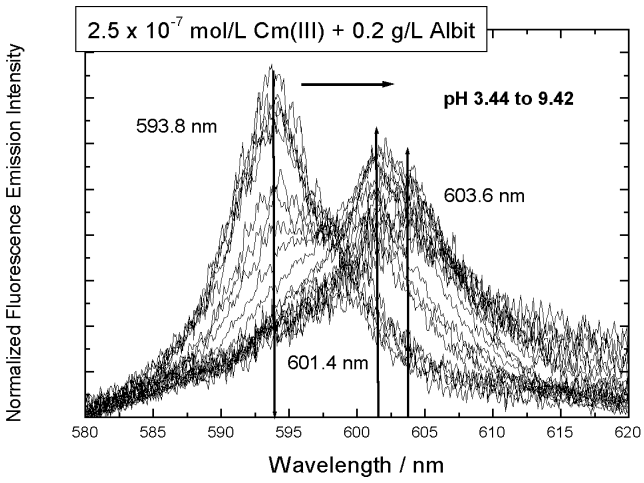

Fig. 1: Fluorescence emission spectra of Cm(III) in the presence of albite with increasing pH

With increasing pH a spectral shift of the peak maximum from 593.8 nm to 603.6 nm is observed. This indicates the sorption of Cm(IIII) onto the mineral surface. The single components (Fig. 2) and the speciation (Fig. 3) are derived by peakdeconvolution /1/. The peak at 593.8 nm corresponds to the Cm^{3+} aquo ion. The sorption species with a peak maximum at 601.4 nm and 603.6 nm are identical for both feldspars. Cm(III) begins to sorb onto albite at lower pH. This behavior can be explained by the more acidic point of zero charge of the mineral compared to the one measured for orthoklas. Lifetime measurements result in 70 ± 3 μs for the Cm^{3+} aquo ion (593.8 nm) as expected and 110 ± 3 μs for both sorption species. According to the correlation found by Kimura et al. these lifetimes indicate a coordination of 9 water molecules for the aquo ion and 5 water molecules for the sorbed species /2/.

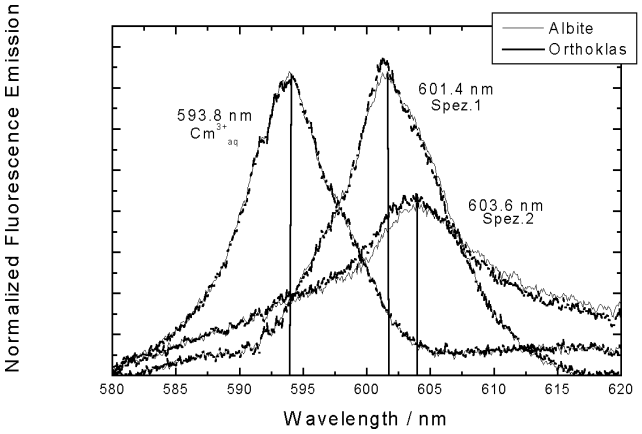

Fig. 2: Spectra of the single components for the sorption of Cm(III) onto albite and orthoklas

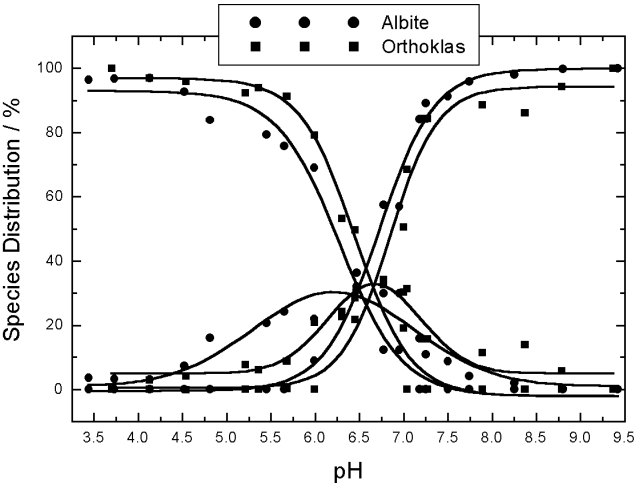

Fig. 3: Speciation plot for the sorption of Cm(III) onto albite and orthoklas

The slope analysis shows the loss of one proton for the reaction Spez.1 -> Spez.2. This can be explained by two mechanisms. 1) Spez.1 is bonded monodentat and converts to a bidentat bonding in a second step. 2) Cm(III) is sorbed as bidentat species from the beginning and Spez.2 is a ternary Cm/feldspar hydrolysis complex. Further experiments are in progress in order to identify the sorption mechanisms.

References

/1/ Roßberg, A., Ph.D. Thesis, TU Dresden (2002)
/2/ Kimura, T. et al., J. Alloys Comp. **213/214**, 313-317 (1994)

NUCLEAR WASTE REPOSITORIES AND ABANDONED MINES: A COMPARISON FROM THE POINT OF VIEW OF COLLOID-FACILITATED CONTAMINANT TRANSPORT

H. Zänker

A critical comparison of the role of colloids in contaminant transport from nuclear waste repositories and from abandoned underground mines shows that "natural analog sites" of repositories are not very representative of large-scale mines.

The colloid-facilitated transport of contaminants (radionuclides) has been investigated in the context of nuclear waste repositories for more than two decades. The scenario typically assumed in such nuclear waste related studies is the migration of radionuclides in waters of slow flow such as slowly-flowing aquifers.

Different transport conditions are encountered in flooded mines. Two distinct transport timescales have to be considered in mines /1/. First, in mines too, there are zones of relatively slow flow. These are regions of the rock matrix, the source of the contaminants. Second, shafts and drifts within the mine, which make up many per cent of the void volume in the mine, can provide fast and possibly even turbulent flow pathways to the accessible environment.

The geochemical colloid research community's attention was first called to ore deposits and mines in the context of nuclear waste repository research. Mining sites were used as natural "analog sites" and the colloids were investigated at these sites. The aim was to identify possible colloid-facilitated processes of radionuclide transport that might also be relevant for nuclear waste repositories. The best-known of these sites are the U deposit at Pocos de Caldas, Brazil, the Koongarra U deposit, Australia, the Cigar Lake U deposit, Canada, the U-Th deposit of Palmottu, Finland, the Krunkelbach mine, Germany, the El Berrocal site, Spain and the Oklo natural reactor site, Gabon. The principal aim of the colloid „analog studies" carried out at these sites was to find out if colloids are able to stimulate radionuclide transport.

In all "analog studies" colloids (size 1 nm to 1 µm) and suspended particles (size > 1 µm) were found in the mine waters. The most important constituent of these colloids and particles was amorphous iron(III) oxyhydroxide. Also amorphous Al and Si compounds often played an important role. Significant fractions of Th and the rare earth elements and varying fractions of U were adsorbed by the amorphous colloids and particles. Nevertheless, the stimulation of the transport of these trace heavy metals by the colloids or particles at the "analog sites" investigated was generally regarded as marginal. This was mainly because of the low mobility of the colloids and particles. Even immobilizing effects due to the colloids were reported.

The disadvantage of the "analog site" studies regarding the assessment of colloid-facilitated contaminant transport in large-scale mines is that sites were selected showing a groundwater hydrology as undisturbed as possible. Thus the conditions at the sampling points often more resembled those of an unaffected aquifer than those of a mine. We asked ourselves if colloid studies on dynamic systems such as mixing zones in rivers receiving acid mine drainage (AMD) or mixing zones in estuaries might be more relevant to large-scale mines than colloid studies at the "analog study" sites.

There has been a number of investigations into the behavior of colloids in such mixing zones (e.g. /2,3/). The outcome of these studies was that crystalline silicate mineral particles, though often higher concentrated in rivers than in the slow-flow waters of the "analog study" sites, could be neglected as carriers of adsorbed trace contaminants. The colloid-borne contaminants were detected almost exclusively on freshly-formed particles of Fe(III), Al and Mn(IV) oxyhydroxides or hydroxysulfates, i.e. on nondetrital material. The studies on natural mixing zone water from a river receiving AMD correspond quite well with published solubility data of Fe(III), Al and Mn(IV) oxyhydroxides and hydroxysulfates /3/. The pH dependence of trace element adsorption onto such compounds can be described by sigmoidal curves that exhibit a steep increase in the middle pH region („adsorption edges"). There is also good agreement of the mixing zone water results with published adsorption isotherms of Zn, Cu, Co, Ni, Pb and Cd on Fe(III), Al and Mn(IV) oxyhydroxides and hydroxysulfates /3/. One might speculate that organic compounds play a more pronounced role for the colloids of surface waters such as river waters than for those of groundwaters. However, for AMD-river mixing zones this is not really corroborated by the results. The adsorption isotherms of the trace contaminants at the colloids and particles can be explained without the assumption of an influence of organics /3/.

The results from AMD-river mixing zones and the experimental findings from abandoned large-scale ore mines such as the Freiberg Zn-Pb-Ag mine or the Königstein uranium mine /4,5/ are strikingly alike. This is due to the fact that a lot of processes typical of such mixing zones are also encountered in large-scale mines: the access of oxygen, rapid pH changes, rapid changes in ion concentrations, rapid redox processes, the spontaneous formation of colloids and particles, the formation of precipitates and coatings. Thus the conditions in natural mixing zones can be much more representative of large-scale mines than the exceptional mine conditions of the "natural analog sites".

References

/1/ Viswanathan, H.S., Sauter, M., Proc.10th Int. Symp. on Water-Rock Interaction, Villasimius, Italy 2001, A.A. Balkema Publishers 2001, p. 1285
/2/ B.A. Kimball et al., Appl. Geochem. **10**, 285 (1995)
/3/ Lee, G. et al., Appl. Geochem. **17**, 569 (2002)
/4/ Zänker, H. et al., Radiochim. Acta **88**, 619 (2000)
/5/ Zänker, H. et al., Coll. Surf. A, in print (2003)

CONSEQUENCES OF COLLOID BEHAVIOR FOR PERFORMANCE ASSESSMENT OF ABANDONED URANIUM MINES

H. Zänker

Whereas the influence of colloids on the transport of contaminants from nuclear waste repositories is a problem of a long-term timescale, the influence on the transport of contaminants from abandoned mines is rather a question of a months to years timescale ("first flush" of the mine).

One of the most important questions in the assessment of colloid influences on trace element transport via the water path is the question if the binding of the trace elements to the colloids is reversible or irreversible (see e.g. /1/). In flooded mines the impact of colloids on trace element transport is often rather a transport-reducing than a transport-enhancing one since the colloids scavenge and immobilize the trace elements by colloid aggregation and sedimentation /2,3/. In this context the question is whether the trace elements are captured and deposited temporarily or permanently in the drifts, galleries and shafts of the mine. It is discussed in the following for uranium(VI), the most important trace heavy metal contaminant in the Königstein uranium mine /3/.

The reaction of the colloid-borne U fraction to relatively small changes in pH and in carbonate concentration that can be concluded from /3/ indicates a reversible binding of the U(VI) to the colloids. The change of the colloid-borne U fraction caused by the acidification of „Rothschönberger Stolln“ adit water to pH values of 4 to 6 /4/ also suggests rather reversible than irreversible U(VI) binding to the colloids. The behavior of the uranium in estuaries /5/ and the $^{234}U/^{238}U$ isotope ratios on iron-rich groundwater colloids /6/, too, indicate that the U(VI) on iron-rich colloids is in a dynamic equilibrium with the truly dissolved U(VI) and not bound irreversibly. Nevertheless, XAS measurements proved that a chemical interaction between U(VI) and synthetic iron oxyhydroxides and hydroxysulfates exists, i. e. that the U(VI) is bound by inner-sphere surface complexes and not only by outer-sphere complexes /7, 8/ .

The aggregated Fe(III)/Al oxyhydroxide and hydroxysulfate colloids form deposits and coatings on the rock surfaces. The important question is if and how the trace elements such as the uranium are built in into these precipitates. It is well-known that adsorbed/co-precipitated U(VI) gradually escapes from freshly-formed iron(III) oxyhydroxide. Payne et al. /9/ found that uranium-contaminated Fe(III) oxyhydroxide released about 70% of the U to the solution in the course of precipitate aging. The remainder of the U might have been incorporated irreversibly.

However, another effect is more important. It is obvious that in the performance assessment for nuclear waste repositories only processes able to influence the state of a repository in the very long run are really important. This is different for abandoned mines. In the case of mines, a critical phase, if not *the* critical phase occurs when the flood water reaches the level where connections to unprotected surface waters or underground drinking water resources exist, i. e. where there are natural or artificial spillways to the unprotected environment. This phase is characterized by the „first flush“ of the mine /10/. Taking into consideration that pH values exist where almost 100% of the U(VI) can be attached to colloids /3/, one must assume that the scavenging and immobilization of U(VI) by colloids can influence the „first flush“ of a flooded uranium mine, even if this immobilization only lasts for few months or years. This influence is always a flattening and broadening of the „first flush“ uranium concentration profiles. It can be of relevance for the safety precautions that need to be taken during the flooding of a mine and thus, for instance, for licensing the flooding. The effect should therefore be studied more thoroughly and tried to be described (modeled) quantitatively. Currently, we prepare XAS measurements to characterize the binding of U(VI) onto mine water colloids, coatings and crusts as well as attempts at modeling the colloid influence on the “first flush”.

The situation is similar to that of U(VI) for other trace elements. There is some difference compared to U(VI) since many of the other elements are regarded as immobile in mine performance assessment and the influence of colloids can thus only be a „mobilizing“ one, not an „immobilizing“ one. Another difference is that many of these other elements show a higher tendency to adsorb irreversibly to the Fe(III)/Al colloids than does U(VI). This is for instance the case for arsenic. Furthermore, the other elements show much less tendency to form dissolved carbonate complexes than does uranium(VI) which is of importance at pH values above 6.

References

/1/ Ryan, J.N., Elimelech, M., Coll. Surf. A **107**, 1 (1996)
/2/ Zänker, H., Report FZR-373, p.24 (2003)
/3/ Zänker, H. et al., Coll. Surf. A, in print (2003)
/4/ Zänker, H. et al. Radiochim. Acta **88**, 619 (2000)
/5/ Andersson, P.S. et al., Geochim. Cosmochim. Acta **65**, 13 (2001)
/6/ Ivanovich, M. et al., CEC Symposium, Brussels 1987, 300-313; Report EUR-11037-EN (eds. B. Cöme and N. Chapman), Graham and Trotman, London 1987
/7/ Reich, T. et al., J. Electron Spectroscopy and Related Phenomena **96**, 237 (1998)
/8/ Walter, M. et al., Environ. Sci. Technol. (2003) (submitted)
/9/ Payne, T.E. et al., Radiochim. Acta **66/67**, 297 (1994)
/10/ Younger, P.L. et al., *Mine Water*, Kluwer 2002

INORGANIC COLLOIDS IN THE ELBE RIVER

K. Opel, G. Hüttig, H. Zänker

Water of the Elbe River at Dresden was investigated by centrifugation, filtration, ICP-MS, AAS, REM, EDX and photon correlation spectroscopy. It contains particles primarily consisting of clay minerals, $Al(OH)_3$, Fe and Mn oxyhydroxides as well as diatoms and organic suspended matter.

Introduction

Colloids play an important role in the migration of contaminants in the environment. In rivers they may impact the seepage behavior of contaminants below the river, the bioavailability and toxicity of the contaminants or the fate of the contaminants in mixing zones such as confluences or estuaries. The determination of their concentration, size distribution and composition in river waters is therefore of interest (see e.g. /1/). The techniques of colloid investigation used for waters from abandoned mines /2/ were also used to analyze the inorganic colloids of the Elbe River.

Experimental

Aliquots of the raw sample were centrifuged at several accelerations and filtered through Nucleopore filters of varying pore size. The filtrates and centrifugates were analyzed by ICP-MS, AAS and PCS. Particles on the filter membranes were visualized by REM and their chemical composition determined by EDX.

Results

With decreasing pore size of the filters the decay of the autocorrelation function is shifted to lower delay times (Fig. 1). A reproducible determination of the particle size by deconvolution of the autocorrelation functions is not possible because of its wide and polymodal distribution.

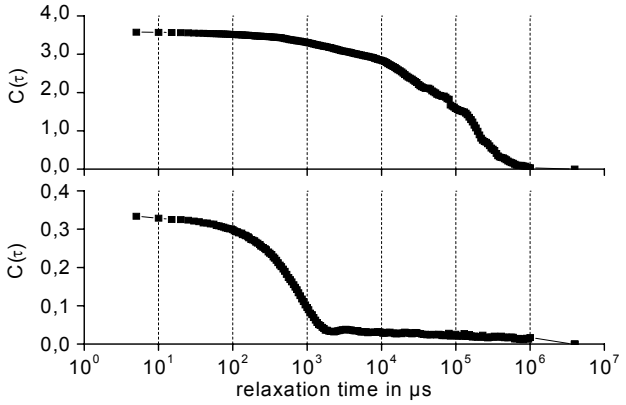

Fig. 1: Autocorrelation function of raw sample and 1 µm-filtrate

Tab. 1 shows a rough estimate of the removable particle size of various minerals as a function of the centrifugal acceleration.

Centrifugal Acceleration	d_{max}(Muscovite)/nm (ρ = 2,82 g/cm^3)	d_{max}(Goethite)/nm (ρ = 3,80 g/cm^3)
1 x g	4177	3368
13 x g	1446	1165
35 x g	867	699
110 x g	482	388
1250 x g	145	117
3500 x g	87	70
6800 x g	62	50

Tab. 1: Removable particle sizes at varying accelerations (sedimentation and centrifugation time: 1 h)

The decrease in the concentration of various colloid-forming elements with increasing centrifugal acceleration is shown in Fig. 2. More than 50% of the content of these elements is removed by gravitational sedimentation. According to the data in Table 1 the diameter of these particles exceeds the submicron range. The continued decrease in element concentration at higher accelerations proves the presence of colloids. The successive decrease in Fe, Al and Mn concentrations (for Fe from 1 x g to 6,800 x g) indicates a wide particle size distribution.

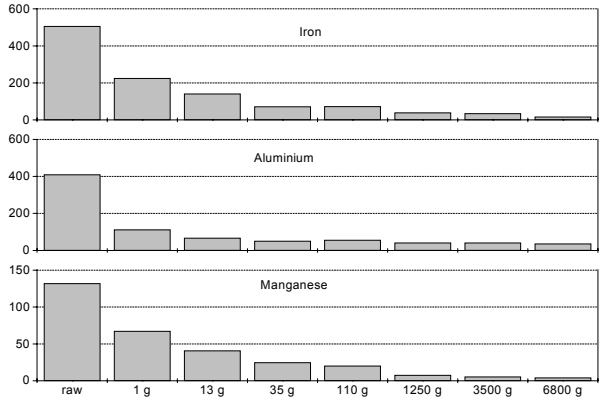

Fig. 2: Concentration of colloid-forming elements in various centrifugates (centrifugation time: 1 h)

The behavior of Fe and Al is similar to that observed in the adit water investigations in /2/. However, the behavior of Mn in the Elbe River differs from that in the adit water. In the Elbe water (pH 8.4) more than 95% of Mn is removed at 6,800 x g whereas in adit water (pH 7.2) Mn is virtually not centrifugable or filterable. This difference is due to the slightly higher pH of the Elbe River; Mn(IV) precipitation does not occur at pH values around 7 but it does at pH>8 /3/.

According to our centrifugation, filtration and EDX results (the latter two not given here), the inorganic colloids mainly consist of clay minerals, quartz and hydroxides/oxyhydroxides of Fe(III), Mn(IV) and Al(III). Their stabilization in suspension should be attributable to electrostatic effects and to organic constituents (cf. /1/) that have not been analyzed in this study. From the sedimentation behavior of the elements Fe, Al, Si and Mn (Fig. 2) at centrifugal accelerations $\geq$35 x g (the boundary at which all micron-sized particles are eliminated; cf. Tab. 1) one can conclude that the concentration of the inorganic colloids is about 200 to 400 µg/l. Thus we find a composition of the submicron particles very similar to that found in the Rhine River /1/ but a colloid concentration which exceeds it by almost one order of magnitude.

References

/1/ Perret, D. et al., Wat. Res. **28**, 91 (1994)
/2/ Zänker, H. et al., Radiochim. Acta **88**, 619 (2000)
/3/ Lee, G. et al., Appl. Geochem. **17**, 569 (2002)

MEASUREMENT OF PARTICLE GROWTH IN A FILTERED ACID ROCK DRAINAGE WATER

W. Richter, H. Zänker, G. Hüttig

Acid rock drainage (ARD) water from an abandoned ore mine was ultrafiltered and subsequently ultracentrifugated. The particle growth in this solution was observed by photon correlation spectroscopy.

Acid Rock Drainage (ARD) waters are highly mineralized, red-colored solutions which are formed by the sulfide oxidation process in ore mines. We took samples of ARD from the abandoned Zn-Pb-Ag Mine "Himmelfahrt Fundgrube" at Freiberg for colloid-chemical investigations. For details concerning the concentration, the size and the composition of the colloid particles see /1/. In new experiments we filtered the water in a stirred ultrafiltration cell from Amicon with a 1 kD YM membrane. The filtrate was ultracentrifugated for 1 h with an ultracentrifuge OPTIMA XL-100K from Beckman Coulter at a centrifugal acceleration of 200 000 x g. The centrifugates, filtrates and retentates were analyzed by ion chromatography (Jasco), ICP-MS (Elan 5000) and/or AAS (AAS 4100, Perkin Elmer). The size of the colloid particles was measured by PCS (BI-90, Brookhaven Instruments).

Results and discussion

The salt content of the water (pH 2.5) is dominated by sulfate, Mg, Fe, Zn and Mn. Tab. 1 gives selected cation and sulfate concentrations of the raw water and the filtrate (1 kD = ca. 1 nm). One can see that about 50% of the iron, 90% of the arsenic and 98% of the lead occurred as colloidal particles of > 1 nm.

Component	Concentration [Mol/L]	
	Raw water	1 kD filtrate
Mg	7.9×10^{-2}	7.6×10^{-2}
Al	4.5×10^{-2}	3.5×10^{-2}
Si	1.9×10^{-3}	1.6×10^{-3}
Ca	1.2×10^{-2}	1.0×10^{-2}
Mn	2.0×10^{-2}	nd
Fe	7.3×10^{-2}	3.3×10^{-2}
Zn	6.9×10^{-2}	nd
As	6.1×10^{-3}	5.5×10^{-4}
Pb	1.2×10^{-4}	4.9×10^{-6}
U	7.5×10^{-6}	6.0×10^{-6}
Sulfate	0.39	0.32

Tab. 1: Results of ICP-MS, AAS and Ion Chromatography on the ARD water and the filtrate

Probe	Count Rate [kcps]	Particle Size [nm]
Raw water	150	150 - 300
1kD-filtrate after 13min	16.4	1.3
after 24min	18.3	1.6
after 58min	11.8	1.5
after 97min	15.2	1.5; 150
after 138min	14.9	1.8; 160
after 177min	20.2	150 - 200
after 1d	112.8	200 - 400

Tab. 2: Results of the PCS-measurements of raw water and 1 kD-filtrate in the course of time

Tab. 2 shows the PCS results from the raw water and the 1-kD filtrate. PCS of the raw water revealed a prevailing particle size of about 150-300 nm.

In /1/ we have shown that these particles of > 100 nm contribute only little to the total colloid inventory of the ARD solution. The major colloidal component is a population of ultrafine particles of less than 5 nm in size which account for about 98 % of the total colloid mass concentration of ca. 1 g/l. However, the particles of the minor component (the > 100 nm particles) entirely govern the scattered light intensity in light scattering experiments. This is due to the r^6 dependence of the scattering intensity on the particle radius r in the particle size range of Rayleigh scattering. We succeeded in removing this perturbing colloidal component by applying a combination of ultrafiltration and subsequent ultracentrifugation. Tab. 2 shows the behavior of the BI-90 photomultiplier count rate (the scattered light intensity) of such an ultracentrifuged filtrate which is continuously increasing and reaches values comparable to that of the raw sample within one day. The change of the autocorrelation function of the scattered light fluctuations within one day is given in Fig. 1.

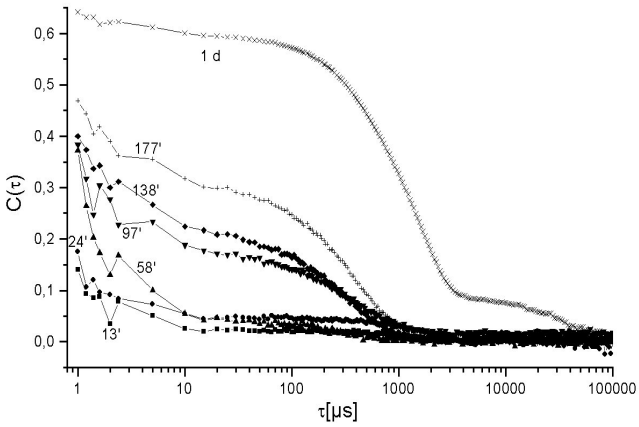

Fig. 1: Autocorrelation functions of the light scattered from the 1-kD filtrates depending from the time after centrifugation

A systematic shift toward higher relaxation times is visible in this figure. After 1 day a shape of the autocorrelation function very similar to that of the raw sample (not given in the figure) is observed. This is also reflected in the deconvolution of the autocorrelation function in Tab. 2 which was done with the CONTIN procedure: During the first hour ultrafine particles of 1 to 2 nm are indicated, during the second hour the >100 nm component reappears and the particle size distribution becomes bimodal and after 3 h the ultrafine particles become entirely masked again. The experiments show that ARD is a dynamic chemical system. If it is disturbed by filtration, it adjusts itself by formation of new particles.

References

/1/ Zänker, H. et al., Appl. Geochem. **17**, 633-648 (2002)

THERMOCHROMATOGRAPHIC VOLATILITY STUDIES OF ACTINIDE OXIDES

S. Hübener, Th. Fanghänel

The volatility of oxides of the light actinides Th, Pa, U, and Np in the O_2-$H_2O_{(g)}$/$SiO_{2(s)}$ system has been studied by thermochromatography. The experimental results reveal the formation of volatile oxide hydroxides of uranium and neptunium.

Introduction

The thermochromatographic volatility studies of oxidic U and Pu species in the O_2-$H_2O_{(g)}$/$SiO_{2(s)}$ system /1, 2/ were extended to Np oxides. Th and Pa oxides were processed as reference oxides of actinides having a maximal oxidation state of +4 or +5, respectively.

Experimental

The experimental setup was nearly the same as used in the U and Pu studies /1, 2/. The commercial gradient oven HTM LORA 36 and open tubular quartz glass columns with an inner diameter of 3.5 mm were applied. The pairs Np/Pa and U/Th were studied separately. The thermochromatographic samples were prepared from nitric acid solutions either of ^{237}Np and its daughter nuclide ^{233}Pa or ^{233}U containing trace amounts of ^{228}Th. Up to 10^{16} actinide atoms per sample were applied. Silica boats were used as sample carriers. The actinide solutions were evaporated to dryness. Fuming with HNO_3 was repeated three times to remove residual chloride ions. The actinide nitrate samples were inserted into the column in the starting position of thermochromatography. A mixture of He and O_2 in the ratio of 1:1 was used as the carrier gas at a total flow rate of 100 cm^3 min^{-1}. The carrier gas was moistened by bubbling through H_2O. Prior to thermochromatography the actinide nitrates were converted into oxides by heating at 700 K for 10 min. To start thermochromatography the hot oven was shifted into the working position. A temperature of 1375 K was chosen as maximal temperature at the starting position of the thermochromatographic column in order to diminish actinide diffusion into the silica bulk. To end a thermochromatography experiment the carrier gas flow was interrupted and the column removed from the oven within 10 seconds. Then, the column was cut into 2 cm sections which were leached with hot nitric acid. Thin-layer samples were prepared from the acidic solution by evaporation on glass disks. The actinide concentration of these samples was determined by alpha spectrometry. Gamma spectrometry was used to measure ^{233}Pa.

Results and Discussion

Fig. 1 combines thermochromatograms of U and Np after 30 min chromatography time at 1375 K at the starting position and a water vapor pressure of 2.5 kPa. The chromatograms represent the actinide fractions soluble in hot nitric acid. As can be seen from Fig. 1 Np exhibits a broad distribution along the whole column with a small peak at 1000 K, about 200 K lower than the U peak. The broad distribution of Np is presumably a result of the diffusion of Np species into the silica bulk. The actinide fractions removed from the gas chromatographic process due to diffusion into the silica are not depicted. They amount to about 10 % in case of uranium and up to 99 % for neptunium.

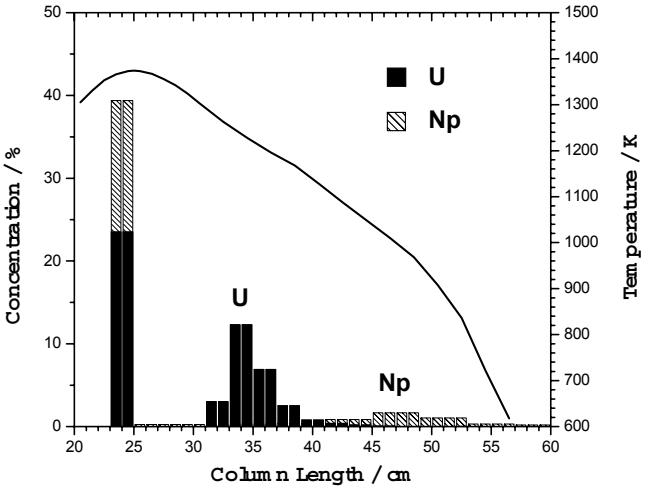

Fig. 1: Thermochromatograms of ^{233}U and ^{237}Np

However, even the low volatilization yield of Np indicates the oxidation of NpO_2, the primary product of the neptunium nitrate calcination /3/, to Np(VI) or Np(VII) by the reactive carrier gas components O_2 and H_2O. Np(VI) is volatile presumably as oxide hydroxide which should be formed according to reaction (1) in analogy to the formation of volatile $PuO_2(OH)_2$ /4/:

$$NpO_{2(s)} + 1/2O_{2(g)} + H_2O_{(g)} \rightarrow NpO_2(OH)_{2(g)} \quad (1)$$

The behavior of Th and Pa supports this interpretation. Both Th and Pa are quantitatively retained in the silica boat because actinides in the oxidation state 4+ and 5+ are unable to form volatile oxide hydroxides. The position of the Np peak at lower temperatures than the U peak may result from the formation of a volatile Np(VII) oxide hydroxide. However, the evidence for this interpretation from these indirect thermochromatographic studies is very weak in particular as the main part of the Np evades the chromatographic process due to diffusion into the silica bulk as mentioned above. The behavior of Pu under experimental conditions as used in the present Np studies is still more dominated by the diffusion into the silica bulk. The alternative column materials Al_2O_3 and ZrO_2 proved to be even less suitable than SiO_2. Nevertheless, in spite of all these drawbacks our thermochromatographic volatility studies proved to be conclusive enough to give evidence for the oxidation of NpO_2 and PuO_2 to higher oxides by moist oxygen.

References

/1/ Hübener, S., Taut, S., Vahle, A.. Report FZR-318 (2001) p.60

/2/ Hübener, S., Taut, S., Vahle, A., Fanghänel, Th., Report FZR-343 (2002) p.19

/3/ Marquart, R., Hoffmann, G., Weigel, F., J. Less-Common Met. **91**, 119 (1983)

/4/ Krikorian, O.H. et al., J. Nucl. Materials, **247**, 161 (1997)

Actinides / Radionuclides in Biosystems

ARCHAEAL DIVERSITY IN SOILS OF THE URANIUM MINING WASTES

G. Radeva, S. Selenska-Pobell

Archaeal communities were studied in the uranium mining waste pile Haberlandhalde and in the uranium mill-tailings Gittersee/Coschütz. In both environments the populations of Archaea were not very dense and they were limited to several related not yet cultured groups of Crenaechaeota.

Recently, we demonstrated that bacterial communities in uranium mining waste piles and in the U mill tailings are site-specific and very diverse /1/. In this work the distribution and diversity were studied of the members of the second phylogenetic prokaryotic domain (*Archaea*) in two uranium wastes, namely in the mining pile near the town of Johanngeorgenstadt and in the mill tailings Gittersee/Coschütz near the city of Dresden.

Two archaea-specific 16S rDNA clone libraries (A21F-A958R and A12F-A1513R) were constructed for the same soil samples of the two mentioned environments in which bacterial diversity was formerly studied /1, 2/. As estimated in this work, in contrast to the previously reported extremely complex composition of the bacterial communities, the archaeal communities in the samples are limited to only a few populations of uncultured Crenarchaeota. In Fig. 1 a phylogenetic tree based on the predominant archaeal 16S rDNA clones obtained from the soil samples of Gittersee/Coschütz (Gitt) and of the Haberlandhalde (JG36) is presented. As shown in the figure, most of the clones recovered from the Gitt samples were affiliated to the so called **SCA** clones which represent a deeply branching group within Crenarcheota that has no close affiliation to any cultivated member of the Archaea. However, this group is considered to be characteristic for a large variety of terrestrial environments /3/. One archaeal population of Gittersee/ Goschütz represented by the clone Gitt-GR-27 was affiliated to another uncultured Crenarchaeotic 16S rDNA sequence (44a-A1-1) which was found in a ZnS-prodicing biofilm of a subsurface acid mine drainage system. The main part of the JG36 16S rDNA clones was affiliated to the **S**outh **A**frican **G**old **M**ine **A**rchaeal (**SAGMA**) group consisting also of not yet cultured Crenarchaeota /4/. A relatively dense archaeal population was represented by the clone JG36-GR-12 and was affiliated to the clone HTA-B10, which was found in a very interesting mixed microbial community associated with metal-rich particles from a freshwater reservoir /5/. Interestingly, no representatives of the known bacterial oxidizers or reducers of metals were found in that community. On the basis of their results the authors considered that possibly members of novel uncultured bacterial and archaeal lineages, which they identified in the metal-rich samples, are involved in the metal biotransformation processes occurring at that environment /5/.

In addition to the above mentioned clones representing large and small groups of closely related RFLP-types, all individual clones of the archaeal 16S rDNA libraries were sequenced as well. Due to the already described low archaeal diversity the number of these clones was limited to 10 for both 16S rDNA libraries. All individual sequences were affiliated to the mentioned Crenarchaeota lineages (see the example presented by the clone Gitt-GR-78). Because all sequences obtained in this study showed no close phylogenetc affiliation to any cultured Archaea, it is difficult to predict the phenotipic properties and the ecological role of the corresponding organisms. However, it is significant that the most related sequences from the Gene Bank are recovered from environments with ecological properties similar to those of the uranium wastes, such as acid mine drainage system, gold mining wastes or metal-rich particles.

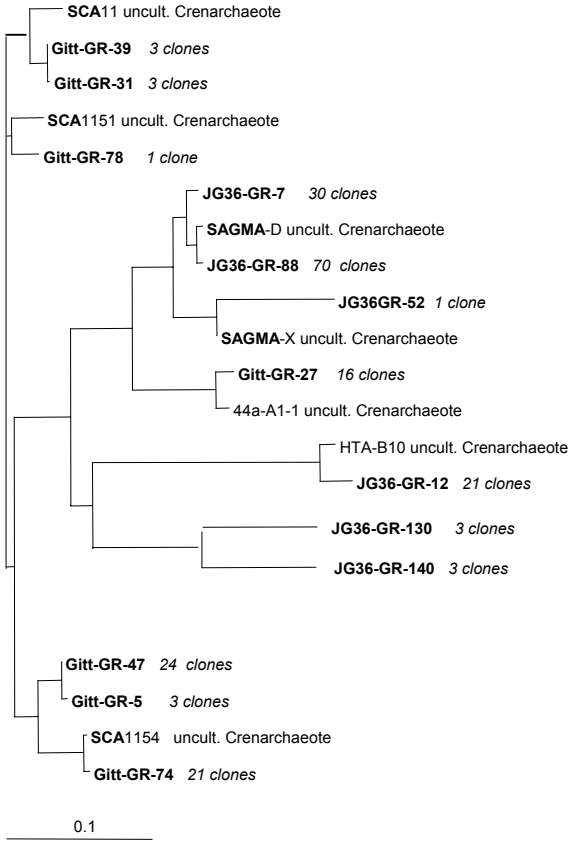

Fig. 1: Phylogenetic tree of the archaeal 16S rDNA-clones recovered from the soil samples of the uranium wastes.

Acknowledgements

This work was supported by grant SMWK 7531.50-04-844-02/4 from the Sächsisches Staatsministerium für Wissenschaft und Kunst, Dresden, Germany.

References

/1/ Selenska-Pobell, S., In: *Interactions of Microorganisms with Radionuclides*, Elsevier Sciences, Oxford, UK , pp. 225-253, (2002)
/2/ Flemming, K. et al., FZR-Report **318**, p. 35 (2001)
/3/ Bintrim, S. et al., PNAS **94**, 277-282 (1997)
/4/ Takai, K. et al., Appl. Env. Microbiol. **67**, 5750-5760 (2001)
/5/ Stein, L. et al., FEMS Microb. Ecol. **42**, 431-440 (2002)

NATURAL BACTERIAL COMMUNITIES IN UNDERGROUND WATERS NEAR THE DEEP-WELL INJECTION SITE TOMSK-7, SIBERIA, RUSSIA

M. Nedelkova, G. Radeva, S. Selenska-Pobell

Bacterial diversity was studied by using the 16S rDNA retrieval in deep underground waters near the radioactive waste injection site Tomsk-7. A population of a β-proteobacterial Dechlorosoma species was found to be predominant there. The presence of a large variety of diverse not yet cultured bacteria was demonstrated as well.

Natural bacterial communities were studied in underground water at depths of 290-324 m at the monitoring site S15 closely located to the Russian deep-well radioactive waste injection boreholes near the town of Tomsk, Siberia. For this the 16S rDNA retrieval was applied as described in /1/. The choice of this direct molecular approach was based on the knowledge that at present only a few percent of the bacteria in nature can be cultured and studied in laboratory conditions due to the limited information about their life-necessities /2/. About 1 μg of total DNA was recovered per a water sample with a volume of 1 L. This amount corresponds to a bacterial community with a size of about 10^8 cells/L. One hundred thirty two full length 16S rDNA clones were constructed via PCR amplification of the total DNA. Results obtained after the sequence analysis of the predominant 16S rDNA clones from the library are presented in Fig. 1. As evident from the phylogenetic tree presented in the figure a large and micro-diverse population of one β-proteobacterial *Dechlorosoma* sp. was identified in the sample studied. More than 65% of the clones from the library were affiliated with two closely related isolates of the same species with a 99.2 % of identity. Cultured strains of the *Dechlorosoma* sp. are capable to reduce perchlorate and chlorate and to obtain energy for growth by this metabolic process /3/. However, *Dechlorosoma* isolates were cultured not only from industrial wastes contaminated with the above mentioned pollutants but also from a very diverse environments such as pristine, hydrocarbon contaminated soils, aquatic sediments, etc. /3/. It is obvious that in the environments not polluted with per(chlorate) the bacterial populations affiliated to *Dechlorosoma* sp. are involved in some different, possibly not yet described, metabolic processes.

As seen in the Fig. 1, representatives of α–, γ– and δ–proteobacteria were also identified in the studied water sample. The clone S15A-MN75 represents an α–proteobacterial population closely related to the genus *Sphingomonas*. The latter is characteristic for oligotrophic environments where it's representatives can be found in a form of ultramicrobacteria. Another α– proteobacterial population was represented by the clone S15A-MN24, related to a chemolithoautotrophic arsenite-oxidizing bacterium BEN-5 which was recovered from a gold mine. The clone S15A-MN135 represents a relatively dense population of γ –proteobacteria related to a not yet cultured group of this subclass which was identified in another extreme environment, the Mammoth Hot Spring in the Yellowstone National Park, USA. The number of δ-proteobacteria (clone S15A-MN13) seems to be low and limited to the dissimilatory Fe(III)-reducing *Geobacter* sp. Interestingly, much higher is the density of another group of Fe(III)-reducing bacteria which were affiliated to *Geothrix fermentas* of the *Holophaga* group (clone S15A-MN55). In contrast to the other metal reducing bacteria, *G. fermentas* is able to release chelating compounds into the environment which can influence the solubility of Fe(III) and possibly of some other metals as well /4/. Populations with not known functions belonging to *Cytophaga / Flavobacterium / Bacteroides* **(CFB),** Planctomycetales **(Pl)** and to the Gram positive bacteria with a low G+C content were found in the studied sample as well.

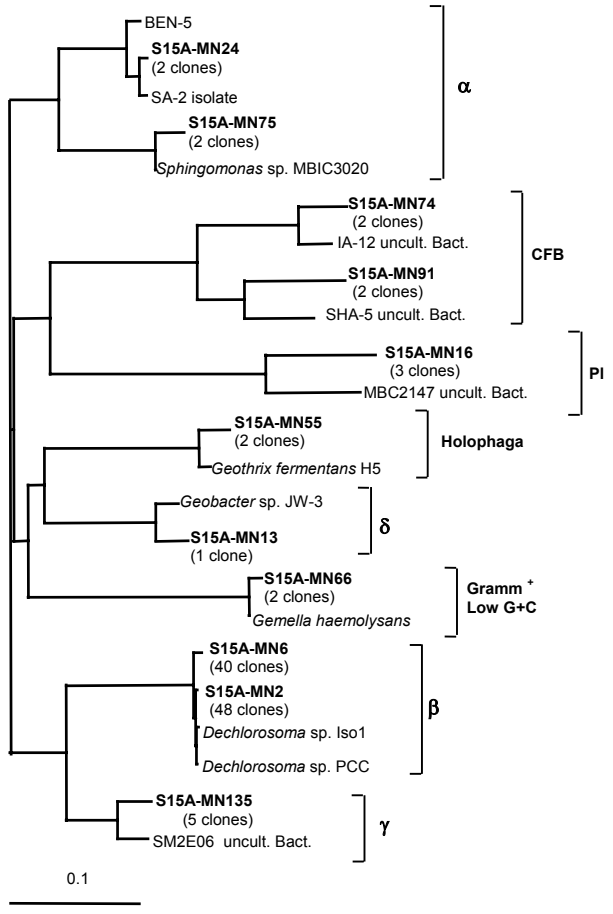

Fig.1: Phylogenetic tree of the predominant bacteria in the "BORIS" sample S15

Acknowledgements

This work was supported by a grant FIKW-CT-2000-00105 "BORIS" from the EU.

References

/1/ Selenska-Pobell, S. et al., Antonie van Leewenhoek **79**, 149-161 (2001)

/2/ Dojka, M. et al., Appl. Env. Microbiol. **66**, 1617-1621 (2000)

/3/ Coates, J.D. et al., Appl. Env. Microbiol. **65**, 5234-5241 (1999)

/4/ Nevin, K. et al., Appl. Env. Microbiol. **68**, 2294-2299 (2002)

INTERACTION OF ACTINIDES WITH *Desulfovibrio äspöensis* DSM 10631^T. PART I: URANIUM

H. Moll, M. Merroun, S. Selenska-Pobell, G. Bernhard

We are presenting the first results on interactions of the sulfate-reducing bacterium D. äspöensis DSM 10631^T with uranium(VI). 80 % of the U(VI), solved initially in a concentration of 0.02 mM in a liquid medium supplemented with lactat (10 mM), was removed by the cells of this strain after 72 h of incubation at pH 5.

Introduction

Motamedi and Pedersen showed that sulfate reducing bacteria (SRB) are frequently distributed in the deep granitic rock aquifers at the Äspö hard rock laboratory (Sweden) /1/. The interaction of actinides with SRB have not been studied in the Äspö aquifer. We are focussing our work on the strain *Desulfovibrio äspöensis* DSM 10631^T recovered from the deep granitic groundwater at the Äspö site /1/. The strain was grown under anaerobic conditions in 250 ml bicarbonate-buffered medium containing a trace amount of ferrous chloride ($7.5x10^{-7}$M) at 22 °C. The biomass was separated by centrifugation and washed 3 times with 0.9% NaCl. To study the interaction of *D. äspöensis* with U(VI), 96-hour cultures were prepared. The collected biomass was 1.10 $g_{dry\ weight}$/l. The purity of the *D. äspöensis* cultures was verified using Amplified Ribosomal DNA Restriction Enzyme Analysis (ARDREA). For this 16S rDNA PCR amplicons were generated and digested with the endonucleases *Rsa*I, *Msp*I, *Hae*III and *Hinf*I (see Fig. 1).

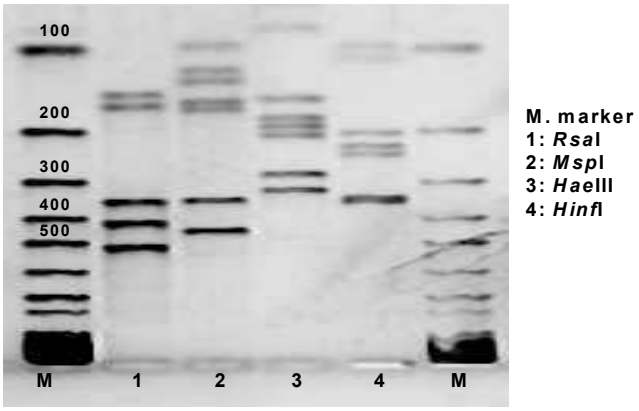

Fig. 1: 16S-ARDREA of *D. äspöensis* DSM 10631^T

Results

We could show the removal of uranium from the solution due to the activity of *D. äspöensis* (Fig. 2, 3).

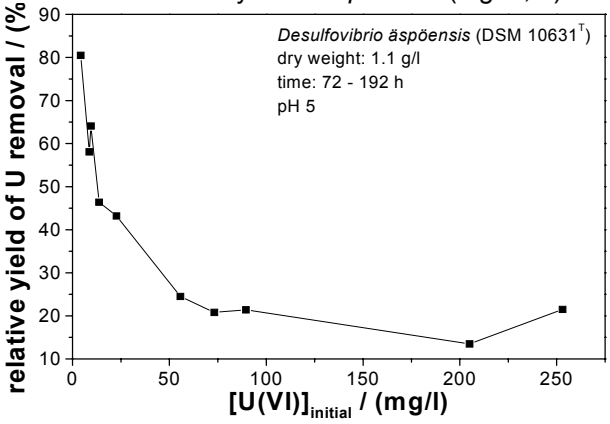

Fig. 2: Removed uranium from the solution in the presence of *D. äspöensis*

In all samples where no cells were added, the uranium concentrations measured by ICP-MS did not differ significantly from the initial values. Ferrous chloride concentrations ranging from $1.9x10^{-6}$ to $7.5x10^{-7}$ M in the growing medium do not affect the efficiency of the uranium removal. At $[U(VI)]_{initial}$ < 5 mg/l a removal efficiency of 80% could be achieved. Besides the pH (Fig. 3), the uranium concentration in solution is another factor limiting the removal efficiency (Fig. 2). At $[U(VI)]_{initial}$ > 50 mg/l, the removal efficiency decreased to a level of 20 to 25 %. Comparing our findings with the literature /2, 3/, one might speculate that *D. äspöensis* is tolerating less uranium compared to *D. desulfuricans*, to achieve a maximum on removed uranium. On the other hand, we observed with increasing $[U(VI)]_{initial}$ increasing total amounts of removed U by the biomass.

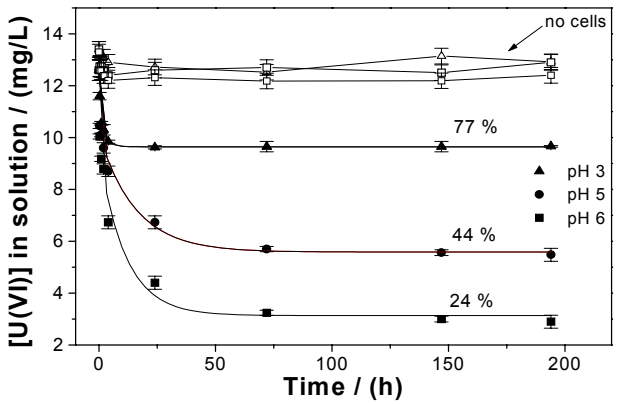

Fig. 3: Decrease of the U(VI) concentration ($[U(VI)]_{initial}$ = 12.6 mg/l) in solution in dependency of the contact time and the pH

The main U(VI) removal occurred after the first 24 h. After 72 h, limiting values are reached. A decrease from 77 to 24 % was observed when the pH changed from 3 to 6, respectively. This is reasonable because this bacterium grows at an optimum pH of 7. However, we detected a strong decrease, 7 %, in the removal activity of the cells at pH 8. On the basis of these results and those found in the literature with *D. desulfuricans* one may speculate that *D. äspöensis* enzymatically reduces U(VI) /2, 3/. The time dependencies shown in Fig. 3 could only be fitted to a bi-exponential law. This leads to the conclusion that probably two different processes occur after adding the biomass. Additional experiments showed that uranium reduction takes place also without addition of an electron donor. Further experiments exploring the reaction mechanism are in progress.

Acknowledgement

This work is supported by the BMWi (no. 02E9491).

References

/1/ Motamedi, M. et al., Int. Syst. Bacteriol. **48**, 311 (1998)

/2/ Panak, P. et al., J. Alloys Comp. **271-273**, 262 (1998)

/3/ Lovley, D.R. et al., Appl. Environ. Microbiol. **58**, 850 (1992)

Desulfovibrio äspöensis DSM 10631^T AND URANIUM – FIRST XAS RESULTS

H. Moll, M. Merroun, S. Selenska-Pobell, C. Hennig, H. Funke, A. Roßberg, G. Bernhard

The precipitates formed by D. äspöensis (DSM 10631^T) in a medium containing U(VI) and lactate were characterized by XANES. The formation of U(IV) was demonstrated.

Introduction

Strains of the genus *Desulfovibrio* are widespread and have the ability to immobilize heavy metals, e.g. uranium by reduction. XAS with synchrotron radiation is a powerful tool to determine the near order surrounding and changes of the oxidation state of actinides in biological samples.

Experimental

After culturing of *D. äspöensis* DSM 10631^T in optimized growth medium, the bacterial cells were collected by centrifugation. They were washed and resuspended in a solution of 0.9% NaCl. Two parallel samples were prepared. In the sample A, the cells were incubated with 0.63 mM U(VI) solution at pH 5. In the sample B the uranium concentration and the pH used were 0.1 mM and 6, respectively. After shaking the samples for 7 days under nitrogen atmosphere, the biomass was separated by centrifugation, washed with 0.9% NaCl solution, and sealed in polyethylene cuvettes. The XAS data were recorded at the Rossendorf Beamline (ROBL) at the ESRF in Grenoble /1/.

Results

The pattern of the XANES spectrum of the sample A clearly indicates the presence of uranium in both oxidation states +4 and +6 (see Fig. 1).

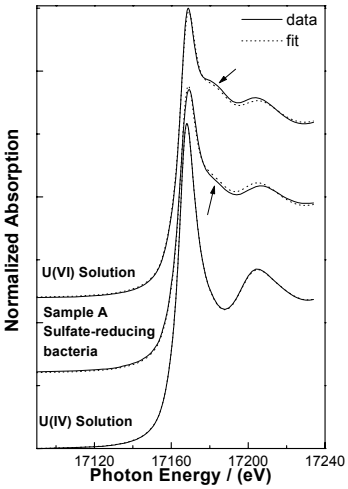

Fig. 1: U L_{III}-edge XANES spectra of 0.03 M U(IV) and 0.04 M U(VI) reference solutions in 1 M $HClO_4$ and after bacterial reduction of U(VI) (sample A). Solid line – experiment; dots – calculated spectrum.

We applied the Factor Analysis described in /2/ to determine the amounts of U(IV) and U(VI) present in sample A. The calculations revealed a mixture containing 20 % U(IV) and 80% U(VI). An attempt to fit the EXAFS data of sample A is presented in Tab. 1 and Fig. 2. The amplitude of the axial oxygen atoms is clearly reduced compared to sample B indicating the presence of two oxidation states of uranium. To the knowledge of the authors, this is the first experimental prove that *D. äspöensis* can reduce U(VI) to U(IV).

On the other hand, the identification of U(IV) in the sample B failed. The XANES spectrum indicates that almost all of the uranium is present as U(VI). The reasons for this observation are not clear at the moment. One possibility could be a re-oxidation of U(IV) to U(VI) during the time between sample preparation and the measurement.

Sample	Shell	N	R (Å)	σ (Å^2)
A	U-O_{ax}	1.2±0.4	1.74±0.01	0.0027
	U-O_{eq}	6.7±2.0	2.31±0.01	0.0131
B	U-O_{ax}	2.2±0.3	1.76±0.003	0.0036
	U-O_{eq}	6.4±1.5	2.31±0.01	0.0160
	U-C	1.8±2.1	2.84±0.02	0.0011
	U-P	0.6±0.5	3.62±0.05	0.0040[f]

f: value fixed for calculation

Tab. 1: EXAFS structural parameter

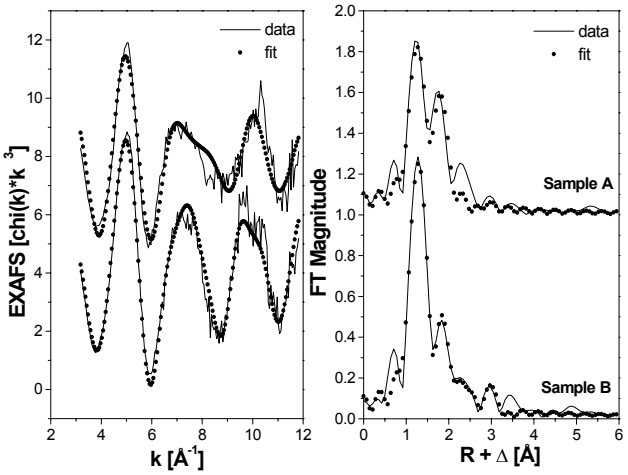

Fig. 2: Uranium L_{III}-edge k^3-weighted EXAFS spectra (left) and corresponding FT (right) of the *D. äspöensis* DSM 10631^T uranium samples.

The evaluation of the EXAFS data of sample B (Tab. 1, Fig. 2) yielded an relatively short U-O_{eq} distance of 2.31 Å. This indicates an intensive interaction of uranyl with functional groups at the surface of the bacteria. The third and fourth peaks in the FT at 2.84 and 3.62 Å could be fitted using U-C and U-P phase and amplitude functions. The interaction of *D. äspöensis* with uranium could probably consists of more than one process /3/. We suggest, that the mechanism of the U removal involves biosorption and bioreduction. As a result a mixed precipitate consisting of UO_2, bacteria, and bound U(VI) to them is formed. Further investigations to throw more light on the interactions of uranium with *D. äspöensis* are in progress.

Acknowledgement

This work is supported by the BMWi (no. 02E9491).

References

/1/ Reich, T. et al., Radiochim. Acta **88**, 633 (2000)
/2/ Roßberg, A., Ph.D. Thesis, TU Dresden (2002)
/3/ Moll, H. et al., Report FZR-373, p.31 (2002)

EXAFS INVESTIGATIONS OF URANIUM COMPLEXES FORMED BY DIFFERENT BACTERIA ISOLATED FROM URANIUM MINING WASTES

M. Merroun, A. Roßberg, C. Hennig, T. Reich, S. Selenska-Pobell

Extended X-ray absorption fine structure (EXAFS) measurements were used at the U L3-edge to directly determine the functional groups responsible for the absorption of aqueous UO_2^{2+} by Bacillus sphaericus JG-A12, Pseudomonas stutzeri ATCC 17588, P. migulae CIP 105470, Acidithiobacillus ferrooxidans D2 and Stenotrophomonas maltophilia JG-2 at pH 4.5.

Contamination of the environment with radionuclides, toxic metals, metalloids and organo-metals is of considerable economic and environmental significance. There is a considerable interest in the microbiological processes which affect the behavior of these contaminants in natural and engineered environments and also in the potential to bioremediate them. In this work, we present results of U L_{iii}-edge Extended X-ray Absorption Fine Structure (EXAFS) spectroscopy of the uranium complexes formed by strains of *Acidithiobacillus ferrooxidans*, *Stenotrophomonas maltophilia, Bacillus sphaericus*, *Pseudomonas stutzeri* and *Pseudomonas migulae,* relevant to uranium mining wastes.

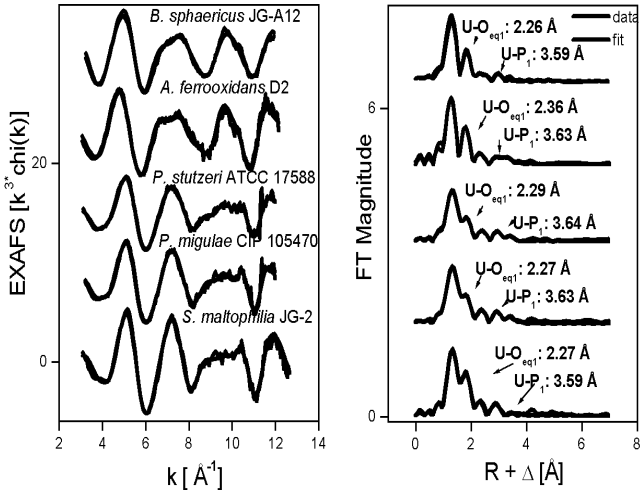

Fig.1: Uranium L_{III}-edge k^3–weighted EXAFS spectra (left) and corresponding FT (right) of the bacterial uranium complexes.

The k^3-weighted spectra determined from extended X-ray absorption spectroscopy (EXAFS) analyses of the uranium species formed at pH 4.5 by the above mentioned bacteria are presented in Fig. 1 along with the best fits obtained from the fitting procedure.

Fit results indicate that the adsorbed U(VI) has the common linear trans-dioxo structure: two axial oxygens at about 1.78 Å, and an equatorial shell of 4 to 5 oxygens at 2.26-2.41 Å.

The U-O_{eq1} bond distances of the *B. sphaericus* JG-A12 uranium complexes (2.27 ± 0.02 Å); *A. ferrooxidans* D2 (2.36 ± 0.02 Å); *P. stutzeri* ATCC 17588 (2.29 ± 0.02 Å); *P. migulae* CIP 105470 and *S. maltophilia* JG-2 (2.27 ± 0.02 Å) are within the range of previously reported values for the oxygen atom of the phosphate bound to uranyl /1/. The FT spectra of the uranium complexes formed by *B. sphaericus* JG-A12 required other oxygen shell to obtain reasonable fits (U-O_{eq2}). This longer equatorial oxygen bond length (2.42 ± 0.02 Å) is similar to previously reported values for the oxygen atom of the carboxyl or water bound to uranyl (2.41 to 2.51 Å) /2/.

For the same sample of *B. sphaericus* JG-A12, the 4th FT peak was modelled to the contribution of carbon atom. The best-fit value for the U-C Path length (r= 2.91 ± 0.02 Å). The FT spectra of the uranium complexes formed by the other bacteria studied in this work (*P. stutzeri*, *P. migulae*, *S. maltophilia, A. ferrooxidans*) also contain a FT peak at the same bound distance as those found in *B. sphaericus* which was modeled as mentioned above as contribution of the carbon atom. However in the case of *Pseudomonas* and *Stenotrophomonas* strain this peak was modeled to a contribution of oxygen atoms.

The broad FT peak between 2.7 and 3.9 Å could according to Kelly et al. /1/ arise from:

- a phosphorus and the twofold degenerated 3-legged MS path U-O_{eq1}-P_1
- or from a phosphorus and an additional SS path U-P_2 instead of the MS path U-O_{eq1}-P_1 .

Fits to the EXAFS spectra indicate that in the case of *B. sphaericus* JG-A12, the U(VI) is coordinated to carboxyl groups in a bidentate fashion with an average distance between the U atom and the C atom of 2.91 ± 0.02 Å and to phosphate groups in a monodentate fashion with an average distance between the U atom and the P atom of 3.59 ± 0.02 Å. In the case of the other bacteria, however the phosphate groups are mainly implicated in the complexation of uranium in a monodentate mode, with an average distance between the U atom and the P atom of 3.63 ± 0.02 Å.

Acknowledgments

This study was supported by grant No. 03I4004B from the Bundesministerium für Bildung und Forschung, Germany.

References

/1/ Kelly et al., Geochim. Cosmochim. Acta, **65** (2002)
/2/ Bargar et al., Geochim. Cosmochim. Acta, **64** (2000)

SPECTROSCOPIC CHARACTERIZATION OF THE URANIUM (VI) COMPLEXES FORMED BY THE CELLS OF *PSEUDOMONAS* STRAINS

M. Merroun, K. Brottka, A. Roßberg, C. Hennig, T. Reich, R. Nicolai, K-H. Heise, S. Selenska-Pobell

A combination of extended X-ray absorption fine structure (EXAFS) spectroscopy and infrared (IR) spectroscopy were used to determine the structural parameters of the uranium complexes formed by different Pseudomonas strains. The results demonstrated that uranium(VI) is bound by these bacteria via phosphate groups.

Microorganisms have a potential to affect mobility and overall environmental behavior of heavy metals and radionuclides through solubility and speciation changes, biosorption, bioaccumulation or other biotransformations. In this study we used a combination of EXAFS spectroscopy and infrared (IR) spectroscopy to characterize the uranium complexes formed by different bacterial strains such as, *P. stutzeri* DSMZ 5190, *P. stutzeri* DSMZ 7190 and *P. migulae* CIP 105470. These strains represent the predominant indigenous bacterial populations of the uranium wastes.

In order to identify the type of bacterial functional groups implicated in the interaction with uranium, the FTIR study was carried out (Fig. 1).

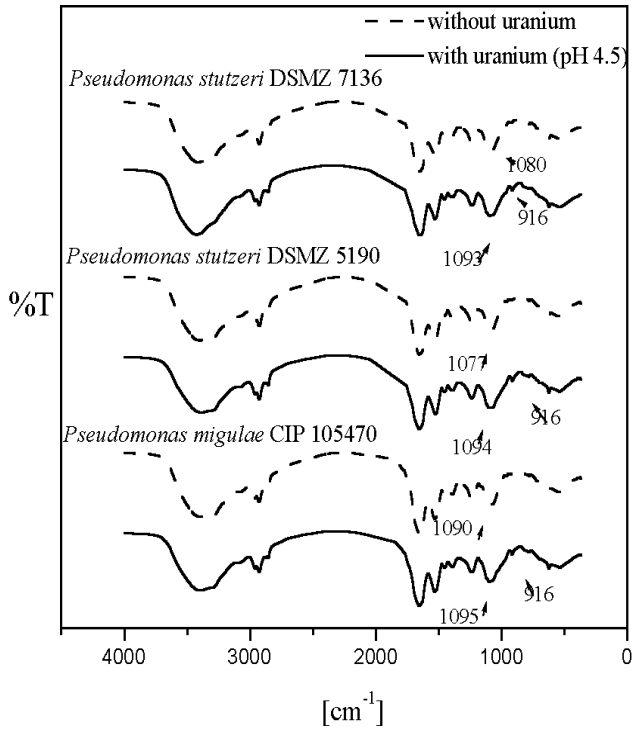

Fig. 1: IR spectra of native and uranium treated cells of*, P. stutzeri* DSMZ 7136*, P. stutzeri* DSMZ 5190 and *P. migulae* CIP 105470.

The absorption spectra of uranium treated biomass were compared to those of untreated biomass (Fig. 1). The treated biomass was washed, dried and powdered under the same conditions used for the preparation of untreated biomass.

The absorption band at 916 cm^{-1} (*P. migulae* CIP 105470, *P. stutzeri* DSMZ 5190 and *P. stutzeri* DSMZ 7190) originates from the asymmetric stretching vibration of the uranyl unit. The FTIR spectra of the strains treated with uranium revealed a significant shift of the absorption peak to higher wave numbers which is corresponding to phosphorus residues.

Uranium L_{III}-edge EXAFS spectra of the uranium species formed by *P. stutzeri* DSMZ 7136*, P. stutzeri* DSMZ 5190, *P. migulae* CIP 105470 and their corresponding Fourier Transforms (FT) are shown in Fig. 2.

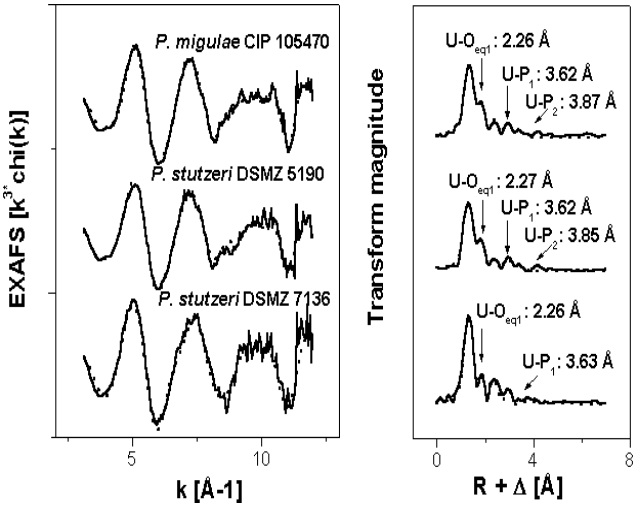

Fig. 2: Uranium L_{III}-edge k^3–weighted EXAFS spectra (left) and corresponding FT (right) of the *P. stutzeri* DSMZ 7136, 5190 and *P. migulae* CIP 105470 uranium complexes

The most prominent peak in all samples occurs at 1.3 Å and arises from the backscattering caused by the axial oxygen atoms (O_{ax}). Backscatters from oxygen atoms laying in the equatorial plane of the uranyl ion appear as a single broad peak at 1.7-1.8 Å. As evident from Figure 1 a weak peak appears in all samples at about R + ΔR = 3 Å (not corrected from phase shift) in the FT, which was modelled to the interaction of uranium with phosphorous giving a distance of 3.62 ± 0.02 Å. Therefore, one may conclude that the phosphate groups of the bacterial strains studied are the main uranium binding sites.

EXAFS and IRS measurement of the U(VI) complexes formed by *P. stutzeri* DSZM 7136, *stutzeri* DSZM 5190 and *P. migulae* CIP 105470 demonstrate that phosphorous residues of these bacteria are involved in the interaction with uranium.

Acknowledgments

This study was supported by grant No.03I4004B from the Bundesministerium für Bildung und Forschung, Germany.

EXAFS STUDIES ON COMPLEXATION OF URANIUM(VI) BY *BACILLUS SPHAERICUS* JG-A12 CELLS, SiO_2-XEROGEL AND BIOCERS

J. Raff, M.L. Merroun, A. Roßberg, C. Hennig, U. Soltmann[1], S. Matys[2], H. Böttcher[1], W. Pompe[2], S. Selenska-Pobell

[1]Department of Functional Layers, GMBU e.V., Dresden, Germany

[2]Institute of Materials Science, Technical University Dresden, Dresden, Germany

U(VI) complexes formed by vegetative cells of B. sphaericus JG-A12 cells, by SiO_2-xerogel and the corresponding biocers were investigated using extended X-ray absorption fine structure (EXAFS) spectroscopy. The spectra demonstrated that, depending on the case, carboxyl, phosphate, hydroxyl or/and silicate groups were involved in the interaction with U.

Highly contaminated environments as uranium mining waste piles are an enormous pool for heavy metal resistant bacteria. These bacteria possess mechanisms to survive in the extreme conditions such as bioaccumulation, biotransformation, biomineralization or biosorption of metals. The latter is of special interest for bioremediation. Cells of the uranium mining waste pile isolate *Bacillus sphaericus* JG-A12 bind selectively U, Cu, Pb, Al, and Cd /1/. Therefore this strain was used for construction of biological ceramics (biocers) for bioremediation. In the present work *B. sphaericus* JG-A12 cells were embedded in a porous SiO_2-matrix by using sol-gel techniques /2,3/. 36.4 mg dry weight of vegetative cells, 163.6 mg of the SiO_2-matrix (xerogel) and 200 mg of the biological ceramic were incubated in $9x10^{-4}$ M uranyl nitrate solved in 0.9 % $NaClO_4$, pH 4.5 for 48 h at 30 °C. The uranyl complexes were investigated by using EXAFS spectroscopy. The uranium L_{III}-edge (17185 eV) X-ray absorption spectra were collected at room temperature in the fluorescence mode at the Rossendorf Beamline (ROBL) using Si(111) double-crystal monochromator.

The structural parameters of the uranium complexes formed by the different components are shown in Tab. 1. The EXAFS spectra and the corresponding Fourier transforms (FT) are shown in Fig. 1.

	shell	N	R [Å]	σ^2 [Å^2]	ΔE[eV]
Bacillus cells	$U\text{-}O_{ax}$	2[a]	1.76	0.0017	-11.0
	$U\text{-}O_{eq1}$	2.2(1)	2.26	0.0040	
	$U\text{-}O_{eq2}$	2.8(1)	2.41	0.0024	
	U-C	1.4	2.91	0.0038[a]	
	U-P	1	3.59	0.0050	
xerogel	$U\text{-}O_{ax}$	2[a]	1.77	0.0016	-10.0
	$U\text{-}O_{eq1}$	3.2(2)	2.28	0.0068	
	$U\text{-}O_{eq2}$	2.5(2)	2.44	0.0030	
	U-Si	0.5(1)	3.10	0.0040 [a]	
biocer	$U\text{-}O_{ax}$	2[a]	1.77	0.0021	-14.0
	$U\text{-}O_{eq}$	5.7(5)	2.26	0.0080	
	U-Si	0.7(2)	3.10	0.0040 [a]	
	U-P	1.3(3)	3.59	0.0040 [a]	

a: value fixed for calculation

Tab. 1: Structural parameters of the studied complexes

In the first sample uranium is coordinated to two axial oxygen atoms at a distance of 1.76 ± 0.02 Å. The second and third peak were modeled to a contribution of 2 different equatorial oxygen shells (O_{eq1} and O_{eq2}) at distances of 2.26 and 2.41 ± 0.02 Å. The fourth peak was modeled to C neighbors at 2.91 Å, which is typical for coordination of U(VI) to carboxyl groups in a bidentate fashion. The fifth peak arises from an interaction of uranium with phosphorous giving a distance of 3.59 Å /4/. In the case of the SiO_2 matrix, the uranium is coordinated by two axial oxygen atoms at a distance of 1.77± 0.02 Å. The second shell corresponds to the coordination of uranium to 3 equatorial oxygen atoms at a distance of 2.28 ± 0.02 Å. The third peak could be split in two individual peaks, one could be modeled to interaction between uranium and a second equatorial oxygen (2.44 ± 0.02 Å). This oxygen atom arises from water molecules. The second peak could be modeled to interaction between uranium and silicon atoms at a distance of 3.10 Å. In the biocer samples uranium is coordinated by two axial oxygen atoms at a distance of 1.77 ± 0.02 Å. The second shell corresponds to the coordination of uranium to 5 equatorial oxygen atoms at a distance of 2.26 ± 0.02 Å. The third peak corresponds to interaction of uranium with a silicon atom at a distance of 3.10 Å. The fourth peak is modeled to an interaction between uranium and phosphorous atoms with a U-P distance of 3.59 Å.

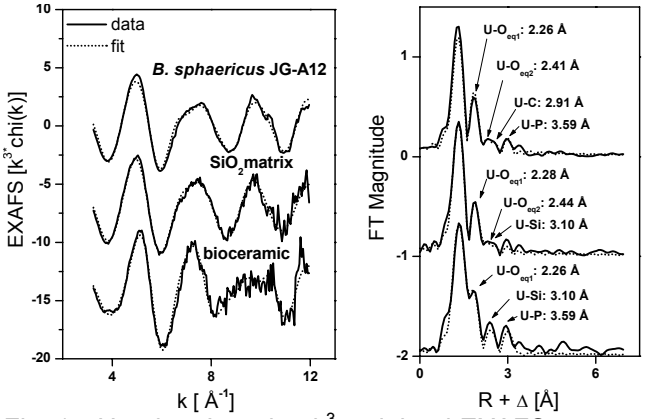

Fig. 1: Uranium L_{III}-edge k^3-weighted EXAFS spectra (left) and corresponding FT (right) of the complexes formed by *B. sphaericus* JG-A12 cells, the xerogel and the biocer.

In summary, the EXAFS analysis of the uranium complexes formed by *B. sphaericus* JG-A12 cells demonstrates the implication of carboxyl and phosphate groups. For the uranium complexes formed by the SiO_2 matrix, the implication of silicate and hydroxyl groups (water molecules) in the interaction with uranium is shown. The sorption of uranium by the biocer occurs mainly via silicate and phosphate groups.

Acknowledgements

This work was supported by grant SE 671/7-1 from the Deutsche Forschungsgemeinschaft.

References

/1/ Selenska-Pobell, S. et al., FEMS Microbiol. Ecol. **29**, 59-69 (1999)

/2/ Raff, J. et al., Chem. Mater. **15** (1), 240-244 (2003)

/3/ Raff, J., PhD thesis, Report FZR-358 (2002)

/4/ Merroun, M. et al., ROBL, Bi-Annual Report 2001 /2002

EXAFS STUDY OF URANIUM(VI) COMPLEXES FORMED BY NATIVE AND RECRYSTALLIZED S-LAYERS OF THE *BACILLUS SPHAERICUS* STRAINS JG-A12 AND NCTC 9602

J. Raff, M.L. Merroun, A. Roßberg, C. Hennig, S. Selenska-Pobell

Uranium(VI) complexes formed by native and recrystallized S-layers of the Bacillus sphaericus strains JG-A12 and NCTC 9602 were investigated using extended X-ray absorption fine structure (EXAFS) spectroscopy. In all cases uranium was coordinated to carboxyl and phosphate groups.

Biosorption on the cell walls is one possible mechanism of bacteria to immobilize and detoxify heavy metals or radionuclides. An important component of the cell walls of many bacteria and archaea are the so called surface layer proteins (S-layers). As outermost cell wall component, they are of particular importance for the sorption processes. In the present work the complexation of uranium by the S-layers of the uranium mining waste pile isolate *Bacillus sphaericus* JG-A12 and of the reference strain *B. sphaericus* NCTC 9602 was investigated. Both S-layers are phosphorylated and those of the natural isolate contains six times more phosphate than the S-layer protein of the reference strain /1/. The complexation of uranium by the native and the recrystallized S-layers was compared.

The experiments were carried out at pH 4.5. As the S-layer lattices are not stable at pH values below 5, the purified S-layers were stabilized with 1-Ethyl-3-(N,N´-di-methyl-aminopropyl)-carbodiimid. 20 mg native or recrystallized S-layers were incubated with $9x10^{-4}$ M uranium nitrate solved in 0.9 % $NaClO_4$, pH 4.5. The uranyl complexes were investigated by using EXAFS spectroscopy. The structural parameters of the complexes are shown in Tab.1. The EXAFS spectra and the corresponding Fourier transforms (FT) are shown in Fig. 1 and Fig. 2.

	shell	N	R [Å]	σ^2 [Å^2]	ΔE[eV]
NCTC 9602 S-layer native	$U\text{-}O_{ax}$	2[a]	1.77	0.0038	-1.0
	$U\text{-}O_{eq1}$	1.9(1)	2.24	0.0050	
	$U\text{-}O_{eq2}$	2.8(1)	2.42	0.0050	
	U-C	1.4(1)	2.91	0.0040	
	$U\text{-}P_1$	1.0(1)	3.64	0.0040[a]	
	$U\text{-}P_2$	1.0(1)	3.85	0.0040[a]	
JG-A12 S-layer native	$U\text{-}O_{ax}$	2[a]	1.78	0.0031	2.9
	$U\text{-}O_{eq1}$	1.2(1)	2.30	0.0050	
	$U\text{-}O_{eq2}$	2.4(1)	2.47	0.0050	
	U-C	1.2(2)	2.91	0.0040	
	$U\text{-}P_1$	0.8(2)	3.64	0.0040[a]	
	$U\text{-}P_2$	1.0(2)	3.87	0.0040[a]	
NCTC 9602 S-layer recrystallized	$U\text{-}O_{ax}$	2[a]	1.77	0.0022	2.9
	$U\text{-}O_{eq1}$	2.0(3)	2.32	0.0046	
	$U\text{-}O_{eq2}$	2.8(5)	2.47	0.0065	
	U-C	1.4	2.91	0.0038	
	$U\text{-}P_1$	0.9(2)	3.65	0.0040[a]	
	$U\text{-}P_2$	1.0(1)	3.87	0.0040[a]	
JG-A12 S-layer recrystallized	$U\text{-}O_{ax}$	2[a]	1.78	0.0022	4.0
	$U\text{-}O_{eq1}$	1.7(3)	2.33	0.0044	
	$U\text{-}O_{eq2}$	2.8(3)	2.49	0.0053	
	U-C	1.4	2.89	0.0038	
	$U\text{-}P_1$	0.8(2)	3.67	0.0040[a]	
	$U\text{-}P_2$	1.2(2)	3.89	0.0040[a]	

a: value fixed for calculation

Tab. 1: Structural parameters of the studied complexes

In all samples the first peak corresponds to coordination of uranium to two axial oxygen atoms (O_{ax}) at a distance of 1.77-1.78 Å. The second and the third peak were modeled to two different equatorial oxygen shells (Oeq_1 and Oeq_2) at distances of 2.24-2.33 Å and 2.42-2.49 Å, respectively. All FTs of the spectra obtained from the U complexes formed by both S-layers contain a fourth peak, which was fitted by C neighbors at 2.89-2.91 Å. This distance is typical for the coordination of U(VI) to carboxyl groups in a bidentate fashion /2/. This is also in a good agreement with the results obtained for the $U\text{-}O_{eq2}$ distance in this work. The fifth peak was modeled to the interaction of uranium with phosphorous at a distance of 3.64-3.67 Å. The sixth peak could arise from a additional SS path $U\text{-}P_2$ or a twofold degenerated 3-legged MS path $U\text{-}O_{eq1}\text{-}P1$.

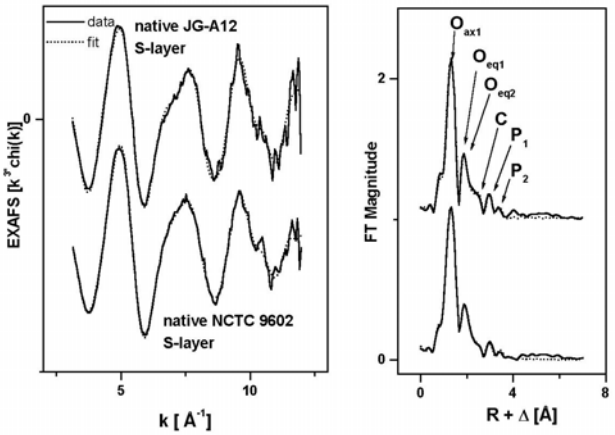

Fig. 1: Uranium L_{III}-edge k^3-weighted EXAFS spectra (left) and the corresponding FT (right) of the uranium complexes formed by the native S-layers of *B. sphaericus* JG-A12 and NCTC 9602.

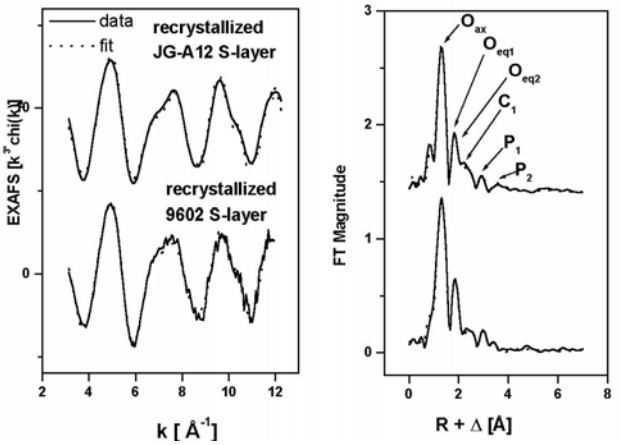

Fig. 2: Uranium L_{III}-edge k^3-weighted EXAFS spectra (left) and the corresponding FT (right) of the uranium complexes formed by the recrystallized S-layers.

In summary, EXAFS analysis of the uranium complexes formed by both S-layers demonstrate the implication of carboxyl and phosphate groups in the interaction with uranium.

Acknowledgements

This work was supported by grant SE 671/7-1 from the Deutsche Forschungsgemeinschaft.

References

/1/ Raff, J., PhD thesis, Report FZR-358 (2002)

/2/ Bargar et al., Geochim. Cosmochim. Acta **64**, 2737-2749 (2000)

INVESTIGATION OF SEVERAL CELL COMPONENTS OF DANDELION BY TIME-RESOLVED LASER-INDUCED FLUORESCENCE SPECTROSCOPY

A. Günther, G. Bernhard

We separated the cell sap and solid cell components of uranium-containing plant samples. Depending on the uranium concentration in the hydroponic solution, uranium species were detected in the separated cell components by TRLFS.

A detailed knowledge of the nature of the uranium complexes formed after the uptake into plants is essential for describing the migration behavior of uranium in the environment. We used TRLFS and EXAFS to determine the uranium speciation in plants. The spectroscopic results showed that uranium(VI) is predominantly bound to inorganic and/or organic phosphorus groups inside the plants /1/. The aim of this study was to determine the uptake of uranyl into the cell sap and solid cell components.

Dandelion plants were grown in uncontaminated soil and then transferred into hydroponic solutions. The uranium concentration in the hydroponic solutions ranged from $1 \cdot 10^{-4}$ M to $2.65 \cdot 10^{-2}$ M at pH 3. After harvesting the plants were washed and separated into roots and leaves, followed by the preparation of section samples. The cells of the section samples were destroyed in an oscillating mill while being cooled with liquid nitrogen. The light microscopy pictures in Fig. 1 and Fig. 2 show plant cells of a dandelion sample before (Fig. 1) and after destruction of the cells (Fig. 2). The pictures were taken with an Olympus BX61 light microscope and enlarged 400 times.

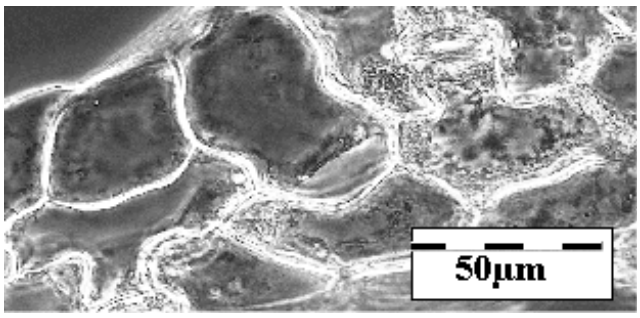

Fig. 1: Intact plant cells

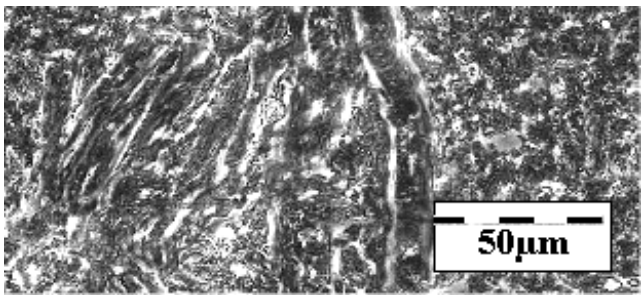

Fig. 2: Destroyed plant cells

The "green mass" was centrifuged and the cell sap separated from solid cell components. Then the section samples, the cell sap and the solid cell components were investigated by TRLFS. The results of some examples are shown in Fig. 3 and Tab. 1.

In hydroponic solution with a high uranium concentration, uranium species were found in the cell sap and on the solid cell components of roots and leaves.

But when the uranium concentration in the hydroponic solution was in the range of 10^{-4}M, uranium species were only detected on the solid cell components of the roots.

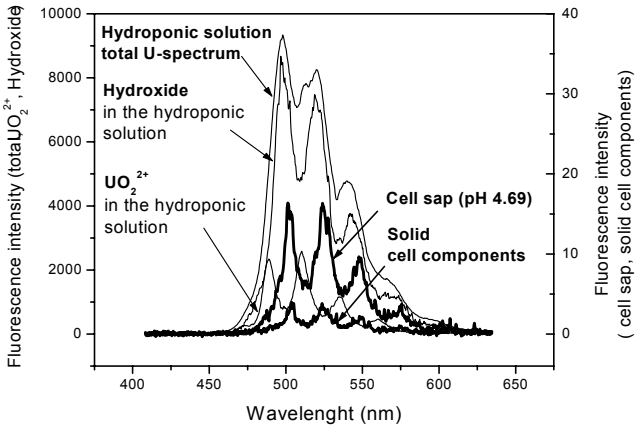

Fig. 3: Comparison of TRLFS spectra of the uranium species in the hydroponic solution, in the cell sap and on the solid cell components of a dandelion root sample

Sample		Main emission bands (nm)				
H	UO_2^{2+}	471.5	488.9	510.6	535.1	560.4
	Hydroxides	481.2	498.2	519.5	543.8	569.8
Section			500.2	521.2	547.2	568.7
Cell sap		493.8	503.7	524.5	548.2	574.7
Solid cell components		494.0	502.4	524.8	547.9	574.2

Tab. 1: Fluorescence data of uranium species in the hydroponic solution (H, $2.65 \cdot 10^{-2}$M U, pH 3.18) and different samples of an uranium containing dandelion root

The main emission bands of the uranium species always showed a bathochromic shift against the spectral lines of free uranyl and hydroxides in the hydroponic solution. The fluorescence data of the uranium species in the cell sap and on the solid cell components are comparable with the data records of the section samples. They are identical with the fluorescence data obtained for liquid or solid uranyl phosphate complexes. This confirms the statements about the formation of uranyl phosphates as the main species after the uptake of uranium(VI) into plants /1/. The detection of uranium species in the samples of solid cell components can be described as precipitation of solid products from the cell sap or/and as uranium species sorbed on the cell wall components.

Acknowledgment

We thank Tabea Birk and Sabine Matys for the sample preparation.

References

/1/ Günther, A. et al., Radiochim. Acta (in press)

Reactive Transport of Actinides / Radionuclides

SURFACE COMPLEXATION MODELING FOR NEPTUNIUM(V) SORPTION ONTO HEMATITE

V. Brendler, T. Arnold

Based on high-quality experimental sorption data sets provided by the NEA Sorption Project Phase II , the modeling capability of SCM approaches was examined. The Constant Capacity SCM was superior to a non-electrostatic model, but both gave a satisfactory data fit. The inclusion of carbonate species left some inconsistencies, however.

The NEA Sorption Project Phase II started a comparative application assessment for the present fitting and predictive capabilities of Surface Complexation Modelling (SCM). Six test cases were supplied, one being experimental data for the sorption of neptunium(V) onto hematite /1/. The data comprised of 107 acid-base titration data points, 11 data points for carbonate sorption, and 52 data points for the Np(V) sorption at varied pH, ionic strength, solid/liquid ratio, Np content, and pCO_2. Based on a literature survey covering hematite, goethite, and ferrihydrite, only the two carbonate complexes **=FeOH-CO_2 (a)** and **=FeO-CO_3^{3-} (b)**, one Np(V) complex **=FeO-NpO_2 (c)** and one ternary Np(V)-carbonate complex **=FeO-$NpO_2(HCO_3)_2^{2-}$ (d)** turned out to be realistic.

FITEQL version 3.2 /2/ was used as fitting software. The Constant Capacitance Model (CCM) was chosen as a simple SCM, with the Non-Electrostatic Model (NEM) approach as alternative. Also, just one type of surface sites was assumed. All this supports the major goal to minimize the number of parameters. In a first step, acid-base titration data were used to optimize simultaneously the surface site density (SSD in sites / nm²) and the reaction constants for the two surface protolysis steps (pK_1 and pK_2). FITEQL can not fit the capacitance value C required by the CCM, thus it was varied manually. The obtained parameters exhibit a strong correlation, thus two scenarios were selected for CCM for all further computations: one with a nominal low weighted sum of squares over degree of freedom (WSOS/DF) and one with more realistic parameters from the plateau region (Fig. 1).

Scenario	C in F/m²	SSD	pK_1	pK_2
CCM I	1.36	9.7	8.06	11.09
CCM II	1.70	2.32	8.52	10.64
NEM	-	1.17	8.23	10.86

Tab. 1: Parameter fits for hematite surfaces

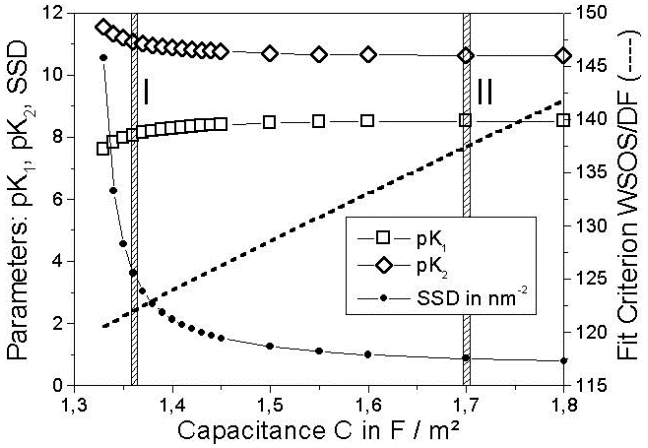

Fig. 1: Hematite surface data: Mutual dependence of the protolysis constants and the binding site density as function of the capacitance for CCM. Shaded areas indicate parameter scenarios I and II.

Next, formation constants for carbonate surface complexes were obtained from separate data sets. The above scenarios were tested with each of the two carbonate complexes, and a combination of them. For the CCM, the best fit was obtained for protolysis scenario II and the combination of the two carbonate surface complexes, with pK_a = -4.33 and pK_b = 3.21. For the NEM, only one species (a) was significant, with pK_a = -7.47. Finally, formation constants for Np(V) surface complexes were determined. For the CCM, again protolysis scenario II including both Np(V) surface species gave the best fit, with pK_c = 2.64 and pK_d = 13.84. The NEM model was not able to fit the ternary complex, leading to pK_c = 1.47.

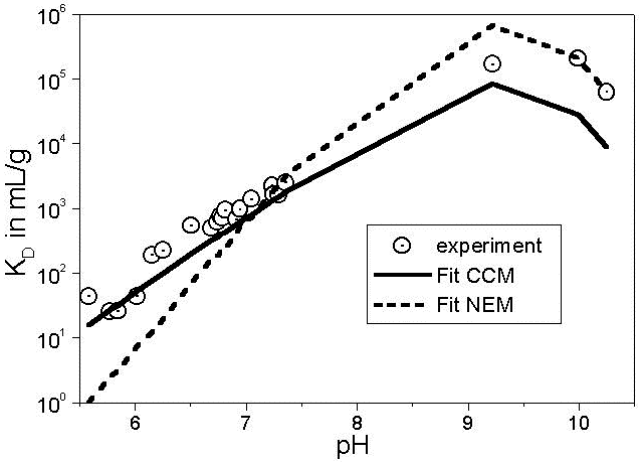

Fig. 2: Quality of fit of distribution coefficients K_D, with CCM and NEM, for sorption data at variable ionic strength, at 1 g/L Hematite, with 1.2×10^{-7} M Np, in air

Fig. 2 illustrates the quality of the sorption data fit. It can be concluded, that both the Constant Capacitance SCM and the Non-Electrostatic SCM are able to describe the sorption of Np(V) onto hematite. Formally, the pure fitting quality (WSOS/DF) is better for the electrostatic model (788 vs. 3028). CCM also better than NEM reflects chemical reality by being able to realistically include the carbonate sorption. There are no data for comparison of the surface complexation itself in the open literature.

References

/1/ Kohler, M., Honeyman, B.D., Leckie, J.O., Radiochim. Acta **85**, 33-48 (1999)

/2/ Herbelin, A.L., Westall, J.C., *FITEQL -Version 3.2.* Report 96-01, Department of Chemistry, Oregon State University, Corvallis (1996)

CURRENT PREDICTIVE CAPABILITIES OF SURFACE COMPLEXATION MODELS

V. Brendler, T. Arnold, A. Richter

The mineral-specific sorption database RES³T was exploited to extract surface complexation model parameter sets for the sorption of neptunium onto hematite. These data then were used in a blind prediction exercise and compared to sorption data records from the literature. Distribution coefficients K_D almost always differed less than one order of magnitude.

One of the major goals of the RES³T database /1/ is providing a sound foundation for the use of surface complexation models (SCM) in risk assessment studies. RES³T should finally be able to deliver recommended data sets for such SCM applications. It is, however, essential to check the general predictive capabilities of SCM before.

Experimental raw data for the sorption of neptunium(V) onto hematite, as summarized in /2/, have been provided by the NEA sorption project, see the article before. Here, the 52 data points for the Np(V) sorption at varied pH, ionic strength, solid/liquid ratio, [Np], and pCO_2 were used. This data set is especially challenging due to the measured high PZC and the sparse system information available from other sources.

The Diffuse Double Layer model was chosen as SCM variant to keep the number of parameters at a minimum. Therefore, also just one type of surface sites was assumed. The modeling was performed with the FITEQL software, version 3.2 /3/.

In a first step, a literature survey helped to define the chemical system, i.e. the set of surface species. Based on data for hematite, goethite, magnetite and ferrihydrite, two carbonate complexes and one binary Np(V) complex were selected. There was no independent information about a ternary Np(V)-carbonate surface complex available other than from /2/, thus it was not included. Below the selected species are given, with their reaction constants, averaged from literature values that were normalized to a surface site density of 12.05 sites/nm^2 according to Kulik /4/.

$\equiv FeOH_2^+$	log K = 6.58
$\equiv FeO^-$	log K = -10.15
$\equiv Fe\text{-}HCO_3$	log K = -4.75
$\equiv FeO\text{-}CO_3^{3-}$	log K = 3.10
$\equiv FeO\text{-}NpO_2$	log K = -3.31

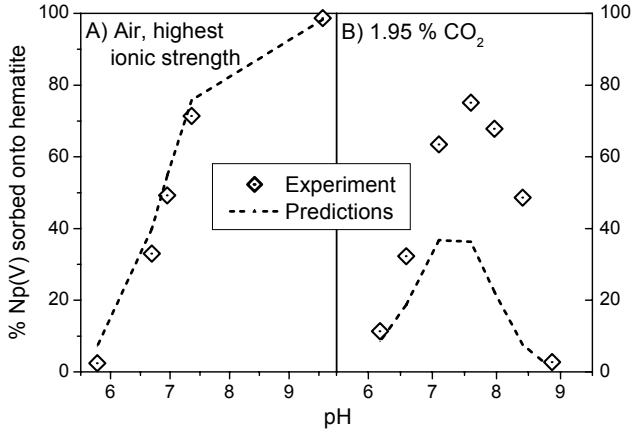

Fig. 1: Predicted percentage of Np(V) sorbed onto hematite, compared with experimental values, for the best (A) and worst (B) cases of coincidence

Fig. 1 illustrates the prediction quality for selected sorption subsets, with the best matching for the sorption under air and at the highest ionic strength of 0.1 M $NaClO_4$. The largest deviations are observed for the experiments at highest CO_2 partial pressure (1.95 % in N_2 atmosphere). These differences are clearly due to the exclusion of a ternary Np-carbonate surface complex. Fig. 2 shows, that the simulation congruence for all data subsets is within one order of magnitude when focusing on the conventional distribution coefficient K_D.

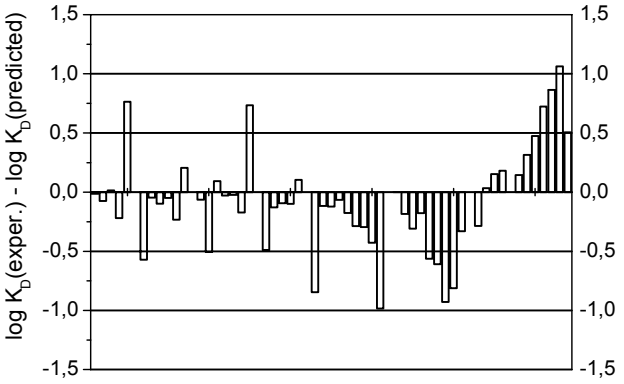

Fig. 2: Predicted Np(V) distribution coefficients K_D, compared to experimental values.

It can be concluded, that the application of SCM can indeed be very valuable for estimating distribution coefficients for contaminants in well defined mineral systems. The SCM database so far assembled within the RES³T project is able to provide the respective parameter sets. Incomplete chemical system setup is the main reason for deviations.

Acknowledgments

Funding by the German Federal Ministry of Economics and Labour (BMWA) under contract No. PtWt+E 02E9471 is gratefully acknowledged.

References

/1/ Brendler, V. et al., J. Contam. Hydrol. (2003), in press

/2/ Kohler, M. et al., 1999, Radiochim. Acta, **85**, 33-48

/3/ Herbelin, A.L., Westall, J.C., *FITEQL -Version 3.2*. Report 96-01, Department of Chemistry, Oregon State University, Corvallis (1996)

/4/ Kulik, D., Radiochim. Acta **90**, 815-832 (2002)

PREDICTING THE URANIUM(VI) SORPTION ON QUARTZ

T. Arnold, G. Bernhard

Two different U(VI) sorption data sets on quartz were provided by the NEA. The first one was used to calculate surface complex formation constants. These constants were then used to predict the K_d of U(VI) on a second quartz substrate. The K_d predictions were excellent and were all within one order of magnitude compared to experimental K_d values.

Introduction

The uranium(VI) sorption on quartz (test case 3) was studied in the framework of the NEA Sorption Project. It was a goal of this test case to determine whether the dependence of the K_d values for U(VI) sorption on chemical variables can be described with surface complexation models. The task was using the first data set of /1/ to calculate surface complex formation constants and use these calculated constants for a blind prediction of the K_d of a second data set /2/. The first data set contained U(VI) sorption data on cleaned quartz powder (Min-u-Sil 30). The specific surface area of the Min-u-Sil 30 quartz was 0,33 m^2/g and the grain size ranged from 8 to 30 µm. The sorption experiments were performed using a solid concentration of 100 g/L, with varying U(VI) concentration ranging from 1×10^{-5} M to 1×10^{-8} M in 0,01 M $NaNO_3$ solution, in air as well as 7,5 % CO_2 atmosphere. For one series a 5×10^{-4} M NaF concentration was used.

The second data set contained U(VI) sorption on a different quartz powder (Wedron #510) /2/. The specific surface area of this substrate was 0,03 m^2/g and the grain size range from 150 to 250 µm. The experimental condition of this U(VI) sorption data set on quartz in 0,1 M $NaNO_3$ covered U(VI) concentrations of $2x10^{-6}$ to $2x10^{-8}$ and a solid concentration of 2 to 50 g/L.

Approach

Acid Base titration data were provided to extract necessary values for the surface site density and the surface acidity constants. The surface acidity constant is shown in Tab. 1 and a surface site density of 0,81 sites/nm^2 was determined. The modeling was performed by using a single or a combination of the following mono- and bidentate uranium(VI) surface species:

$(SiOUO_2OH)^0$, $(SiOUO_2)^+$, $(SiOUO_2CO_3)^-$,

$(SiO_2UO_2)^0$, $(SiO_2UO_2OH)^-$,

$(SiO_2UO_2OHCO_3)^{3-}$, and $(SiO_2UO_2CO_3)^{2-}$.

Surface reaction	Log K (I = 0)
$XOH = XO^- + H^+$	-6,84
$Si(OH)_2 + UO_2^{2+} = SiO_2UO_2 + 2H^+$	-4,83
$Si(OH)_2 + UO_2^{2+} + H_2CO_3 = (SiO_2UO_2CO_3)^{2-} + 4H^+$	-12,72

Tab. 1: Surface reactions on quartz

The best fit, see Fig. 1, for the first U(VI) sorption data set was obtained for a combination of the two bidentate surface species $(SiO_2UO_2)^0$ and $(SiO_2UO_2CO_3)^{2-}$. The respective surface complex formation constants were calculated with FITEQL using the Diffuse Double Layer Model (DDLM). They are shown in Tab. 1.

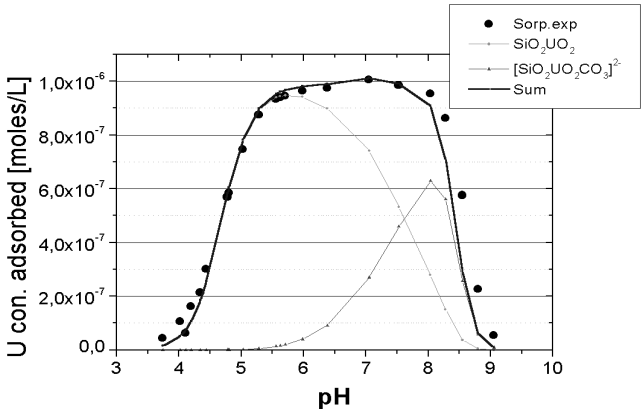

Fig. 1: Modeling the U(VI) sorption on quartz with one surface site and two surface species (1×10^{-6} M U(VI) in air)

Prediction of K_d for the second data set

The constants listed in Tab. 1 were used for a blind prediction of the sorption behavior of U(VI) on a second quartz. The prediction of the K_d for the data set 2 is shown in Fig. 2 and compared with the experimental K_d values. The predictions were excellent and were within one order of magnitude for all experimental values.

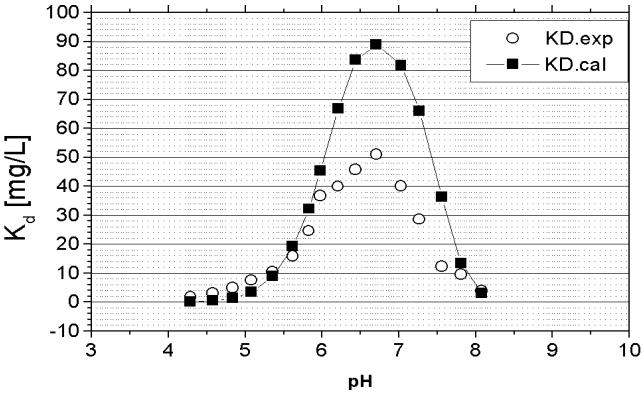

Fig. 2: Predicted K_d values compared to exp. K_d values of /2/ (2×10^{-7} M U(VI), 0,1 M $NaNO_3$, S = 50 g/L.)

References

/1/ Davis, J.A. (ed.) *Surface Complexation Modeling of Uranium(VI) Adsorption on Natural Mineral Assemblages*, Report NUREG/CR-6708, p.214 (2001)

/2/ Pabalan, R.T., Turner, D.R., Bertetti, F.P., Prikryl, J.D.; In: E.A. Jenne (ed.) *Adsorption of Metals by Geomedia*, Academic Press, Chap. 3, p.99-130 (1998)

SET UP OF A COLUMN EXPERIMENT DEVICE WITH AUTOMATED CONTROL, SAMPLING AND MEASUREMENT

J. Mibus, A. Richter, N. Betzl [1]
[1] UFZ Center for Environmental Research Leipzig-Halle, Department of Hydrogeology

A column experiment device was set up for experimental investigation of radionuclide migration in porous media. Automated operation of routine work was to improve efficiency as well as the reproducibility of experiments.

Laboratory column experiments are an important tool for analyzing the migration of radionuclides in the subsurface as well as for parameter estimation for reactive transport codes. The automation of control, sampling and measurement was to minimize the personnel and material effort, improve the reproducibility of the results and thus increase the efficiency of experimental work.

The automated multi measure point analyzer SAMSON, developed by the UFZ Center for Environmental Research Halle /1/, was adapted to these requirements. It permits fluid sampling from the saturated or unsaturated zone, measurement of physico-chemical parameters and sample conservation. Closed fluid handling guarantees compliance with radiation protection. Its modular set up makes for flexibility in experimental design.

A simplified scheme of the system is shown in Fig. 1. The base module with an integrated adjustable peristaltic pump drives the fluid flow from the sampling site via the hydraulic interface and the sensor cell to the fraction collector. Hermetically sealed pipes and fluid storage under inert gas prevent sample alteration or contamination.

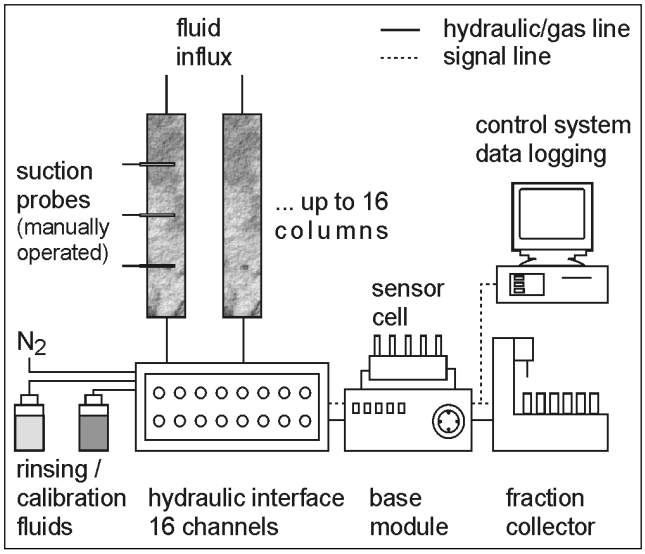

Fig. 1: Simplified scheme of the column experiment-device and the multi measure point analyzer

Every sampling procedure is preceded by a controlled multi-step rinsing procedure. The hydraulic channels for rinsing, calibration or sample fluids are selected by valves in the hydraulic interface. Sample temperature, electrolytic conductivity, pH, E_H, and dissolved oxygen are measured in the sensor cell. The cell may also be equipped with ion sensitive electrodes.

A software was developed in cooperation with the UFZ Halle for operating hydraulic components, and for data acquisition. It facilitates time-controlled or event-controlled sampling, automatic multi-point calibration at set time intervals, signal recording, statistical evaluation of measurement series and structured data storage. The software is easy to use by way of a graphical user interface.

Experimental work focuses on the characterization of source terms of radionuclides in the aeration zone. Right now the kinetic dissolution of non-radioactive model substances (such as gypsum) with homogeneous or heterogeneous distribution of the material is being investigated and modeled /2/. Than the weathering of uraninite (UO_2) and the release of uranium will be studied. A fine sand is used as matrix material in all cases.

Emphasis is also placed on the adsorption of radionuclides on materials that are typical of geological or engineered barriers, such as calcite or hydroxyapatite (HAP). A well-suited application is the monitoring of tracer breakthrough (e.g. tritiated water).

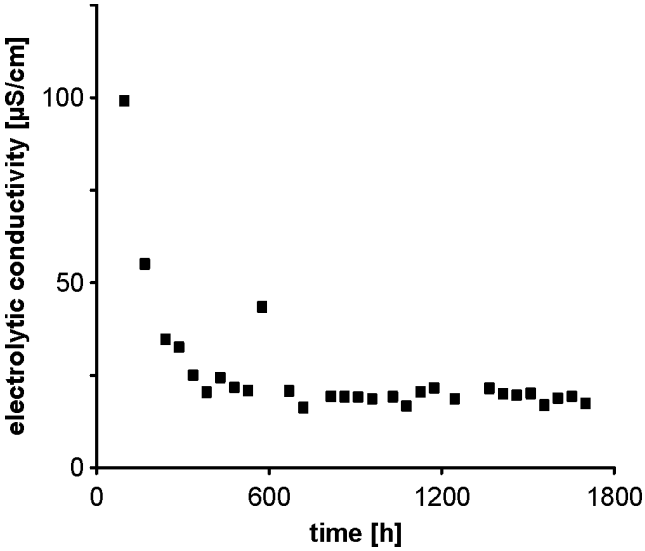

Fig. 2: Electrolytic conductivity at the outflow of the HAP column

Some first results are shown in Fig. 2. After a first flush-out of dissolved components from the aquifer material, an equilibration to HAP is observed. The next step will be the injection of uranyl solution for sorption studies.

Long-term operation of the device should prove that the automated system produces more stable and reproducible results than manual measurement.

References

/1/ Lazik, D. et al.: Modulares Vielkanalprobenahme- und Meßsystem zur automatischen Langzeitanalyse von Fluiden für hydrogeologische Feld- und Laborversuche. Patent DE19758356A1 (1999)

/2/ Mibus, J. et al., Report FZR-343 (2002) p. 43

Spectroscopic Speciation Methods

WAVELET ANALYSIS OF EXAFS DATA – FIRST APPLICATION

H. Funke, M. Chukalina[1], A. Roßberg
[1]Institute of Microelectronics Technology RAS, Chernogolovka, Russia

We propose to complement the conventional method of EXAFS analysis, Fourier transform, with wavelet transform. The method of operation and the advantage of the wavelet analysis is demonstrated by using EXAFS spectra of U (VI) complexes with acetic, formic and glycolic acid.

Introduction

Complementing the conventional Fourier transform (FT), the wavelet transform (WT) is able to extract more information from the k-dependence of the absorption signals. While the FT analyzes the distances of the back scattering atoms, WT reveals additionally at which energies, that means at which wave-numbers k, the back scattering takes place. Thus wavelet analysis can differentiate between heavier and lighter back scattering atoms, even if they are at the same distance from the central atom.

The expression of the WT of the k^3-weighted EXAFS data is

$$W_\chi^\psi(k,R) = \sqrt{2R}\int \chi(k')k'^3\psi(2R(k'-k))dk'$$

where χ(k) is the EXAFS signal, ψ(x) is the wavelet (Morlet), k is the wave number, and R corresponds to the R+Δ value in the FT. Like the FT, the WT is a mathematical one-to-one transformation of a signal, here the EXAFS spectrum. Hence, its inverse transformation recovers again the primary EXAFS signal without any loss of information. For more details see /1/ or, more general, e.g. /2/.

We applied the WT to improve the interpretation of EXAFS spectra of U(VI)-carboxylate complexes. As model compounds we used acetic acid (U-Acet), formic acid (U-Form), and glycolic acid (U-Glyc). For ligands U-Acet and U-Form, U(VI) can interact with carboxylic oxygen atoms only. For ligand U-Glyc, however, U(VI) may interact with both the hydroxyl and the carboxylate groups.

Experimental

Three aqueous solutions were prepared at room temperature. U-Acet: [U(VI)] = 0.025 mol/L, [acetic acid] = 0.5 mol/L, pH = 4.5. U-Form: [U(VI)] = 0.053 mol/L, [formic acid] = 1.0 mol/L, pH = 4.5. U-Glyc: [U(VI)] = 0.02 mol/L, [glycolic acid] = 0.25 mol/L, pH = 8. U L_{III}-edge EXAFS spectra were measured at ROBL/ESRF. The spectra were processed following standard procedures using EXAFSPAK.

Results

The FT of all three samples show maxima in the range R+Δ = 3.0…4.0 Å. The source of these maxima is, however, different for the different complexes. For U-Acet, FT maxima in the region R+Δ = 3.4…3.9 Å are caused by the six fold degenerated, 3-legged, multiple scattering path U-C_1-C_2 and by the single scattering path U-C_2. /3/. For U-Glyc, FT maxima in a similar FT-range are caused by backscattering from uranium at a distance of 3.81 ±0.02 Å /4/. The FT of U-Form shows a broad peak between R+Δ = 3.1…4.0 Å, which cannot be analyzed and separated using conventional FT-filtering technique.

We analyzed the WT of all three spectra within the range R+Δ = 3.2…4.1 Å, and plotted the resulting WT against the distance R and the wavenumber k. The plot of U-Acet is dominated by a maximum at 7.5 $Å^{-1}$, corresponding to multiscattering from relatively light C atoms at a distance of 3.7 Å from U. The plot of U-Glyc shows a maximum at about 12 $Å^{-1}$, corresponding to the heavy backscatterer U at a distance of 3.6 Å from another U atom.

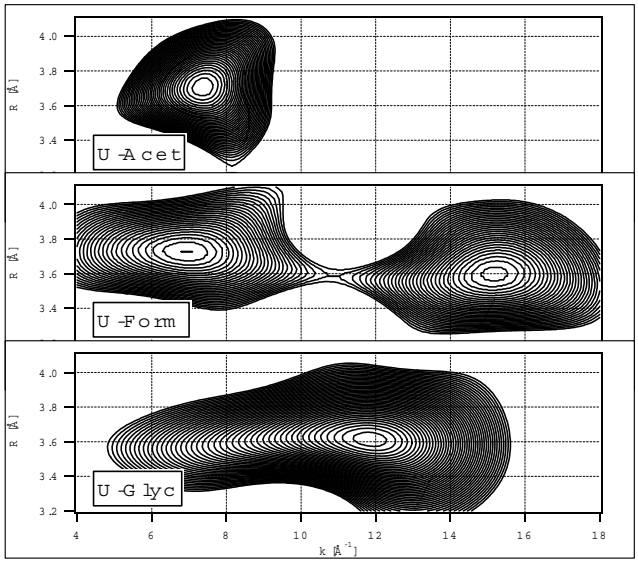

The plot of U-Form shows two separated peaks, one at about 7 $Å^{-1}$ and a distance of 3.7 Å, the second at about 15 $Å^{-1}$ and a distance of 3.6 Å. This means that WT is able to detect a light and a heavy backscatterer at very similar distances (ΔR = 0.1 Å). The extinction in the center of the WT of U-Form is a consequence of the interference of the similar backscattering waves from uranium and multiscattering waves from carbon. Therefore, the WT analysis suggests for U-Form both U-O_{ax}-U and U-O_{eq}-C structural elements, which may be interpreted as the formation of poly-nuclear U(VI)/formic acid complexes.

In contrast to the clear separation by WT of the two different atoms at very similar distances, FT analysis was not able to resolve the two types of atoms.

This example shows that the combined application of WT and FT analysis is able to provide both short range distances and identity of neighboring atoms with unprecedented precision, and therefore may significantly improve the elucidation of complex structures.

References

/1/ Funke, H. et al., Report FZR-343, p. 45 (2002)
/2/ Mallat, S., *A wavelet tour of signal processing,* Academic Press, 1999
/3/ Roßberg, A., Ph.D. Thesis, TU Dresden, (2002)
/4/ Moll, H. et al., Radiochimica Acta **90**, 1-10 (2002)

EXAFS INVESTIGATION OF URANIUM(VI) ADENOSINE PHOSPHATE COMPLEXES

C. Hennig, G. Geipel, G. Bernhard

The local structure of U(VI) adenosine monophosphate (U-AMP) and triphosphate (U-ATP) was investigated by U L_{III}-edge EXAFS. In both structures, U(VI) forms monodentate complexes with the phosphate groups.

Introduction

Previous EXAFS experiments have shown, that U(VI) accumulated by various bacteria is bound to phosphoryl groups /1-3/. Important phosphate-containing enzymatic compounds in living cells are nucleoside phosphates. Divalent metal ions like Ca^{2+} and Mg^{2+} catalyze the dephosphorylation of nucleoside phosphates, while UO_2^{2+} inhibits the functionality of Ca^{2+} and Mg^{2+} adenosine triphosphatase /4/ and other enzymatic molecules. Hence, understanding the complex formation between adenosine phosphates and UO_2^{2+} ions helps to understand the interaction of U(VI) with organisms, which in turn may be relevant to predict the fate of U(VI) in the environment. Due to the lack of crystallinity, only spectroscopic methods are useful for investigation of uranium (VI) adenosine phosphate structures. EXAFS measurements were performed in order to determine the uranyl ion binding sites in ATP and AMP.

Experiment

U-ATP and U-AMP were prepared by mixing 1 M uranyl nitrate solution with 1 M adenosine 5'-triphosphoric acid and adenosine 5'-monophosphoric acid solutions at pH 1.8 - 2.5 and room temperature. The yellow, gelatinous precipitates were filtered, washed and dried. X-ray powder diffraction showed that the precipitates are non-crystalline. EXAFS experiments were performed at the ROBL beam line at ESRF.

Results and Discussion

Uranium may bind to adenosine phosphate via bonds involving the oxygen atoms of the phosphate groups, the oxygen atoms of the ribose and the nitrogen atoms of the adenine heterocycle. In contrast to the octahedral coordination of Mg^{2+}-ATP, the coordination geometry of UO_2^{2+}-ATP is restricted to the equatorial plane. Fig. 1 shows the U L_{III}-edge EXAFS spectra of U-AMP and U-ATP. The first peak of the Fourier Transform (FT) originates from the uranyl oxo groups (O_{ax}). Due to the possible arrangement of U (VI) with phosphate, ribose or adenine groups, the second shell may arise from either O or N in the equatorial plane of uranyl. Both backscatterers cannot be distinguished by EXAFS, hence O was chosen for the fit. The fit results (Tab. 1) reveal different coordination distances for U-AMP and U-ATP: U-ATP has an U-O_{eq} distance of 2.36 Å, whereas the equatorial shell of U-AMP is split into two distances of 2.36 Å and 2.54 Å. Hence, complex formation of U-AMP and U-ATP is clearly different, but the U-N,O_{eq} distances do not allow to distinguish between coordination via adenine N, ribose O or phosphate O. The lack of U-U interaction allows to exclude the formation of polynuclear species.

The weak but significant peak at R+Δ = 3 Å was best fit with P. The U-P distance of 3.87 Å (U-AMP) and 3.61 Å (U-ATP) indicate monodentate binding of U to phosphate groups. The observed low coordination number of U-P may be biased by multiple scattering effects and could be higher. In contrast to the data shown here, formation of a bidentate coordination between U and the terminal phosphate groups of AMP have been observed for asparagine synthease /5/. This indicates, that U(VI) may bind to adenosine phosphates in several ways, depending on the actual chemical and physiological situation.

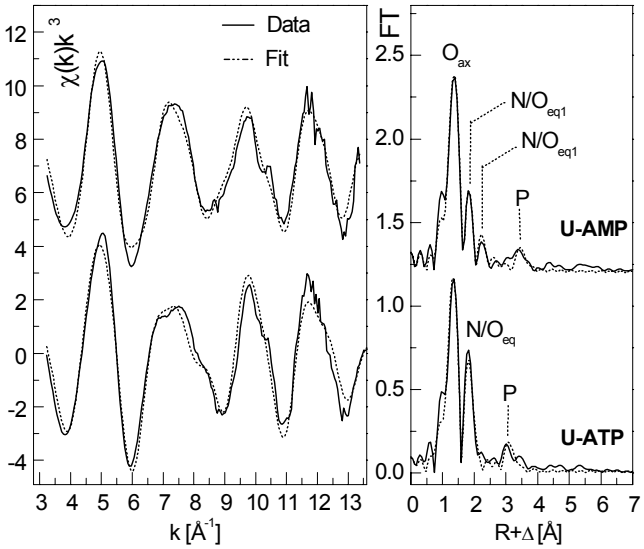

Fig. 1: U L_{III}-edge EXAFS spectra of U-AMP and U-ATP (left) and their Fourier transform (right).

Sample	Shell	R [Å]	N	σ^2 [Å^2]
U-AMP	U-O_{ax}	1.791(2)	2.2(1)	0.0021(2)
	U-MS	3.58	2.2	0.0042
	U-N/O_{eq1}	2.356(4)	2	0.0061(5)
	U-N/O_{eq2}	2.541(8)	3	0.0055(6)
	U-P	3.871(6)	0.9(4)	0.0024(2)
U-ATP	U-O_{ax}	1.773(1)	1.9(1)	0.0019(2)
	U-MS	3.546	1.9	0.0038
	U-N/O_{eq}	2.361(4)	4.1(3)	0.0073(6)
	U-P	3.606(7)	1.0(3)	0.002(1)

Tab. 1: EXAFS structural parameters

References

/1/ Hennig, C. et al., Radiochim. Acta **89**, 625 (2001)
/2/ Merroun, M. et al., Radiochim. Acta, in press
/3/ Kelly, S.D. et al., J. Synchrotron Rad. **8**, 846 (2001)
/4/ Thompson, J.D. et al., J. Tox. Env. Health **7**, 901(1981)
/5/ Larsen, T.M. et al., Biochemistry **39**, 733 (2000)

THE STRUCTURE OF URANIUM (VI) OXYISOBUTYRATE: AN XRD AND U L_{III} EXAFS STUDY

C. Hennig, W. Kraus[1], H. Moll
[1]Bundesanstalt für Materialforschung und -prüfung, Richard-Willstätter-Str. 11, D-12489 Berlin

In solid $UO_2[OC(CH_3)_2COO]_2$, uranyl forms both monodentate and chelating bonds with the α-hydroxy isobutyrate ligands.

Introduction

Complexation by carboxylate is an important uptake mechanism for U (VI) by plants organisms. We used α-hydroxyisobutyrate as a model compound to study the exact structure of such U (VI) carboxylate complexes in the presence of an α-hydroxy group.

Experimental

Uranium (VI) α-hydroxyisobutyrate was prepared in aqueous solution using 11 mL of 0.09 M uranyl acetate and 5 mL of a 50% α-hydroxyisobutyric acid (H_2IBA) following the procedure of Udupa /1/. To minimize the formation of hydrolytic species of U (VI) the synthesis was performed at pH 1.8. At this pH, the α-hydroxo group is hydrated and the carboxylate group is deprotonated ($HIBA^-$). The calculated speciation of the solution is 65% $UO_2[HIBA]_3^-$, 30% $UO_2[HIBA]_2$ and 5% $UO_2[HIBA]^+$. The precipitate was filtrated, washed and dried, and used for U-L_{III} edge EXAFS analysis to determine the short-range structure. A single crystal was separated and used for structure analysis by XRD. In addition, a solution of 0.01 M U(VI) and 0.6 M H_2IBA at pH 2.6 with a speciation of 50% $UO_2[HIBA]_3^-$, 38% $UO_2[HIBA]_2$ and 12% $UO_2[HIBA]^+$ was investigated with EXAFS.

Results and discussion

The crystal structure of $UO_2[OC(CH_3)_2COO]_2$ as determined by XRD contains two symmetry-independent α-oxyisobutyrate ligands. Uranium (VI) is coordinated in a distorted pentagonal bipyramid as shown in Fig. 1.

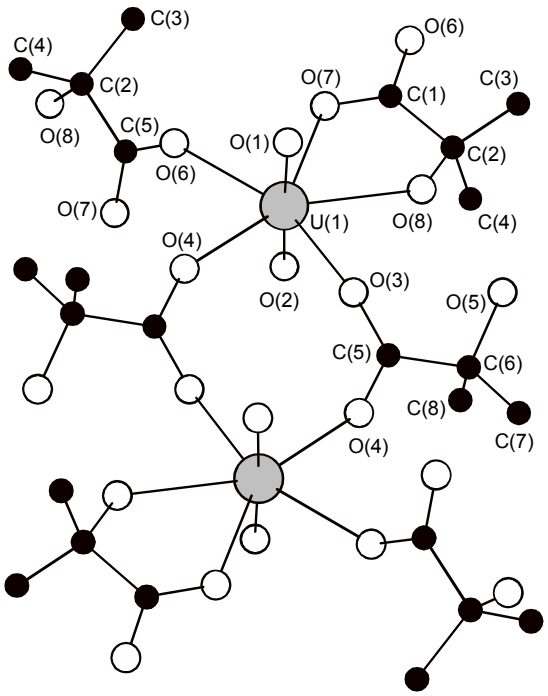

Fig. 1: Uranium (VI) $[OC(CH_3)_2COO]_2$ coordination

The apices of the bipyramid are occupied by the uranyl oxygens O(1) and O(2). The equatorial plane contains three carboxylic oxygen atoms in monodentate fashion (O(3), O(4), O(6)). In addition, U(VI) forms a chelate complex with the carboxylic oxygen O(7) and the oxo atom O(8). The second isobutyrate ligand keeps its hydroxo hydrogen atom O(5) and is not involved in the coordination.

XRD		(^{c} – chelate, ^{m} – monodentate)			
U-O(1)	1.78	U-O(5)	4.21	U-C1^c	3.28
U-O(2)	1.78	U-O(6)	2.37	U-C1^m	3.42
U-O(3)	2.30	U-O(7)	2.41	U-(C2)	3.48
U-O(4)	2.33	U-O(8)	2.48	U-U	5.78
EXAFS					
Solid sample		$U\text{-}O_{ax}$	1.77	$U\text{-}O_{eq2}$	2.44
		$U\text{-}O_{eq1}$	2.35	U-U	4.02
Liquid sample /4/		$U\text{-}O_{ax}$	1.78	U-C	2.86
		$U\text{-}O_{eq1}$	2.42		

Tab. 1: Selected atomic distances in Å

Uranium glycolate in solution is coordinated exclusively via carboxylate groups at low pH, whereas the proton of the α-hydroxy group dissociates just above pH 3.5 forming chelate sequences such as $UO_2[OCH_2COO]_p^{2-2p}$ /2/. XRD and IR analysis of the solid, $UO_2[OHCH_2COO)_2$, showed that the α-hydroxy-group is protonated /3/. It is a surprising result that the corresponding solid of uranium (VI) α-dioxoisobutyrate prepared at pH 1.8 contains deprotonated α-hydroxy groups as confirmed by IR spectroscopy.

The structural parameters obtained by EXAFS are summarized in Tab. 1. The $U\text{-}O_{eq}$ distances of 2.35 Å and 2.44 Å are in line with monodentate and bidentate coordination, respectively. Both values agree with the average distances derived by XRD. However, the U-U distance obtained by XRD is 5.78 Å whereas the one obtained by EXAFS is 4.02 Å. This shorter distance indicates the presence of uranyl dimers in the precipitate. The feature originates probably from UO_2L_1 or UO_2L_3 and seems to be correlated with a significant amorphous background of the XRD pattern, while the resolved sharp peaks correspond to the crystalline structure presented in Fig. 1.

In contrast to the solid compound, the solution is dominated by the $UO_2[HIBA]_3^-$ species. Depending on pH, $U\text{-}O_{eq}$ distances between 2.40 Å at pH 2 and 2.43 Å at pH 4 and a U-C distance of 2.9 Å were observed /4/. In contrast to the solid sample a U-U interaction is missing. The observed distances indicate that U (VI) forms predominantly bidentate complexes with oxyisobutyrate ligands.

References

/1/ Udupa, M.R., Thermochimica Acta **53**, 225 (1982)
/2/ Szabó, Z., Grenthe, I., Inorg. Chem. **39**, 5036 (2000)
/3/ Mentzen, B.F. et al., Acta Cryst. B **36**, 2051 (1980)
/4/ Moll., H. et al., Radiochim. Acta **91**, 11 (2003)

SOLID URANIUM(VI) COMPLEXES WITH DIFFERENT AMINO ACIDS STUDIED BY EXAFS

H. Moll, T. Reich, C. Hennig, H. Funke, A. Roßberg, K. Henkel, A. Scholz, G. Bernhard

Solid uranyl complexes of α-aminoisobutyric acid, ß-aminobutanoic acid, and γ-aminobutanoic acid were synthesized and characterized. The aim was the detection of structural changes of the formed compounds using the EXAFS technique.

As a continuation of our project dealing with the complex formation of uranium with alpha-substituted carboxylic acids in aqueous solution, we investigated the structure of solid complexes of uranyl with selected aminoacids /1/. The aim of this EXAFS study was the observation of structural changes of solid uranium(VI) complexes with selected aminoacids having the amino group at different positions within the organic molecule.

Experimental

The aminoacids (HL) used were α-aminoisobutyric acid (HL^1), ß-aminobutanoic acid (HL^2), and γ-aminobutanoic acid (HL^3). The reactions were performed in aqueous solution at different molar ratios (UO_2:HL = 1:1, 1:2, 1:3). The products were isolated by slow evaporation of the solvent. The elemental composition of the compounds were determined using TOC, TN ICP-MS, and ion chromatography. Furthermore, the solids were analyzed by XRD and thermal analysis. For the EXAFS measurements, the precipitates were mixed with teflon powder and pressed into pellets of 13 mm diameter. The EXAFS data were recorded at the Rossendorf Beamline (ROBL) at the ESRF in Grenoble /2/.

Results

We observed the formation of three types of complexes of uranium(VI) and α-aminoisobutyric acid (1:1, 1:2, 1:3). Only the tris complex was isolated with γ-aminobutanoic acid (HL^3). This is in agreement with the findings of Bismondo et al. /3/. Whereas no solid complexes could be obtained with ß-aminobutanoic acid (HL^2).

Sample	Shell	N	R (Å)	σ (Å^2)
A $UO_2[HL^1](NO_3)_2$	U-O_{ax}	2f	1.76	0.0017
	U-O_{eq}	5.0	2.39	0.0126
B $UO_2[HL^1]_2(NO_3)_2xH_2O$	U-O_{ax}	2f	1.77	0.0017
	U-O_{eq}	5.2	2.36	0.0152
C $UO_2[HL^1]_3(NO_3)_2xH_2O$	U-O_{ax}	2f	1.77	0.0016
	U-O_{eq}	4.8	2.37	0.0103
D $UO_2[HL^3]_3(NO_3)_2xH_2O$	U-O_{ax}	2f	1.77	0.0022
	U-O_{eq}	5.7	2.47	0.0058
	U-C	3.0	2.87	0.0034

The 95% confidence limits for the bond length (R) and coordination numbers (N) are the following: U-O_{ax} ±0.003 Å; U-O_{eq} ±0.01 Å and 16%; U-C ±0.01 Å and 33%, respectively. f: parameter fixed during the fit.

Tab. 1: Summary of the EXAFS structural parameters

Fig. 1 depicts the EXAFS spectra and the corresponding Fourier transforms (FT) measured for the synthesized compounds, whereas Tab. 1 summarizes the structural parameters determined. The U-O_{eq} distance can be used as an indicator for the coordination mode of carboxylate ligands to the uranyl center (see Tab. 1). For sample A we measured an U-O_{eq} distance of 2.39 Å. This value is shorter than expected for a bidentate coordination of the carboxylic group of the aminoacid. Most likely the α-aminoisobutyric acid is coordinated in the 1:1 complex via one oxygen of the carboxylic group to the uranyl center.

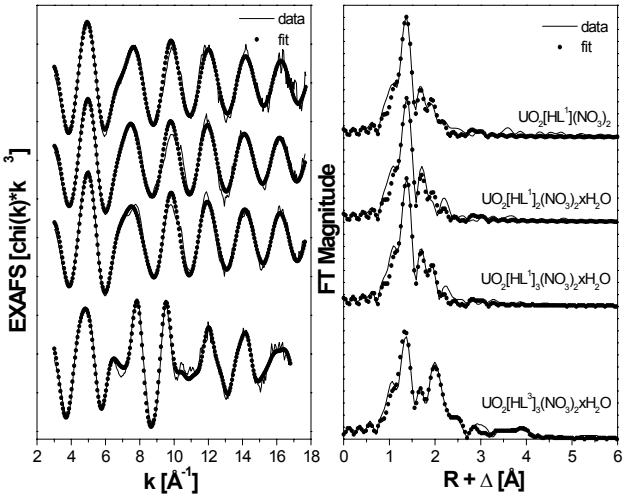

Fig. 1: U L_{III}-edge k^3-weighted EXAFS spectra (left) and corresponding Fourier transforms (right) of the synthesized solids. Solid line – experiment; dots – theoretical fit.

If more than one aminoacid is coordinated, we observed a slight decrease of the U-O_{eq} distance by 0.03 Å. The results indicate that the aminoacid is monodentate coordinated via one oxygen of the carboxylic group independent from the coordination number of the α-aminoisobutyric acid. The presented results are in agreement with findings of these complexes in solution /1/. The EXAFS spectrum of $UO_2[HL^3]_3(NO_3)_2xH_2O$ looks different compared to the other data (see Fig. 1). The measured U-O_{eq} and U-C distances of 2.47 and 2.87 Å, respectively, are characteristic for bidentate coordination of the carboxylic group. The structural parameters are in agreement with those reported by Bismondo et al. /3/. If the amino group moves farther away from the carboxylic group, we detected a bidentate coordinated aminoacid via the two oxygens of the carboxylic group. The coordination mode changed to monodentate coordination of the ligand via one oxygen of the carboxylic group when the amino group is in α-position. Based on the presented experimental results we found no evidence for the formation of chelate species involving the amino group.

References

/1/ Moll, H. et al., Radiochim. Acta **91**, 11-20 (2003)
/2/ Reich, T. et al., Radiochim. Acta **88**, 633 (2000)
/3/ Bismondo, A. et al., Inorg. Chim. Acta **110**, 205 (1985)

COMPLEXATION OF U(VI) AND MONOCHLOROACETIC ACID - ITERATIVE TRANSFORMATION FACTOR ANALYSIS OF EXAFS SPECTRA

A. Roßberg, G. Geipel, G. Bernhard

Iterative Transformation Factor Analysis (ITFA) was used to derive the EXAFS spectrum of the aqueous U(VI)/monochloroacetic acid complex. The isolated EXAFS spectrum shows axial O atoms at a distance of 1.79 Å and equatorial O atoms at 2.30 Å. The source of a third peak, which consistently appears in the Fouriertransform of the spectra of U(VI) complexes in plants /1/, is still unclear.

Introduction

Our goal was the investigation of the interaction of U(VI) with organic compounds, which contain strongly acidic carboxylic groups, using U-L_{III} edge EXAFS. As model we used monochloroacetic acid (Clac) (pK_s = 2.66 at T = 25°C and IS = 1 mol/L). Since the aqueous U(VI)-Clac complex cannot be prepared in chemically pure form, we employed ITFA to derive the EXAFS spectrum of this complex /2/.

Experimental

We prepared three samples with [U(VI)] = 0.075 mol/L, [Clac] = 1.0 mol/L, and a pH of 1.00, 2.25 and 4.00. In this pH range the three complex species $UO_2(H_2O)_5^{2+}$, 1:1 U(VI)/Clac and 1:2 U(VI)/Clac coexist. Using published stability constants /3,4/, we calculated the following compositions: at pH 1.00 60% $UO_2(H_2O)_5^{2+}$, 35% 1:1, 5% 1:2; at pH 2.25 5% $UO_2(H_2O)_5^{2+}$, 36% 1:1, 59% 1:2; at pH 4.00 1% $UO_2(H_2O)_5^{2+}$, 16% 1:1, 83% 1:2. The U L_{III}-edge EXAFS spectra were recorded at the Rossendorf Beamline (ROBL) at the ESRF /5/.

Results

Fig. 1 shows the EXAFS spectra of the U(VI)/Clac samples and their Fourier Transforms (FT) at three pH values. All spectra are well fit by assuming two spectral components (reproductions are shown with dotted lines).

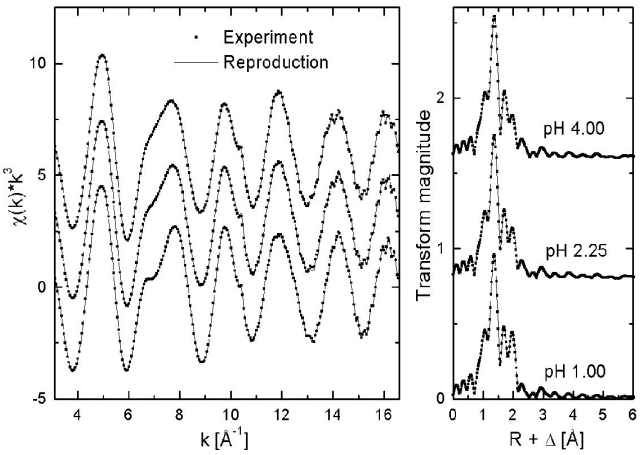

Fig. 1: U L_{III}-edge k^3-weighted EXAFS spectra (left) and corresponding FT (right)

One component is the EXAFS signal of coordinated water molecules. If one assume that for the 1:1 complex 4 water molecules and for the 1:2 complex 3 water molecules coordinate at U(VI), then one can calculate the sum of coordinated water molecules using the result of the speciation calculation. According to these calculations 4.6 water molecules are coordinated to U(VI) atom at pH 1.00, and 3.2 water molecules at pH 4.00. Based on this information, ITFA can be used to derive the EXAFS spectra of the pure complex species (Fig. 2).

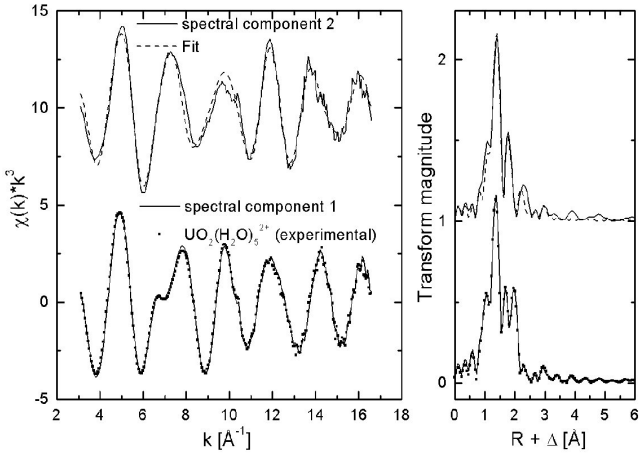

Fig. 2: U L_{III}-edge k^3-weighted EXAFS spectra (left) of the isolated spectral components and corresponding FT (right). Dotted line experimental EXAFS spectrum of $UO_2(H_2O)_5^{2+}$

The isolated spectral component 1 matches the experimental EXAFS spectrum of $UO_2(H_2O)_5^{2+}$ (Fig. 2, bottom). In this species five water molecules are arranged in the equatorial plane of U(VI) with a radial bond distance of 2.41 Å. The fit of spectral component 2 is shown in Fig. 2. The radial distance between U and the axial oxygen atoms is 1.79 Å (first peak in the FT). If one considers two equatorial oxygen shells (O_{eq1}, O_{eq2}) one obtains 3 O_{eq1} at a radial bond distance of 2.30 Å (σ^2 = 0.004 Å^2), and 2 O_{eq2} with a radial bond distance of 2.50 Å (σ^2 was held constant at 0.008 Å^2). Note that the fit does not fully match the third peak at 2.4 Å in the FT (Fig. 2). The origin of this peak is currently under investigation. We suppose that in case of spectral component 2 a special coordination between U(VI) and the carboxylic group exists, which is also present in the U-L_{III} EXAFS spectra of U-exposed plants /6/.

References

/1/ Günther, A. et al., Radiochim. Acta, in press
/2/ Roßberg, A. Ph.D. Thesis, Technische Universität Dresden (2002)
/3/ Hala, J. et al., Coll. Czechoslov. Chem. Commun. **27**, 1697 (1962)
/4/ Ahrland, S., Acta Chem. Scand. **3**, 783 (1949)
/5/ Reich, T. et al., Radiochim. Acta **88**, 633 (2000)
/6/ Roßberg, A. et al., Report FZR-373, p. 48 (2003)

AN UNRESOLVED PROBLEM IN THE U L_{III}-EDGE EXAFS SPECTRA OF ORGANIC COMPLEXES: THE 2.4 Å FOURIER TRANSFORM PEAK

A. Roßberg, A. Günther, G. Geipel, G. Bernhard

The U L_{III}-edge EXAFS spectra of U(VI)-treated plants show a small but significant peak in the Fourier Transform (FT), which is also present in the EXAFS spectra of U(VI) monochloroacetic acid, salicylic acid and 2,3-dihydroxybenzoic acid. While this peak indicates a structural feature common to all the complexes, the feature itself remains unresolved.

Introduction

In the U L_{III}-edge EXAFS spectra of U(VI)-treated plants, a small but significant peak in the Fourier Transform (FT) at 2.4 Å has been previously observed, but could not be fit /1/. In order to resolve the structural cause of this peak, we investigated EXAFS spectra of a suite of U(VI) reference complexes, including monochloroacetic acid (Clac), salicylic acid (Sal), and 2,3-dihydroxybenzoic acid (Diba), and compared them with the spectrum of an U(VI)-treated Lupinus root.

Experimental

The UL_{III}-edge EXAFS spectra of the following systems were analyzed: U(VI)/Clac (mathematically isolated EXAFS spectrum of an U(VI)/Clac complex /2/), the root of Lupinus after 14 days of contact with U(VI) contaminated hydroponic solution ([U(VI)] = $1 \cdot 10^{-4}$ mol/L, pH = 8), U(VI)/Sal (pH 6), and U(VI)/Diba (pH 4). The EXAFS spectra were recorded at room temperature at ROBL/ESRF /3/.

Results

Figure 1 shows the EXAFS spectra of the four samples and their corresponding FT (for comparison purposes the spectrum of Clac is plotted on top of the other spectra). Except for Diba, the FT were calculated using a k-range of 3.1-12.4 $Å^{-1}$. The arrow (Fig. 1) shows that a peak at 2.35 Å is present in all samples except for Diba, where only a shorter k-range was available.

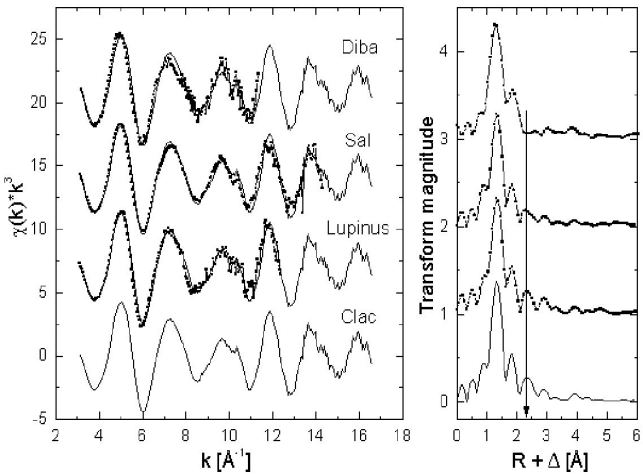

Fig. 1: U L_{III}-edge k^3-weighted EXAFS spectra (left) and their corresponding FT (right) of the U(VI) complexes with Clac (fine line), Lupinus, Sal, and Diba.

The EXAFS spectrum of the U(VI)/Clac complex matches those of the samples Sal and Diba reasonably well, but the best agreement is with Lupinus. All four spectra can be fit with two axial oxygen atoms at a radial distance of 1.78 ±0.02 Å, and with equatorial oxygen atoms at 2.30 ±0.02 Å.

To isolate the peak at 2.35 Å, FT filtering was applied in the R range 2.08 to 2.68 Å. Fig. 2 shows the EXAFS signal and the FT of the filtered peak. The sinusoidal EXAFS oscillations of Clac, Lupinus and Sal are almost perfectly in phase. Furthermore, the EXAFS amplitude envelopes of Clac and Lupinus are very similar.

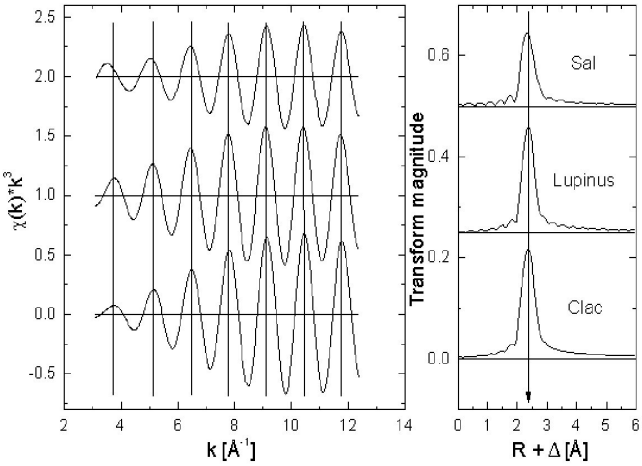

Fig. 2: FT-filtered (3.1-12.4 $Å^{-1}$) EXAFS spectra (left) and their corresponding FT

If this isolated wave function would stem from backscattering of a light element like O or C, one would expect that the maximum of the amplitude function would appear at a lower k-range than the observed 10.5 $Å^{-1}$ (Fig. 2). However, we could model the peak with two light atoms at distances of about 2.80 Å. We currently investigate possible structural arrangements which could explain such a scattering contribution. Since the EXAFS spectra of all four samples are so similar, we expect a very similar short-range structure, which is worthwhile to study in more detail.

References

/1/ Günther, A. et al., Radiochim. Acta, in press
/2/ Roßberg, A. et al., Report FZR-373, p. 47 (2003)
/3/ Reich, T. et al., Radiochim. Acta **88**, 633 (2000)

ENERGY TRANSFER REACTIONS IN LANTHANIDE COMPLEXES

G. Geipel

Up to now we have no experimental data on energy transfer from organic ligands to a complexed uranium(VI) ion. However, several lanthanides are known to show this effect. To obtain information about energy transfer reactions we studied the fluorescence emission of terbium and samarium in combination with several ligands.

To record the fluorescence spectra of terbium and samarium we used the setup for time-resolved laser-induced fluorescence spectroscopy (TRLFS), which is commonly used for TRLFS of uranium. The samples were excited at 266 nm. The applied laser energy was about 300 µJ, so as to avoid destroying the organic ligand. Solutions were prepared by mixing a stock solution of terbium or samarium with the ligand in question. The measured solutions were 5E-5 M in metal concentration and 5E-4 M in ligand concentration. The pH was adjusted to 4.0. For terbium the spectra were recorded in a delay range from 0 to 500 µs and for samarium from 0 to 10 µs.

In the pure lanthanide solutions only terbium shows a low fluorescence emission due to the weak and broad absorption at around 260 nm. Samarium itself does not show any fluorescence, when excited with laser pulses at 266 nm, but it has an absorption band at 401.2 nm.

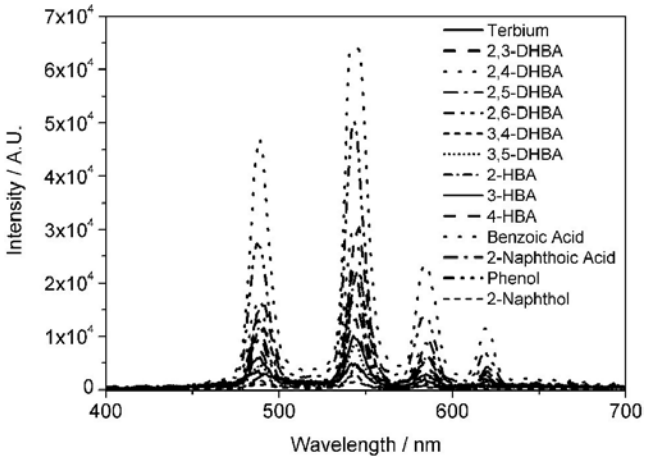

Fig. 1: Change in the fluorescence intensity of terbium depending on the ligand added, 40 µs after the laser pulse

Fig. 1 shows the fluorescence spectra of terbium at a delay of 40 µs after applying the laser pulse. The fluorescence lifetimes vary in a wide range from 26.8 µs for 2-naphthoic acid to around 170 µs for phenol and 2- naphthol. The calculated fluorescence intensities for the emission maximum at 543.5 nm at t = 0 also vary widely. No increase in fluorescence intensity was observed for 3,4-dihydroxybenzoic acid (3,4-DHBA), phenol and 2-naphthol, while benzoic acid, 2-naphthoic acid, 2,4-dihydroxybenzoic acid (2,4-DHBA) and 2,6-dihydroxybenzoic acid (2,6-DHBA) showed the most intense change in fluorescence intensity. A big increase in the fluorescence of terbium was caused by 4-hydroxybenzoic acid (4-HBA) and salicylic acid (2-HBA). 2,3-dihydroxybenzoic acid (2,3-DHBA), 2,5-dihydroxbenzoic acid (2,5-DHBA), 3,5-dihydroxybenzoic acid (3,5-DHBA) and 3-hydroxybenzoic acid (3-HBA) showed only a slight increase in intensity by a factor up to 4.

The recorded TRLFS spectra with the various ligands showed no change in the maxima of fluorescence emission, but the intensity and the fluorescence lifetime changed.

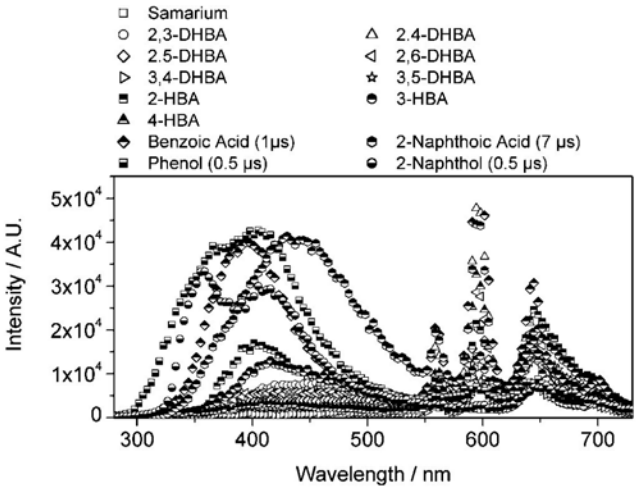

Fig. 2: Change in the fluorescence intensity of samarium and the ligand added.

The results obtained from the samarium fluorescence spectra do not vary greatly from the observations in the terbium systems. Fig. 2 shows the recorded fluorescence spectra at a delay of 0 µs. Exceptions had to be made for benzoic acid and 2-naphthoic acid in vies of the extremely high fluorescence intensity of both components, the ligand and the metal ion. For phenol and 2-naphthol the increased delay was required by the fluorescence of the ligand.

The spectra also show the broad emission of the ligand. We tried to correlate the fluorescence emission at 401.2 nm of the ligand with the fluorescence emission of samarium. However, no constant factor was found for the various ligands used. The most efficient system for energy transfer are 3,4-DHBA and 4-HBA. Here the ratio of the fluorescence of the ligand at 401.2 nm to the fluorescence of samarium at 596.6 nm was found to be more than 10. Most of the other ligands show ratios between 1 and 10. For benzoic acid and 2-naphthoic acid ratios less than 1 were found. However, the fluorescence emission of these two compounds at 401.2 nm is extremely high. The two phenols used in this study show ratios less than 0.1. They also have intense fluorescence emission, but the fluorescence of samarium is very low. From these data we conclude that only in the phenolic systems is there an energy transfer between two separated molecules. In all other cases an intramolecular energy transfer should be observed between the ligand bond to the metal ion . Energy transfer reactions of this type should therefore be a possible way of obtaining complex formation constants.

EXCITED STATE REACTION OF 2-NAPHTHOL

G. Geipel

The excited state chemistry of 2-naphthol is described in the literature /1,2,3/. These data are mostly obtained by using the single photon counting technique. In order to compare these data with measurements obtained by the gated spectroscopic technique.

If 2-napthol excited by light it shows at low pH values an intermolecular proton transfer forming the naptholate ion. The protonation constant for this excited state reaction is assigned to be $pK_a^* = 2.8$.

We studied the fluorescence behavior of a 5E-05 M at an ionic strength of 0.1 M ($NaClO_4$) solution as function of pH. Fig. 1 shows the time-resolved fluorescence spectrum at pH 2.74. One can clearly detect the fluorescence of the 2-naphthol and of the formed naphtholate ion. The center of the maximum emission was found to be located at about 350 nm for the 2-naphthol and 420 nm for the naphtholate, respectively.

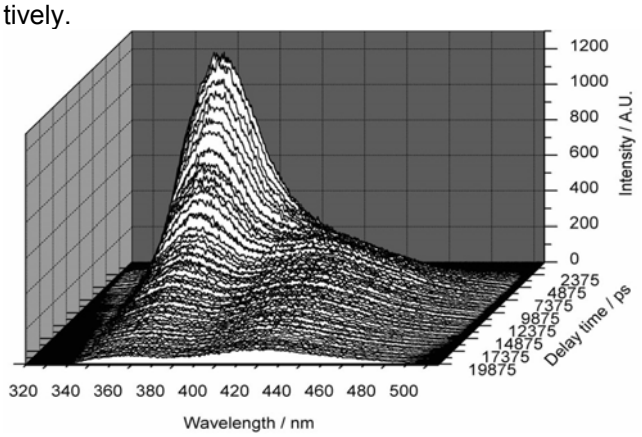

Fig. 1: TRLFS Spectrum of 2-naphthol at pH 2.74

From the time-resolved fluorescence spectra we obtain the decay at the emission maxima. The decay curves are shown for pH 2.74 in Fig. 2. In comparison to the fast inset of the fluorescence of the 2-naphtol the fluorescence of the naphtholate ion is delayed due to its formation upon the excitation process. At high pH values, when only the naphtholate ion exits in the ground state the inset of the fluorescence becomes as fat as for the 2-naphthol in acid solutions. The fluorescence lifetimes were assigned to be 3.7 ± 0.1 ns for the 2-naphthol and 8.8 ± 0.2 ns for the naphtholate respectively.

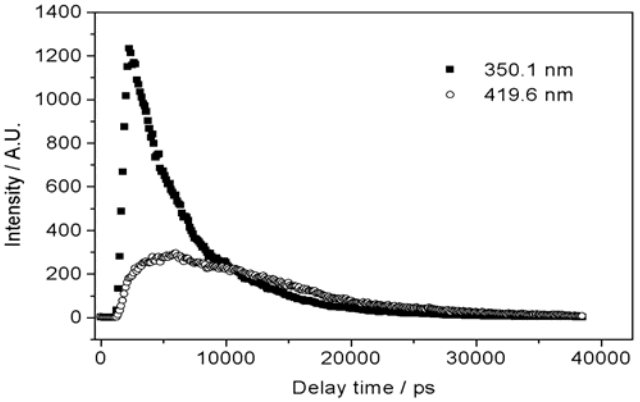

Fig. 2: Fluorescence decay for the 2-naphthol and naphtolate at pH 2.74

However we study the spectroscopic properties of two species in solution which are combined by a chemical equilibrium in the excited state. Therefore in the fluorescence spectra a wavelength point in spectra must exist which is comparable with the isosbestic point in absorption spectroscopy. To simplify the method described in the literature we recalculated all single spectra of one time-resolved spectrum in such a way, that for all spectra the same summarized intensity would be obtained. Fig. 3 shows a part of the resulting spectra.

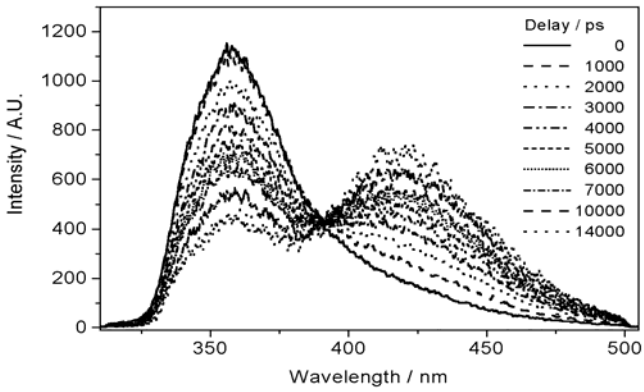

Fig. 3: Determination of the isoemissive point for the equilibrium 2-naphthol – naphtholate

The so called isoemissive point can be clearly detected by this method. This point is located to be at 391.6 nm for the excited state equilibrium 2-naphthol – 2-naphtholate. From fluorescence spectra at different pH values this point can also be obtained (Fig. 4).

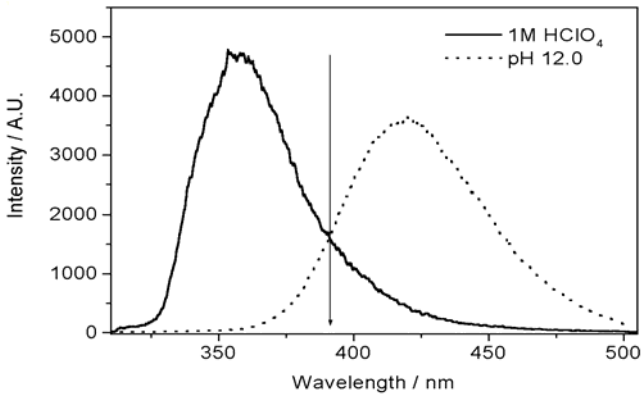

Fig. 4: Determination of the isoemissive point from spectra at various pH

We found in this case the isoemissive point to be located at 391.1 nm. However in this case only spectra from solutions can be used, where also in the excited state only one species exist. This means that conditions have to be selected, where no excited state reaction can occur.

As the kinetics of the formation of the deprotonated species in the excited state play an important role for the description of such equilibria, the excitation behavior will be used to derive the kinetic constants.

References

/1/ Webb, S.P. et al., J. Am. Chem. Soc. **106**, 7286 (1984)

/2/ Lawrence, M. et al., J. Phys. Chem. **95**, 10294 (1991)

/3/ Shizuka, H., Acc. Chem. Res. **18**, 141 (1985)

USING PULSED PHOTO-THERMAL SPECTROSCOPY FOR MICROSPECTROMETRY IN THE INFRARED REGION - A FIRST APPROACH

W. Seidel[1], H. Foerstendorf, K.H. Heise, J.M. Ortega[2], F. Glotin[2], R. Prazeres[2]
[1]Institute of Nuclear and Hadron Physics; [2]LURE, Université de Paris-Sud, Orsay, France

Photo-thermal spectroscopy using a pulsed pump source potentially provide spatial information of a sample surface. This may result in a microspectrometric technique for determining the distribution of metal species on mineral surfaces.

The border range between an implanted and a untreated region of the surface of a germanium substrate was investigated by photo-thermal spectroscopy. The substrate was implanted by oxygen ions (O^+) which was restricted to a distinct region of the substrate by partially covering the surface with a metal plate during the implantation process. This substrate serves as a model system for future investigations of mineral surfaces.

Experimental

We have used this method in order to take advantage of the pulsed character of the infrared laser. The incident energy is deposited in a short time. The heat generation will exhibit a corresponding time dependence, its time constant being of the order of the lifetime of the excited level (ps to ns). A temperature profile then develops in the sample *via* heat diffusion which can be described by a thermal diffusion length which was found in the µm range for solid states /1/. Let us assume that the optical absorption is due to a small defect: Therefore, if one measure the induced deflection with a sufficiently small laser probe, signal will be found only in the vicinity of this defect within one thermal diffusion length. With a probe beam having a small spot diameter one can hope for spatial resolution of a few micrometers, possibly even smaller than the infrared FEL wavelength. This will allow to perform mappings of the absorption profile at the surface of the sample, *i. e.* microspectrometry. It seems even possible to reach a sub-wavelength resolution.

Results

The border range between the O^+-implanted and pure germanium region was investigated by recording time curves of the deflection signal at distinct positions of the substrate surface using a constant FEL wavelength (11.6 µm). Due to absorption the produced germaniumoxide shows an enhanced deflection signal whereas pure germanium is nearly transparent and only a weak deflection signal is observed (Fig.1).

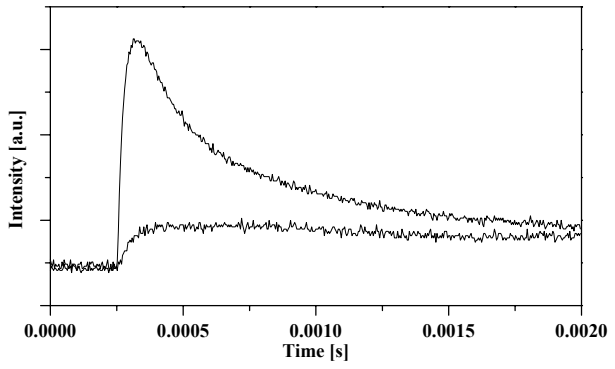

Fig. 1: Beam deflection signals of the different regions of the Ge-substrate. Upper trace: O^+-implanted region. Lower trace: pure Ge.

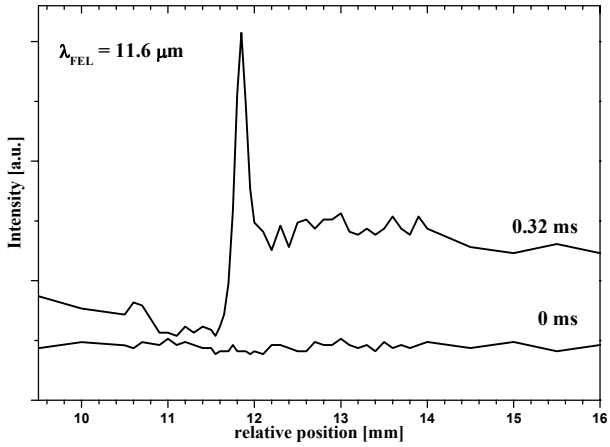

Fig. 2: Intensity of the deflection signal at distinct positions of the Ge-substrate at 0.32 ms (upper trace) and 0 ms after the FEL pulse (lower trace), respectively.

From these time curves profiles representing the absorption at each position of the sample can be obtained reflecting the distribution of the implanted oxygen in the substrate. Figure 2 shows the profiles obtained 0.32 ms after the FEL pulse where maximum deflection was observed. For comparison, the profile at 0 ms where no deflection occurs is also shown. In the border range the step width between two acquisition points was 50 µm and was increased to 100 and 500 µm, respectively, in the outer regions of the substrate. This results in a slightly increased noise of the profiles between 11 and 14 mm relative position.

The two different regions of the substrate can be clearly distinguished by different levels of absorption around 10 and 17 mm relative sample position, respectively. Surprisingly, in the border range around 11.8 mm relative position the concentration of the produced oxide seems to be considerably increased. If this is due to the implantation process, to surface effects or to artifacts of the spectroscopic technique applied has still to be verified. In further studies our aim is to increase the spatial resolution to a few microns which will be achieved by a better focusing of the probe beam and a more sophisticated sample translation.

Acknowledgements

The cooperation with Dr. E. Richter, FWI, is gratefully acknowledged.

References

/1/ Benchikh, O. et al., J. Phys. **46**, 727 (1985)

INFRARED CHARACTERIZATION OF ENVIRONMENTAL SAMPLES BY PULSED PHOTO-THERMAL SPECTROSCOPY

H. Foerstendorf, W. Seidel[1], K.H. Heise, R. Nicolai, A. Schamlott[2], J.M. Ortega[3], F. Glotin[3], R. Prazeres[3]
[1]Institute of Nuclear and Hadron Physics; [2]Central Department Radiation Source ELBE; [3]LURE, Université de Paris-Sud, Orsay, France.

The low metal concentration in environmental samples often limits the interpretation of results of studies investigating the interaction processes between metal ions and environmental compartments by vibrational spectroscopy. We show that photo-thermal infrared spectroscopy performed with a pulsed free electron laser can provide a low detection limit.

The aim of this investigation is to reduce the limits for IR-spectroscopic analyses and to develop *in situ* methods for environmental samples. This is demonstrated on different concentrations of solid neodymium nitrate ($Nd(NO_3)_3 \cdot 6H_2O$) dissolved in a potassium bromide (KBr) matrix serving as a model system.

Experimental

The photo-thermal detection method is based on thermo-elastic deformation bump generated by intermittent laser heating and thermal expansion /1/. A solid sample is irradiated by a modulated beam of monochromatic light produced by a tuneable free electron laser (FEL) and a probe beam (*e.g.* HeNe laser) which is reflected from the sample. Depending on the modulated intensity of the pump beam the photoinduced displacement of the probe beam changes periodically and thus a different reflection angle is observed (Fig.1). At first order the thermal beam deflection (TBD) is proportional to the absorption coefficient of the material under investigation, thus providing direct access to acquisition of absorption spectra. The detection limit is expected to be extremely low since absorptions as low as 10^{-6} to 10^{-8} have been measured in the visible region by this method /2/.

Results

The spectra were recorded within a small spectral range where narrow bands show up. The observed spectral features can be assigned to vibrational modes of the nitrate anion. A comparison of the spectra recorded with FTIR and TBD spectroscopy show a good agreement for the high and middle salt concentration (Fig. 2B,C). whereas spectral deviations are observed at low concentration (Fig. 2A).

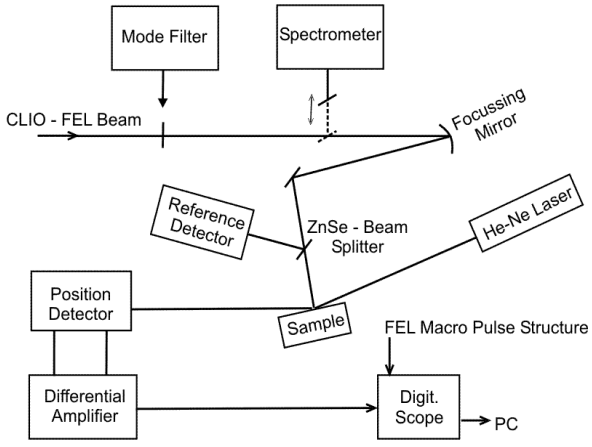

Fig. 1: Schematic diagram of the thermal deflection experiment setup.

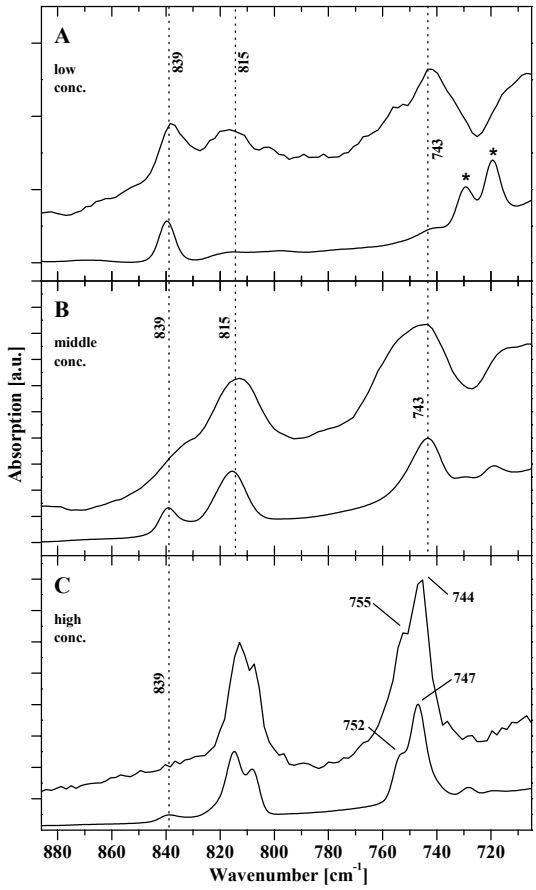

Fig. 2: Photo-thermal (upper traces) and FT-IR (lower traces) spectra of $Nd(NO_3)_3 \cdot 6H_2O$ in KBr matrix at different concentrations. Low conc.: 0.6 mM (A). Middle conc.: 2 mM (B). High conc.: 5 mM (C). *Bands representing impurities of the KBr matrix (A).

From these spectra it appears that the deflection method is more efficient to detect low amounts of substance than conventional FTIR spectroscopy, since weak bands around 815 and 743 cm^{-1} are clearly observed in the FEL spectra which are hardly present in the respective FTIR spectra due to the low concentration. Furthermore, in contrast to transmission FTIR spectroscopy only a small fraction of the sample is detected in the TBD experiment. Therefore, the high quality of the photo-thermal spectra presented here emphasises the high detection efficiency of this acquisition technique /3/.

References

/1/ Olmstead, M.A. et al., Appl. Phys. **A32**, 141 (1983)
/2/ Mandelis, A., Physics Today, Aug. 2000, p. 29
/3/ Seidel, W. et al. (submitted)

SEPARATION OF ^{14}C, ^{234}U AND ^{226}RA IN LIQUID SCINTILLATION SPECTRA

C. Nebelung

The radionuclides ^{14}C, ^{234}U and ^{226}Ra are nuclides of importance for the Morsleben radioactive waste disposal site. Simultaneous determination of these three nuclides in one sample is difficult. The α-active nuclides (^{234}U and ^{226}Ra together with their α-active decay products) and the β-active nuclides (^{14}C and ^{226}Ra β-decay products) were separated by α-β discrimination of the liquid scintillation spectra. Knowing the shape of the spectra of ^{226}Ra and its decay products makes it possible for us to separate ^{234}U from ^{226}Ra as well as ^{14}C from the β-decay products of ^{226}Ra.

The α- and β-active nuclides were determined by analyzing the liquid scintillation (LS) spectra recorded with an LS counter (Wallac system 1414, Perkin-Elmer) which separates α and β counts.

The sample investigated contained 1.2 E-7 mol/L ^{14}C, 1.29 E-9 mol/L ^{226}Ra and 1.36 E-6 mol/L ^{234}U. Fig. 1 shows the spectra obtained (a) immediately after sampling and (b) 5 weeks later.

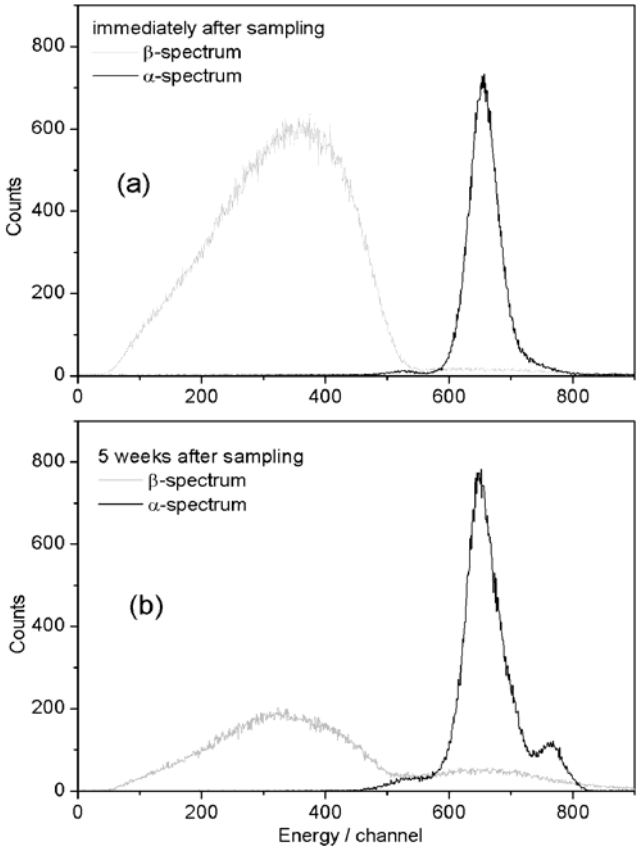

Fig. 1: LS spectra of a mixed ^{14}C, ^{226}Ra, ^{234}U sample

The ^{14}C activity needs to be measured immediately after sampling since a decrease in activity, presumably caused by CO_2 diffusion through the polyethylene scintillation vials, was observed within days. The β-active decay products of ^{226}Ra, i.e. ^{214}Pb, ^{214}Bi, ^{210}Pb and ^{210}Bi, have to be taken into account. An activity of (149±7) cpm of β-active nuclides was measured in LS measurements on pure ^{226}Ra of the same concentration immediately after sampling (24 measurements). This activity has to be subtracted from the total β-activity of (8550±290) cpm for the composite sample in order to calculate the ^{14}C activity.

The α-active nuclides were calculated by peak-fitting. Since the peak is not purely Gaussian, the α-spectra were fitted by a Gauss function with an exponential correction term /1/. The determination of the ^{226}Ra concentration was based on exact knowledge of the activity ratios between ^{226}Ra and its α-active decay products (^{222}Rn, ^{218}Po, ^{214}Po and ^{210}Po) /2/. The first decay product, ^{222}Rn, is gaseous. After sampling the equilibrium between ^{226}Ra and its daughter products is disturbed. Five weeks later this equilibrium has re-adjusted. The α emission energies of ^{234}U (4.775 MeV) and ^{226}Ra (4.784 MeV) are very close together and cannot be resolved by peak-fitting. However, it is possible to separate the daughter products from the joint $^{234}U/^{226}Ra$ peak (1) in Fig. 2 by peak-fitting. In a pure ^{226}Ra sample (under the same conditions as in the composite sample) the radium α activity amounts to 25 % of the total equilibrium α-activity. The ^{210}Po (2), ^{222}Rn (3), ^{218}Po (4) and ^{214}Po (5) activities contribute a fraction of 75 % to the total activity. The ^{234}U content is calculated by subtracting the ^{226}Ra activity from the joint $^{234}U/^{226}Ra$ peak.

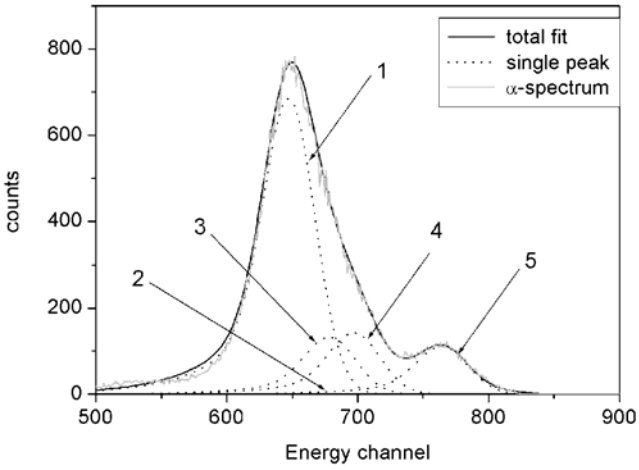

Fig. 2: Peak-fitting results of the α-LS spectrum of a ^{234}U+^{226}Ra sample in equilibrium

Tab. 1 shows the measured and calculated activities and concentrations of all nuclides that have to be considered. A maximum deviation of 8 % was observed between the added and measured concentrations.

Nuclide	Energy MeV	Half life	Activity Bq	Concentration mol/L
^{14}C	0.156	5730 a	140.0	(1.10±0.04) E-7
^{234}U ^{226}Ra	4.775 4.784	245500 a 1600 a	26.1 5.9	(1.36±0.03) E-6 (1.31±0.06) E-9
^{210}Po	5.304	138.2 d	0.1	< 1 E-14
^{222}Rn	5.490	3.82 d	6.1	< 1 E-14
^{218}Po	6.002	3.1 min	6.2	< 1 E-14
^{214}Po	6.787	164.3 µs	5.3	< 1 E-14

Tab. 1: Content of ^{14}C and α-emitting nuclides

References

/1/ Nebelung, C., Nitsche, H., *Schlußbericht* BMBF Fördervorhaben 02 S 7655, (1999)

/2/ Baraniak, L. , Nebelung, C. , Thieme, M., Report FZR-343, p. 48 (2002)

II. PUBLICATIONS, LECTURES, POSTERS, PH.D. THESES, DIPLOMA, PATENTS, AWARDS

PUBLICATIONS

Books, Journals

Artinger, R., Rabung, T., Kim, J.I., Sachs, S., Schmeide, K., Heise, K.H., Bernhard, G., Nitsche, H.
Humic Colloid-Borne Migration of Uranium in Sand Columns
Journal of Contaminant Hydrology **58**, 1-12 (2002)

Bernhard, G.
Radionuklidmigration und ökologische Konsequenzen für Mensch und Umwelt
Acta Academiae Scientiarum **6**, 57-75 (2002)

Brachmann, A., Geipel, G., Bernhard, G., Nitsche, H.
Study of uranyl(VI) malonate complexation by time resolved laser-induced fluorescence spectroscopy (TRLFS)
Radiochimica Acta **90**, 147 (2002)

Brendler, V., Arnold, Th., Nordlinder, S., Zänker, H., Bernhard, G.
Speciation and Sorption for Risk Assessment: Modelling and Database Applications
In: H.D. Schulz, G. Teutsch (Eds.) *Geochemical Processes. Conceptual Models for Reactive Transport in Soil and Groundwater*, Wiley VCH, Weinheim, 2002, p.79-94

Brendler, V., Vahle, A., Arnold, Th., Bernhard, G., Fanghänel, Th.
RES^{3}T-Rossendorf expert system for surface and sorption thermodynamics
Journal of Contaminant Hydrology **61**, 281-291 (2002)

Geraedts, K., Bruggeman, C., Maes, A., Van Loon, L.R., Roßberg, A., Reich, T.
Evidence for the existence of Tc(IV)–humic substance species by X-ray absorption near-edge spectroscopy
Radiochimica Acta **90**, 879 (2002)

Hennig, C., Reich, T., Dähn, R., Scheidegger, A.M.
Structure of uranium sorption complexes at montmorillonite edge sites
Radiochimica Acta **90,** 653-657 (2002)

Hübener, S.
Actinide Elements
In: *Encyclopedia of Physical Science & Technology* – Third Edition, Vol. 1, Academic Press, San Diego, 2002, p. 211-236

Krawczyk-Bärsch, E., Arnold, T., Brandt, F., Bosbach, D. , Bernhard, G.
Formation of Fe-oxyhydroxide particles during the dissolution of Fe-rich chlorite: Fate and behavior of heavy metals in the environment
Beiheft zum European Journal of Mineralogy **14**, 92 (2002)

Merroun, M.L., Hennig, C., Roßberg, A., Geipel, G., Reich, T., Selenska-Pobell, S.
Molecular and atomic analysis of uranium complexes formed by three eco-types of *Acidothiobacillus ferrooxidans*
Biochem. Sc. Trans. **30**, 669-672 (2002)

Mertig, M., Klemm, D., Zänker, H., Pompe, W.
Scanning force microscopy of two-dimensional structure formation in thin humic acid films
Surface Interface Analysis **33**, 113-117 (2002)

Moll, H., Zänker, H., Richter, W., Brendler, V., Hennig, C., Reich, T., Kluge, A., Hüttig, G.
Detection and characterization of colloids in acid rock drainage solution from an ore mine – Application of X-ray Absorption Spectroscopy (XAS)
Mitteilungen der Deutschen Bodenkundlichen Gesellschaft **99**, 201-202 (2002)

Moyes, L.N., Jones, M.J., Reed, W.A., Livens, F.R., Charnock, J.M., Mosselmans, J.F.W., Hennig, C., Vaughan, D.J., Pattrick, R.A.D.
An X-ray absorption spectroscopy study of neptunium(V) reactions with mackinawite (FeS)
Environ. Sci. Technol. **36,** 179-183 (2002)

Plaschke, M., Rothe, J., Schäfer, Th., Denecke, M.A., Dardenne, K., Pompe, S., Heise, K.H.
Combined AFM and STXM in situ Study of the Influence of Eu(III) on the Agglomeration of Humic Acid
Colloids and Surfaces A: Physicochemical and Engineering Aspects **197**, 245-256 (2002)

Sachs, S., Bubner, M., Schmeide, K., Choppin, G.R., Heise, K.H., Bernhard, G.
Carbon-13 NMR Spectroscopic Studies on Chemically Modified and Unmodified Synthetic and Natural Humic Acids
Talanta **57**, 999-1009 (2002)

Selenska-Pobell, S.
Diversity and activity of bacteria in uranium waste piles (invited chapter)
In: M. Keith-Roach, F. Livens (Eds.) *Radioactivity in the Environment (Vol.2); Interactions of Bacteria with Radionuclides*
Elsevier Sciences, Oxford, UK, 2002, p. 225-254

Stumpf, Th., Fanghänel, Th.
A Time-Resolved Laser Fluorescence Spectroscopy (TRLFS) Study of the Interaction of Trivalent Actinides (Cm(III)) with Calcite
J. Colloid Interface Sci. **249**, 119-122 (2002)

Stumpf, Th., Bauer, A., Coppin, F., Fanghänel, Th., Kim, J.I.
Inner-sphere, outer-sphere and ternary surface complexes: A TRLFS study of the sorption process of Eu(III) onto smectite and kaolinite
Radiochimica. Acta **90**, 345-349 (2002)

Stumpf, Th., Fanghänel, Th., Grenthe, I.
Complexation of trivalent actinide and lanthanide ions by glycolic acid: A TRLFS study
J. Chem. Soc., Dalton Trans. 3799-3804 (2002)

Squartini, A., Struffi, P., Döring, H., Selenska-Pobell, S., Tola, E., Giacomini, A., Velazques, E., Mateos, P.F., Martinez-Molina, E., Dazzo, F., Casella, S., Nuti, M.P.
Rhizobium sulae sp. nov. (formerly *"Rhizobium hedizari"*), the root-nodule microsymbiont of *Hedysarum coronarium* L.
Int. J. Syst. Evol. Microbiol. **52,** 1267-1276 (2002)

Tsushima, S., Uchida, Y., Reich, T.
A theoretical study on the structures of $UO_2(CO_3)_3^{4-}$, $Ca_2UO_2(CO_3)_3^0$, and $Ba_2UO_2(CO_3)_3^0$
Chem. Phys. Lett. **357**, 73-77 (2002)

Vahle, A, Hübener, S., Dressler, R., Grantz, M.
Development of an Apparatus for Seaborgium Studies by High Temperature Gas Chromatography
Nucl. Instr. and Meth. A **481**, 637-645 (2002)

Zänker, H., Moll, H., Richter, W., Brendler, V., Hennig, Ch., Reich, T., Kluge, A., Hüttig, G.
The colloid chemistry of acid rock drainage solution from an abandoned Zn-Pb-Ag mine
Appl. Geochem. **17,** 633-648 (2002)

Proceedings, Reports

Amayri, S.
Synthese, Charakterisierung und Löslichkeit von Erdalkaliuranylcarbonaten, $M_2[UO_2(CO_3)_3]\cdot xH_2O$; M: Mg, Ca, Sr, Ba
Report FZR-359, FZ-Rossendorf (2002)

Babanov, Yu.A., Zayarnaya, T.Ye., Reich, T., Funke, H.
EXAFS study of U(VI) compounds: A new approach to data analysis
Speciation, Techniques and Facilities for Radioactive Materials at Synchrotron Light Sources
Workshop Proceedings, Grenoble, France, 10.-12.09.2000
OECD, Paris, France, 2002, p. 105-116

Babanov, Yu.A., Rjashkin, A.B., Deev, A.N., Balijev, R.G., Mijanaga, T., Crosier, D., Gordon, R., Reich, T., Funke, H.
Determination of the distribution function of inhomogeneties of the sample-thickness using X-ray transmission spectra
Digest Reports of the XIV Russian Synchrotron Radiation Conference, Novosibirsk, Russia, 15.-19.07. 2002

Bolvin, H., Wahlgreen, U., Moll, H., Reich, T., Geipel, G., Fanghänel, Th., Grenthe, I.
Structure of neptunium(VII) complexes at high pH
ESRF Highlights 2001, 33-34 (2002)

Funke, H., Böttger, H., Reich, T., Hennig, C., Roßberg, A.
A splice program to connect two different EXAFS spectra of the same sample
Speciation, Techniques and Facilities for Radioactive Materials at Synchrotron Light Sources
Workshop Proceedings, Grenoble, France, 10.-12.09.2000
OECD, Paris, France, 2002, p. 229-236

Geipel, G., Bernhard, G., Brendler, V.
Complex Formation of Uranium(IV) with Phosphate and Arsenate
In: B.J. Merkel, B. Planer-Friedrich, C. Wolkersdorfer (Eds.), *Uranium in the Aquatic Environment*; Proc. of the Internat. Conf. UMH III and the IMWA Symposium, Freiberg, Germany; Springer Verlag Berlin 2002, p. 369-376

Gins, K.A., Sidorenko, A.F., Babanov, Yu.A., Muljukov, R.R., Reich, T., Funke, H.
Thermic stability of sub- microcristallic Copper : an EXAFS study
Digest Reports of the XIV Russian Synchrotron Radiation Conference, Novosibirsk, Russia, 15.-19.07.2002

Günther, A., Bernhard, G., Geipel, G., Roßberg, A., Reich, T.
Uranium speciation in plants
In: B.J. Merkel, B. Planer-Friedrich, C. Wolkersdorfer (Eds.), *Uranium in the Aquatic Environment*; Proc. of the Internat. Conf. UMH III and the IMWA Symposium, Freiberg, Germany; Springer Verlag Berlin 2002, p. 513-520

Günther, A., Bernhard, G.
Identifizierung und Charakterisierung des U(VI) in Pflanzen
Abschlussbericht DFG-Projekt BE 2234/1-1, 1-2 (2002)

Hennig, C., Panak, P., Reich, T., Raff, J., Selenska-Pobell, S., Roßberg, A., Funke, H.,
Merroun, M., Bernhard, G.
EXAFS investigation of U(VI) interaction with bacteria
Speciation, Techniques and Facilities for Radioactive Materials at Synchrotron Light Sources
Workshop Proceedings, Grenoble, France, 10.-12.09.2000
OECD, Paris, France, 2002, p.91

Hennig, C., Reich, T., Funke, H., Roßberg, A., Rutsch, M., Bernhard, G.
Analysis of atomic distances in inaccurately determined heavy-atom crystal structures using EXAFS spectroscopy
Speciation, Techniques and Facilities for Radioactive Materials at Synchrotron Light Sources
Workshop Proceedings, Grenoble, France, 10.-12.09.2000
OECD, Paris, France, 2002, p.237-244

Hennig, C.
Synchrotron Radiation for Study of Radioactive Materials
Digest Report of the XIV Russian Synchrotron Radiation Conference, Novosibirsk, Russia, 15.-19.07.2002

Jansen, K., Buschmann, H.-J., Schmeide, K., Schollmeyer, E.
Modification of Textile Mats with Calixarenes – Separation of Uranium from Mine and Seepage Waters
Proceedings of the 1st International Textile, Clothing and Design Conference – Magic World of Textiles. Dubrovnik, Croatia, 06.-09.10.2002, p. 692-697

Kamenskij, I.Yu., Kunicke, M., Reich, T., Funke, H., Babanov, Yu.A.
EXAFS investigation of the local structure of $UO_2(H_2AsO_4)_2 \times H_2O$ at 305 and 15 Kelvin
Digest Reports of the XIV Russian Synchrotron Radiation Conference, Novosibirsk, Russia, 15.-19.07.2002

Kirjanov, C.A., Sidorenko, A.F., Babanov, Yu.A., Rjashkin, A.B., Romaschev, L.N., Pazelov, A.M., Reich, T., Funke, H., Prokert, F., Schell, N.
Anomal X-ray scattering and EXAFS for near-order investigations of the solid solution $Fe_{78,4}\ Cr_{21,6}$
Digest Reports of the XIV Russian Synchrotron Radiation Conference, Novosibirsk, Russia, 15.-19.07.2002

Koban, A., Geipel, G., Bernhard, G., Fanghänel, Th.
Complex Formation of Uranium(VI) with Glucose-1-Phosphate
In: B.J. Merkel, B. Planer-Friedrich, C. Wolkersdorfer (Eds.), *Uranium in the Aquatic Environment*; Proc. of the Internat. Conf. UMH III and the IMWA Symposium, Freiberg, Germany; Springer Verlag Berlin 2002, p. 537-540

Krawczyk-Bärsch, E., Arnold, T., Schmeisser, N., Brandt, F., Bosbach, D., Bernhard, G.
The effect of chlorite dissolution on the sorption behavior of U(VI)
In: B.J. Merkel, B. Planer-Friedrich, C. Wolkersdorfer (Eds.), *Uranium in the Aquatic Environment*; Proc. of the Internat. Conf. UMH III and the IMWA Symposium, Freiberg, Germany; Springer Verlag Berlin 2002, p. 395-398

Künstler, J.-U., Seifert, S., Reich, T., Funke, H., Johannsen, B.
EXAFS analyses of Tc(I) tricarbonyl complexes – ligand exchange studies
Speciation, Techniques and Facilities for Radioactive Materials at Synchrotron Light Sources
Workshop Proceedings, Grenoble, France, 10.-12.09.2000
OECD, Paris, France, 2002, p. 245-252

Merroun, M.L., Reich, T., Hennig, C., Selenska-Pobell, S.
EXAFS investigation of uranium(VI) complexes formed at *Acidithiobacillus ferrooxidans* types
Speciation, Techniques and Facilities for Radioactive Materials at Synchrotron Light Sources
Workshop Proceedings, Grenoble, France, 10.-12.09.2000
OECD, Paris, France, 2002, p. 261

Merroun, M.L., Hennig, C., Roßberg, A., Reich, T., Nicolai, R., Heise, K.H., Selenska-Pobell, S.
Characterization of uranium (VI) complexes formed by different bacteria relevant to uranium mining waste piles
In: B.J. Merkel, B. Planer-Friedrich, C. Wolkersdorfer (Eds.), *Uranium in the Aquatic Environment*; Proc. of the Internat. Conf. UMH III and the IMWA Symposium, Freiberg, Germany; Springer Verlag Berlin 2002, p. 505-511

Mibus, J.
Column Experiments with Heap Material of Kupferschiefer Mining and Thermodynamic Interpretation
Report FZKA 6721, FZ Karlsruhe (2002) p. 55-59

Mibus, J., Szymczak, P., Hebert, D.
Infiltration water dating from tritium measurements in mining dumps: Methodic specifics and case study
In: B.J. Merkel, B. Planer-Friedrich, C. Wolkersdorfer (Eds.), *Uranium in the Aquatic Environment*; Proc. of the Internat. Conf. UMH III and the IMWA Symposium, Freiberg, Germany; Springer Verlag Berlin 2002, p. 959-964

Mibus J., Szymzcak, P., Hebert, D., Oster, H.
Kombinierter Einsatz von FCKW und Tritium als Tracer
Wissenschaftliche Mitteilungen der TU BA Freiberg **19**, 25-28 (2002)

Moll, H., Zänker, H., Richter, W., Brendler, V., Reich, T., Hennig, C., Roßberg, A., Funke, H., Kluge, A.
XAS study of acid rock drainage samples from an abondoned Zn-Pb-Ag mine at Freiberg, Germany
Speciation, Techniques and Facilities for Radioactive Materials at Synchrotron Light Sources
Workshop Proceedings, Grenoble, France, 10.-12.09.2000
OECD, Paris, France, 2002, p. 263-270

Pompe, S., Schmeide, K., Reich, T., Hennig, C., Funke, H., Roßberg, A., Geipel, G., Brendler, V., Heise, K.H., Bernhard, G.
Neptunium(V) Complexation by Various Humic Acids in Solution Studied by EXAFS and NIR Spectroscopy
Speciation, Techniques and Facilities for Radioactive Materials at Synchrotron Light Sources
Workshop Proceedings, Grenoble, France, 10.-12.09.2000
OECD, Paris, France, 2002, p. 277-284

Raff, J., Soltmann, U., Matys, S., Schnorpfeil, M., Boettcher, H., Pompe, W., Selenska-Pobell, S.
Bacteria-based bioremediation of uranium mining waste waters using sol-gel ceramics
In: B.J. Merkel, B. Planer-Friedrich, C. Wolkersdorfer (Eds.), *Uranium in the Aquatic Environment*; Proc. of the Internat. Conf. UMH III and the IMWA Symposium, Freiberg, Germany; Springer Verlag Berlin 2002, p. 615-622

Raff, J., Reich, T., Hennig, C., Roßberg, A., Funke, H., Merroun, M.L., Walter, M., Selenska-Pobell, S.
Interaction between bacterial S-layers and uranium using EXAFS
Bi-Annual Report ESRF(ROBL) 2001/2002

Raff, J., Funke, H., Roßberg, A., Reich, T., Hennig, C., Walter, M., Merroun, M.L., Selenska-Pobell, S.
Uranium binding of sol-gel immobilized cells and S-layers of *Bacillus sphaericus* JG-A12 and NCTC 9602
Bi-Annual Report ESRF(ROBL) 2001/2002

Raff, J.
Wechselwirkungen der Hüllproteine von Bakterien aus Uranabfallhalden mit Schwermetallen
Report FZR-358, FZ Rossendorf (2002)

Selenska-Pobell, S., Flemming, K., Tzvetkova, T., Raff, J., Schnorpfeil, M., Geißler, A.
Bacterial communities in uranium mining waste piles and their interaction with heavy metals

In: B.J. Merkel, B. Planer-Friedrich, C. Wolkersdorfer (Eds.), *Uranium in the Aquatic Environment*; Proc. of the Internat. Conf. UMH III and the IMWA Symposium, Freiberg, Germany; Springer Verlag Berlin 2002, p. 455-464

Schmeide, K., Pompe, S., Reich, T., Hennig, C., Funke, H., Roßberg, A., Geipel, G., Brendler, V., Heise, K.H., Bernhard, G.
Interaction of Neptunium(IV) with Humic Substances Studied by XAFS Spectroscopy
Speciation, Techniques and Facilities for Radioactive Materials at Synchrotron Light Sources
Workshop Proceedings, Grenoble, France, 10.-12.09.2000
OECD, Paris, France, 2002, p. 287-294.

Schmeide, K., Geipel, G., Keil, D., Jansen, K., Praschak, D., Heise, K.H., Bernhard, G.
Separation of uranium from aqueous solution by textile bound calixarenes
In: B.J. Merkel, B. Planer-Friedrich, C. Wolkersdorfer (Eds.), *Uranium in the Aquatic Environment*; Proc. of the Internat. Conf. UMH III and the IMWA Symposium, Freiberg, Germany; Springer Verlag Berlin 2002, p. 417-424

Reich, T., Pompe, S., Heise, K.H., Nitsche, H.
Interaction of uranyl group UO_2^{2+} and Fe(III) ions with natural humic acid
Speciation, Techniques and Facilities for Radioactive Materials at Synchrotron Light Sources
Workshop Proceedings, Grenoble, France, 10.-12.09.2000
OECD, Paris, France, 2002, p. 317-324

Tsushima, S., Reich, T.
Quantum chemical calculation on structures of actinide complexes
Speciation, Techniques and Facilities for Radioactive Materials at Synchrotron Light Sources
Workshop Proceedings, Grenoble, France, 10.-12.09.2000
OECD, Paris, France, 2002, p. 53-62

Walter, M., Arnold, T., Funke, H., Reich, T., Bernhard, G.
Sorption of Uranium(VI) onto Schwertmannite – EXAFS Investigations
In: B.J. Merkel, B. Planer-Friedrich, C. Wolkersdorfer (Eds.), *Uranium in the Aquatic Environment*; Proc. of the Internat. Conf. UMH III and the IMWA Symposium, Freiberg, Germany; Springer Verlag Berlin 2002, p. 395-398

Zayarnaya, T.Ye., Reich, T., Hennig, C., Funke, H.
Application of the Tikhonov regularization method to the EXAFS analysis of $UO_2(H_2AsO_4)_2 \cdot H_2O$
Speciation, Techniques and Facilities for Radioactive Materials at Synchrotron Light Sources
Workshop Proceedings, Grenoble, France, 10.-12.09.2000
OECD, Paris, France, 2002, p. 359-366

Zänker, H., Richter, W., Hüttig, G., Moll, H.
Colloid-borne Uranium in Mine Waters
In: B.J. Merkel, B. Planer-Friedrich, C. Wolkersdorfer (Eds.), *Uranium in the Aquatic Environment*; Proc. of the Internat. Conf. UMH III and the IMWA Symposium, Freiberg, Germany; Springer Verlag Berlin 2002, p. 399

Zänker, H, Richter, W., Hüttig, G., Moll, H., Brendler, V.
Charakterisierung der Kolloidpartikel in den Wasserfließsystemen stillgelegter sächsischer Bergbauanlagen
Abschlußbericht zum DFG-Projekt ZA 238/1-4. FZ Rossendorf, April 2002

LECTURES

Arnold, T.
Thermodynamische Beschreibung von Sorptionsprozessen – Entwicklung reaktiver Barrierematerialien
6. Workshop: Sanierung der Hinterlassenschaften des Uranerzbergbaus. Barrieresysteme – Die Bedeutung hydraulischer und geochemischer Barrieren bei der Verwahrung von Uranbergwerken und bei der Endlagerung radioaktiver Abfälle (invited)
Dresden, Germany, 04.–05.12.2002

Arnold, T., Krawczyk-Bärsch, E., Grossmann, K., Hollenbach, B.
Einsatz von natürlichen Materialien zum Zurückhalten von toxischen Schwermetallen – Von den Grundlagen zur Anwendung
Ausstellung „leben+erde“, Staatliche Naturhistorische Sammlung
Dresden, Germany, 15.-23.11.2002

Arnold, T.
U(VI) sorption on muscovite and biotite studied by TRLFS
ACTAF Meeting
Barcelona, Spanien, 18.-19.11.2002

Arnold, T.
Sorption of U(VI) on granite: experimental versus predicted data
ACTAF Meeting
Kopenhagen, Dänemark, 10.-11.06.2002

Arnold, T.
Uran Sorption auf Quarz
Modellierung-Workshop des NEA Sorptionsprojektes
El Escorial / Madrid, Spanien, 26.-30.10.2002

Bernhard, G.
Uranium speciation in biological systems – plants
The University of Tokyo, Institute of Environmental Studies
Tokyo, Japan, 28.08.2002

Bernhard, G.
Uranium speciation in environmental systems
Institute of Research and Innovation Tokyo
Tokyo, Japan, 27.08.2002

Bernhard, G.
Wohin mit dem Atommüll
FZ Rossendorf
Tag der Offenen Tür
Dresden, Germany, 2002

Bernhard, G.
Zur Umweltchemie des Urans
FZ Karlsruhe, Institut für Nukleare Entsorgung
Karlsruhe, Germany, 2002

Bernhard, G.
Profil und Forschung – Institut für Radiochemie
FZ Rossendorf
Sitzung RSK Ausschuss Grundsatzfragen
Dresden, Germany, 26.06.2002

Brendler, V.
Sorption of Neptunium(V) onto Haematite
Modellierung-Workshop des NEA Sorptionsprojektes
El Escorial / Madrid, Spanien, 26.-30.10.2002

Brendler, V.
Strategien und Konzepte für Geochemische Datenbanken – Sichtweise des Institutes für Radiochemie / FZ Rossendorf
Workshop „Aktueller Stand und Perspektiven der thermodynamischen / geochemischen und Sorptions-Datenbasis“; INE/FZK
Karlsruhe, Germany, 15.10.2002

Brendler, V.
Leistungsmerkmale des Systems EQ3/6
Workshop “Chemsage als Geochemie-Programm ?”
TU BA Freiberg
Freiberg, Germany, 12.04.2002

Brendler, V., Richter, A., Arnold, Th., Bernhard, G., Fanghänel, Th.
RES3T – Rossendorf Expert System for Surface and Sorption Thermodynamic
LBNL Seminar, The Glenn T. Seaborg Center, Lawrence Berkeley National Lab.
Berkeley, USA, 12.07.2002

Brendler, V., Arnold, Th., Bernhard, G., Fanghänel, Th.
RES3T – Rossendorf Expert System for Surface and Sorption Thermodynamic
23rd Rare Earth Research Conference
Davis, USA, 13.-18.07.2002

Brendler, V., Arnold, Th., Richter, A., Bernhard, G., Fanghänel, Th.
From K_D to SCM: Present State of Actinide Data Supply
International Conference Uranium Mining and Hydrogeology III and the International Mine Water Association Symposium
Freiberg, Germany, 15.-21.09.2002

Funke, H., Stumpf, T., Reich, T., Roßberg, A.
EXAFS studies of the Am^{3+} and Cm^{3+} aquoions
32èmes Journées des Actinides
Ein-Gedi, Israel, 19.-22.03.2002

Geipel, G.
Laserspektroskopie im Institut für Radiochemie - Speziation von Schwermetallen am Beispiel der Actiniden
Bundesanstalt für Materialprüfung
Berlin, Germany, 13.03.2002

Geipel, G.
Laserinduzierte Fluoreszenzspektroskopie - Untersuchung der Wechselwirkung von Actiniden mit organischen Liganden (invited)
Institut für Kernchemie
Mainz, Germany, 10.07.2002

Geipel, G., Bernhard, G., Fanghänel, Th.
Studies on Interactions of Actinides with Organic Ligands using Femtosecond-Laser-Induced Spectroscopy
14^{th} Radiochemical Conference 2002
Marianske Lazne, Czech Republic, 14.-18.04.2002

Geipel, G.
New Results in fs-Fluorescence Spectroscopy of Actinides with Organic Ligands (invited)
The University of Tokyo, Institute of Environmental Studies
Tokyo, Japan, 28.08.2002

Geipel, G.
Fs-Fluorescence Spectroscopy of Actinides with Organic Ligands (invited)
Institute of Research and Innovation Tokyo
Tokyo, Japan, 27.08.2002

Geipel, G., Bernhard, G., Brendler, V.
Complex Formation of Uranium(VI) with Phosphate and Arsenate
International Conference Uranium Mining and Hydrogeology III and the International Mine Water Association Symposium
Freiberg, Germany, 15.-21.09.2002

Geipel, G.
Laser Induced Spectroscopy Detection of Species at Low Concentrations
Workshop Elementspeziation
Mainz, Germany, 17.-18.10.2002

Günther, A., Bernhard, G.
Chemische Speziation von Metallen in Pflanzen unter besonderer Berücksichtigung von Uran
Institut für Allgemeine Ökologie und Umweltschutz der TU Dresden
Tharandt, Germany, 26.06.2002

Günther, A., Bernhard, G., Geipel, G., Roßberg, A., Reich, T.
Uranium speciation in plants
International Conference Uranium Mining and Hydrogeology III and the International Mine Water Association Symposium
Freiberg, Germany, 15.-21.09.2002

Hennig, C.
Investigation of Actinide complex compounds with X-ray absorption spectroscopy
ESRF SAC Meeting
Grenoble, France, 08.11.2002

Hennig, C.
Application of X-ray absorption spectroscopy to determine uptake processes of uranium at the clay mineral surface
Polytechnical University of Catalonia
Barcelona, Spain, 18.10.2002

Hennig, C.
Structure of uranium(VI) complexes sorbed at 1:1 and 2:1 clay mineral surfaces – A comparative EXAFS study
Mineral Surface and Colloid Chemistry in Soil and Aquatic Environments
Karlsruhe, Germany, 08.-09.10.2002

Hennig, C.
Synchrotron Radiation for Study of Radioactive Materials
XIV Russian Synchrotron Radiation Conference
Novosibirsk, Russia, 15.-19.07.2002

Hennig, C.
Structure determination by combined X-ray diffraction and X-ray absorption spectroscopy measurements using synchrotron radiation
ANKA FSG Seminar
Karlsruhe, Germany, 14.01.2002

Hübener, S.
Chemische Charakterisierung des Elements Sg (Z = 106) als Oxid Hydroxid
TU Dresden, Institut für Strahlenschutzphysik.
Dresden, Germany, 25.04.2002

Hübener, S., Fanghänel, Th.
Thermochromatographic Oxidation Studies of Plutonium Dioxide
23rd Rare Earth Research Conference
Davis, USA, 13.-18.07.2002

Jansen, K., Buschmann, H.-J., Schmeide, K., Schollmeyer, E.
Modification of Textile Mats with Calixarenes – Separation of Uranium from Mine and Seepage Waters 1st International Textile, Clothing and Design Conference – Magic World of Textiles
Dubrovnik, Croatia, 06.-09.10.2002

Krawczyk-Bärsch, E., Arnold, T., Walter, M., Brandt, F., Bosbach, D., Bernhard, G.
Chlorite dissolution relevant to environmental processes in uranium tailings: Influence on the uranium (VI)
39th Annual Meeting of The Clay Minerals Society
Boulder, Colorado, USA, 08.-13.06.2002

Krawczyk-Bärsch, E., Arnold, T., Brandt, F., Bosbach, D., Bernhard, G.
Formation of Fe-oxyhydoxide particles during the dissolution of Fe-rich chlorite: Fate and behavior of heavy metals in the environment
80. Jahrestagung der Deutschen Mineralogischen Gesellschaft
Hamburg, Germany, 08.–12.09.2002

Koban, A., Geipel, G., Bernhard, G., Fanghänel, Th.
Complex Formation of Uranium(VI) with Fructose and Glucose Phosphates
14th Radiochemical Conference 2002
Marianske Lazne, Czech Republic, 14.-18.04.2002

Merroun, M.L.
Uranium complexes formed by different bacteria isolated from uranium mining waste piles: molecular and spectroscopic studies
University of Granada
Granada, Spain, 17.12. 2002

Merroun, M.L., Hennig, C., Rossberg, A., Reich, T., Nicolai, R., Heise, K.H., Selenska-Pobell, S.
Characterization of uranium (VI) complexes formed by different bacteria relevant to uranium mining waste piles
International Conference Uranium Mining and Hydrogeology III and the International Mine Water Association Symposium
Freiberg, Germany, 15.-21.09.2002

Merroun, M.L.
Spectroscopic characterization of uranium complexes formed by bioceramics
Innoregio Treffen
Dresden, Germany, 10.11.2002

Merroun, M.L., Hennig, C., Roßberg, A., Geipel, G., Reich, T., Selenska-Pobell, S.
Molecular and atomic analysis of the uranium complexes formed by three eco-types of *Acidithiobacillus ferrooxidans*
The 3rd International Biometals Symposium
London, UK, 11.-13.04.2002

Mibus, J., Szymzcak, P., Hebert, D., Oster, H.
Kombinierter Einsatz von FCKW und Tritium als Tracer
Workshop „Isotope und Tracer in der Wasserforschung“
Freiberg, Germany, 21.06.2002

Moll, H., Zänker, H., Richter, W., Brendler, V., Hennig, C., Reich, T., Kluge, A., Hüttig, G.
Detection and characterization of colloids in acid rock drainage solution from an ore mine – Application of X-ray Absorption Spectroscopy (XAS)
DBG Conference on Mineral Surface and Colloid Chemistry in Soil and Aquatic Environments
Karlsruhe, Germany, 08.-09.10.2002

Nebelung, C., Baraniak, L.
Sorption von Uran, Radium und [^{14}C]-Carbonat an endlagerrelevanten Materialien
Projektzwischenbericht ERAM-Projekt
Karlsruhe, Germany, 24.04.2002

Nebelung, C., Baraniak , L.
Löslichkeits- und Sorptionsuntersuchungen von Uran, Radium und [^{14}C]-Carbonat unter den Bedingungen des Endlagers Morsleben
Projektbericht ERAM-Projekt
Karlsruhe, Germany, 05.12.2002

Pollmann, K.
Molecular analyses and engineering of S-layer genes
Kick Off Meeting Project BIO-CAT
Birmingham, UK, 24.06.2002

Pollmann, K.
Molecular analyses of S-layer proteins and genes
BIO-CAT Projekttreffen
Dresden, Germany, 01.-02.11.2002

Raff, J., Soltmann, U., Matys, S., Schnorpfeil, M., Böttcher, H., Pompe, W., Selenska-Pobell, S.
Biological sol-gel ceramics with specific metal binding capacity
VAAM-Jahrestagung
Göttingen, Germany, 24.-27.03.2002

Raff, J., Soltmann, U., Matys, S., Schnorpfeil, M., Böttcher, H., Pompe, W., Selenska-Pobell, S.
Microbial bioremediation of uranium mining waste waters using sol-gel ceramics
International Conference Uranium Mining and Hydrogeology III and the International Mine Water Association Symposium
Freiberg, Germany, 15.-21.09.2002

Raff, J.
Wechselwirkung der Hüllproteine von Bakterien aus Uranabfallhalden mit Schwermetallen
Zentrumskolloquium, FZ Rossendorf
Rossendorf, Germany, 19.12.2002

Reich, T.
Spektroskopische Speziation von Actiniden mittels Synchrotronstrahlung
Wissenschaftliches Symposium der GDCh-Fachgruppe Nuklearchemie
Mainz, Germany, 22.02.2002

Reich, T., Roßberg, A., Hennig, C., Funke, H., Bernhard, G.
An EXAFS study of uranium(VI) complexation with protocatechuic acid in the pH range 4-10

Hamburg Workshop "Application of Synchrotron Radiation in Chemistry - Status and Future"
Hamburg, Germany, 16.-17.09.2002

Richter, A.
Wechselwirkung mit Oberflächen
Workshop BfS/FZK/FZR zum Projekt „Geochemische Prozesse bei der Ausbreitung von Schadstoffen aus einem Endlager für radioaktive Abfälle“
Karlsruhe, Germany, 07.11.2002

Roßberg, A.
Anwendung der Faktorenanalyse auf die Röntgenabsorptionsspektroskopie zur Bestimmung der Speziation von Uran in Lösungen
Zentrumskolloquium, FZ Rossendorf
Rossendorf, Germany, 19.12.2002

Sachs, S.
Synthesis and Characterization of Humic Acids with Different Functional Properties
Workshop zum Forschungsvorhaben "Humic Substances in Performance Assessment of Nuclear Waste Disposal: Actinide and Iodine Migration in the Far-Field"
Paris, France, 23.-24.04.2002

Sachs, S., Heise, K.H., Bernhard, G.
Synthetische und modifizierte Huminsäuren zur Untersuchung des Wechselwirkungsverhaltens von Huminsäuren mit Metallionen. Symposium über Torfpräparate in der Medizin, Veterinärmedizin und Körperpflege
Bad Langensalza, Germany, 23.-24.05.2002

Sachs, S.
Aktuelle Ergebnisse zur Synthese und Charakterisierung von Huminsäuren mit ausgeprägter Redoxfunktionalität
Workshop zum Forschungsvorhaben „Untersuchungen über die Komplexierung und die Migration von Actiniden und nichtradioaktiven Stoffen mit Huminsäuren unter geogenen Bedingungen - Komplexierung von Huminsäuren mit Actiniden in der Oxidationsstufe IV Th, U, Np“
Leipzig, Germany, 26.-27.06.2002

Sachs, S., Schmeide, K., Heise, K.H., Bernhard, G.
Synthetic Humic Acids: A Useful Tool to Study the Interaction of Humic Acids with Actinides in the Environment
20th Anniversary Conference of the International Humic Substances Society
Boston, Massachusetts, USA, 21.-26.07.2002

Sachs, S.
Progresses in the Development of Highly-Reducing Synthetic Humic Acids and in the Study of the Influence of Phenolic OH Groups on the Interaction Behavior of Humic Acids with Neptunium(V)
Workshop zum Forschungsvorhaben "Humic Substances in Performance Assessment of Nuclear Waste Disposal: Actinide and Iodine Migration in the Far-Field"
Manchester, Great Britain, 25.-26.11.2002

Sachs, S., Mibus, J., Bernhard, G.
Sampling and Characterization of Natural Rock Material
Workshop zum Forschungsvorhaben "Humic Substances in Performance Assessment of Nuclear Waste Disposal: Actinide and Iodine Migration in the Far-Field"
Manchester, Great Britain, 25.-26.11.2002

Schmeide, K.
Abtrennung von Uran aus wässriger Lösung durch calixarenausgerüstete Polyestervliese
Workshop zum Forschungsvorhaben "Abtrennung von Uranylionen aus Sicker- und Grundwässern mit uranophilen Calixarenen – Integrierter Umweltschutz in der Textilindustrie"
Düren, Germany, 26.-27.03.2002

Schmeide, K., Geipel, G., Keil, D., Heise, K.H., Bernhard, G., Gloe, K.
Complex Formation Between Uranium(VI) and Calix[6]arenes Studied by Time-resolved Laser-induced Fluorescence Spectroscopy
14th Radiochemical Conference 2002
Marianske Lazne, Czech Republic, 14.-18.04.2002

Schmeide, K.
Determination of Structural Parameters of Actinide Humate Complexes by Means of XAFS Spectroscopy

Workshop zum Forschungsvorhaben "Humic Substances in Performance Assessment of Nuclear Waste Disposal: Actinide and Iodine Migration in the Far-Field", CEA
Paris, France, 22.-24.04.2002

Schmeide, K., Geipel, G., Keil, D., Jansen, K., Praschak, D., Heise, K.H., Bernhard, G.
Separation of Uranium from Aqueous Solution by Textile Bound Calixarenes
International Conference Uranium Mining and Hydrogeology III and the International Mine Water Association Symposium
Freiberg, Germany, 15.-21.09.2002

Selenska-Pobell, S.
Biologische Synthese von Metallclustern an Proteinen und deren technische Nutzung
Nanoverbund Treffen, TU Dresden
Dresden, Germany, 14.06.2002
Selenska-Pobell, S.
Novel precious metal-based bionanocatalysts from scrap
BioCat Meeting – EU
Birmingham, United Kingdom, 24.06.2002

Selenska-Pobell, S.
Bacteria in uranium mining wastes and their interactions with uranium and other metals
BORIS meeting – EU
Moscow, Russia, 08.07.2002

Selenska-Pobell, S.
Bacterial communities in uranium mining waste piles and their interaction with heavy metals
University of Hiroshima
Hiroshima, Japan, 22.08.2002

Selenska-Pobell, S.
Bacterial diversity and activity in uranium mining wastes
Tono Geoscience Center of Japan Nuclear Cycle Development
Tono, Japan, 28.08.2002

Selenska-Pobell, S.
Bacterial communities in uranium mining waste piles and their interaction with heavy metals
International Conference Uranium Mining and Hydrogeology III and the International Mine Water Association Symposium
Freiberg, Germany, 15.-21.09.2002

Selenska-Pobell, S.
Heavy metal polluted environments as a reservoir for biodiversity
Department of Geomicrobiology, University of Sofia
Sofia, Bulgaria, 11.10.2002

Stumpf, Th., Bauer, A., Coppin, F., Fanghänel, Th., Kim, J.I.
Inner-sphere, outer-sphere and ternary surface complexes: A TRLFS study of the sorption process of Eu(III) onto smectite and kaolinite
23rd Rare Earth Research Conference
Davis, USA, 13.-18.07.2002

Walter, M., Arnold, T., Funke, H., Reich, T., Bernhard, G.
Sorption of Uranium(VI) onto Schwertmannite – EXAFS Investigations
International Conference Uranium Mining and Hydrogeology III and the International Mine Water Association Symposium
Freiberg, Germany, 15.-21.09.2002

Yakushev, A.B., Buklanov, G.V., Chelnokov, M.L., Chepigin, V.I., Dmitriev, S.N., Gorshkov, V.A., Hübener, S., Lebedev, V.Ya., Malyshev, O.N., Oganessian, Yu.Ts., Popeko, A.G., Sokol, E.A., Timokhin, S.N., Türler, A., Vasko, V.M., Yeremin, A.V., Zvara, I.
On the Way to Chemically Identify Element 112
14th Radiochemical Conference
Marianske Lazne, Czech Republic, 14.-19.04.2002

Zänker, H., Richter, W., Brendler, V., Moll, H., Hüttig, G.
The Sorption of Toxic and Radiotoxic Heavy Metals by Inorganic Colloids in Mine Waters
GeoProc2002
Bremen, Germany, 04.–07.03.2002

Zänker, H., Moll, H., Richter, W., Brendler, V., Hennig, C., Reich, T., Kluge, A., Hüttig, G.
Detection and Characterization of Ultrafine Fe-As-Pb Colloids in Acid Rock Drainage Solution from an Ore Mine
XXVII General Assembly of the European Geophysical Society (EGS 2002)
Nice, France, 22.–26.04.2002

Zänker, H., Richter, W., Hüttig, G., Moll, H.
The Role of Inorganic Colloids in the Waters of Abandoned Ore Mines
European Materials Research Society (E-MRS) Spring Meeting
Strasbourg, France, 18.–21.06.2002

Zänker, H., Richter, W., Hüttig, G., Moll, H.
Colloid-borne Uranium in Mine Waters
International Conference Uranium Mining and Hydrogeology III and the International Mine Water Association Symposium
Freiberg, Germany, 15.-21.09.2002

POSTERS

Arnold, T., Krawczyk-Bärsch, E.
Bildung von Eisenhydroxid-Partikeln durch Gesteinsverwitterung – Auswirkungen auf den Urantransport
Ausstellung „leben+erde“, Staatliche Naturhistorische Sammlung
Dresden, Germany, 15.-23.11.2002

Arnold, T., Krawczyk-Bärsch, E.
Einsatz von Gesteinen und Mineralen zum Zurückhalten von toxischen Schwermetallen – von den Grundlagen zur Anwendung
Ausstellung „leben+erde“, Staatliche Naturhistorische Sammlung
Dresden, Germany, 15.-23.11.2002

Arnold, T., Krawczyk-Bärsch, E.
Ehemaliger Uranerzbergbau in Sachsen und Thüringen
Ausstellung „leben+erde“, Staatliche Naturhistorische Sammlung
Dresden, Germany, 15.-23.11.2002

Flemming, K., Tzvetkova, T., Selenska-Pobell, S.
Analysis of bacterial communities in uranium mining wastes piles, depository sites and mill tailings
BAGECO 8
Bergen, Norway, 15.-20.06.2002

Flemming, K., Tzvetkova, , T., Geißler, A., Selenska-Pobell, S.
Distribution Ecology of Bacteria in Soil Samples of Uranium Mining Waste Piles
International Conference Uranium Mining and Hydrogeology III and the International Mine Water Association Symposium
Freiberg, Germany, 15.-21.09.2002

Geipel, G., Bernhard, G., Vulpius, D.
Interaction of Organic Ligands with Metal Ions Studied by Time-resolved Laser-Induced Fluorescence Spectroscopy
Euroanalysis-12, European Conference on Analytical Chemistry
Dortmund, Germany, 08.-13.09.2002

Koban, A., Geipel, G., Bernhard, G., Fanghänel, Th.
Complex Formation of Uranium(VI) with Glucose-1-Phosphate
International Conference Uranium Mining and Hydrogeology III and the International Mine Water Association Symposium
Freiberg, Germany, 15.-21.09.2002

Krawczyk-Bärsch, E., Arnold, T., Brandt, F., Bosbach, D., Bernhard, G.
The effect of chlorite dissolution on the sorption behavior of U(VI)

International Conference Uranium Mining and Hydrogeology III and the International Mine Water Association Symposium
Freiberg, Germany, 15.-21.09.2002

Merroun, M., Hennig, C., Roßberg, A., Reich, T., Nicolai, R., Heise, K.H.., Selenska-Pobell, S.
Characterization of uranium (VI) complexes formed by different bacteria relevant to uranium mining waste piles
International Conference Uranium Mining and Hydrogeology III and the International Mine Water Association Symposium
Freiberg, Germany, 15.-21.09.2002

Merroun, M.L., Hennig, C., Roßberg, A., Geipel, G., Reich, T., Selenska-Pobell, S.
Complexation of uranium (VI) by different bacteria recovered from uranium mining waste piles
International Conference Uranium Mining and Hydrogeology III and the International Mine Water Association Symposium
Freiberg, Germany, 15.-21.09.2002

Merroun, M.L., Hennig, C., Roßberg, A., Geipel, G., Reich, T., Nicolai, R., Heise, K.H., Selenska-Pobell, S.
Localization and characterization of uranium (VI) complexes formed by three eco-types of *Acidithiobacillus ferrooxidans*
VAAM-Jahrestagung
Göttingen, Germany, 24.-27.03.2002

Merroun, M.L, Hennig, C., Roßberg, A., Reich, T., Geipel, G., Selenska-Pobell, S.
Complexation of uranium (VI) by three eco-types of *Acidithiobacillus ferrooxidans*: spectroscopic characterization
ESRF/ILL Workshop on Complementary Methods in Structural Biology
Grenoble, France, 14.-15.02.2002

Mibus, J.
Column Experiments with Heap Material of Kupferschiefer Mining and Thermodynamic Interpretation
Workshop „TrePro 2002 – Modelling of Coupled Transport Reaction Processes“, FZ Karlsruhe
Karlsruhe, Germany, 20.-21.03.2002

Mibus, J.
Infiltration water dating from tritium measurements in mining dumps: methodic specifics and case study
International Conference Uranium Mining and Hydrogeology III and the International Mine Water Association Symposium
Freiberg, Germany, 15.-21.09.2002

Raff, J., Soltmann, U., Matys, S., Böttcher, H., Pompe, W., Selenska-Pobell, S.
Reversible accumulation of uranium by bacteria based sol-gel ceramics
International Conference Uranium Mining and Hydrogeology III and the International Mine Water Association Symposium
Freiberg, Germany, 15.-21.09.2002

Raff, J., Soltmann, U., Matys, S., Böttcher, H., Pompe, W., Selenska-Pobell, S.
Biosorption of heavy metals by *Bacillus sphaericus* JG-A12 cells, spores and S-layer proteins embedded in sol-gel ceramics
VAAM-Jahrestagung
Göttingen, Germany, 24.-27.03.2002

Roßberg, A., Reich, T., Hennig, C., Funke, H.
XAFS Analysis of Mixtures using Factor Analysis
Experimental Division Science Days
Aussois, France, 22.-24.05.2002

Satschanska, G., Flemming, K., Tzvetkova, T., Selenska-Pobell, S.
Extensive analysis of bacterial diversity in uranium waste piles by using two alternative PCR amplification primer pairs
International Conference Uranium Mining and Hydrogeology III and the International Mine Water Association Symposium
Freiberg, Germany, 15.-21.09.2002

Tzvetkova, T., Flemming, K., Selenska-Pobell, S.
Comparative analysis of bacterial communities in uranium mining wastes, depository sites and mill tailings
VAAM-Jahrestagung
Göttingen, Germany, 24.-27.03.2002

Walter, M., Arnold, T., Krawczyk-Bärsch, E., Bernhard, G.
The sorption of uranium(VI) on ferrous chlorite – an EXAFS study
EURESCO Conference „Geochemistry of Crustal Fluids - The Role and Fate of Trace Elements in Crustal Fluids“
Seefeld, Austria, 14.-19.12.2002

Zänker, H., Moll, H., Richter, W., Brendler, V., Hennig, T., Reich, T., Kluge, A., Hüttig, G.
Die kolloidalen Bestandteile von Lettenwasser (Acid Rock Drainage) aus der Himmelfahrt Fundgrube in Freiberg / Sa.
Jahrestagung 2002 der Wasserchemischen Gesellschaft in der GDCh
Eichstätt/Altmühltal, Germany, 06.–08.05.2002

PH.D. THESES

Abraham, A.
Einfluss von Huminstoffen und Holzabbauprodukten auf den Valenzzustand von Uran
Technische Universität Dresden, Germany, 2002

Amayri, S.
Synthese, Charakterisierung und Löslichkeit von Erdalkaliuranylcarbonaten, $M_2[UO_2(CO_3)_3]\cdot xH_2O$; M: Mg, Ca, Sr, Ba
Technische Universität Dresden, Germany, 2002

Roßberg, A.
Anwendung der Faktorenanalyse auf die Röntgenabsorptionsspektroskopie zur Bestimmung der Speziation von Uran in Lösungen
Technische Universität Dresden, Germany, 2002

Raff, J.
Wechselwirkungen der Hüllproteine von Bakterien aus Uranabfallhalden mit Schwermetallen
Universität Leipzig, Germany, 2002

DIPLOMA

Geißler, A.
Molekulare Analyse der bakteriellen Diversität in Uranabfallhalden
TU BA Freiberg, Germany, 2002

PATENTS

Förster, E., Hiller, B., Heise, K.H., Nitsche, H.
Vorrichtung zum Öffnen von Glasampullen
DP 19841722 C2 vom 08.08.2002

AWARDS

Raff, J.
FZR-Doktorandenpreis 2002
Wechselwirkung der Hüllproteine von Bakterien aus Uranabfallhalden mit Schwermetallen

III. SEMINARS, CONFERENCES, WORKSHOPS, TEACHING ACTIVITIES

INSTITUTE SEMINARS (talks of visitors)

Prof. Dr. W. Voigt
TU-BA Freiberg, Institut für Anorganische Chemie
Löslichkeit und Kristallisation von $CaSO_4$-haltigen Phasen
24.01.2002

Dr. A. Mijovilovich
European Molecular Biology Laboratory, DESY Hamburg
Simulation the XANES of Metalloenzymes - a Case Study
05.03.2002

Prof. Dr. R. Salzer
TU Dresden, Institut für Analytische Chemie
Molekulares Imaging mit konventionellen Lichtquellen-Möglichkeiten und Grenzen
10.04.2002

Priv.-Doz. Dr. R. Ludwig
FU Berlin, Institut für Anorg. u. Analyt. Chemie
Calixarene als Komplexbildner für radiochemische Trennungen
26.04.2002

Prof. Dr. H. Nitsche
University of California at Berkeley, The Glenn T. Seaborg Center
Lawrence Berkeley National Laboratory
Aktuelle Ergebnisse aus der Actinidenforschung
04.06.2002

Dipl.-Geol. S. Hurst
Sächsisches Landesamt für Umwelt und Geologie
Oberflächenreaktionen - Die Bedeutung natürlicher Prozesse bei der Uranbergbausanierung
19.06.2002

Prof. Dr. S. Tanaka
The University of Tokyo, Dep. of Quantum Engineering and Systems Science
Desorption of Tritium from the Surface by Photon and Electron Irradation
12.08.2002

Dr. H. Geckeis
Forschungszentrum Karlsruhe, Institut für Nukleare Entsorgung
Wechselwirkung von Radionukliden mit aquatischen Kolloiden - relevante Mechanismen
01.10.2002

Dr. A. Lehmann / Dr. S. Fiedler
Universität Hohenheim, Fakultät für Pflanzenproduktion und Landschaftsökologie
Humose Böden, deren Entstehung, Verbreitung und Eigenschaften (In-situ Redoxdynamik und Schwermetallmobilität)
08.10.2002

Dr. M. Kumke
Universität Potsdam, Institut für Chemie und Physikalische Chemie
Spektroskopische Untersuchungen an natürlichen organischen Wasserinhaltsstoffen
15.10.2002

Dr. W. Dedek
Universität Leipzig
In Memoriam Fritz Strassmann 1902-1980
29.10.2002

Dr. S. Szidat
Universität Bern, Dep. Chemie und Biochemie, Labor für Radiochemie und Umweltchemie
Iod-129 und Kohlenstoff-14: Zwei langlebige Isotope als Tracer von atmosphärischen Emissionen und Transportprozessen
03.12.2002

Prof. Sh. Nagasaki
University of Tokyo, Institute of Environmental Studies
Sorption of Metal on Soil
04.12.2002

Mr. N. Aoyagi
University of Tokyo, Institute of Environmental Studies
Analysis of Eu(III) Ion Complex with Model Compounds of Humic Acid in Aqueous Solutions Using Time-resolved Laser-induced Fluorescence Spectroscopy (TRLFS)
04.12.2002

INTERNAL SEMINARS (open for the public)

Hennig, C.
XAFS-Untersuchungen von Actinidensystemen mittels Synchrotronstrahlung
12.04.2002

Geipel, G.
Komplexbildung mit organischen Liganden
23.06.2002

Amayri, S.
Synthese, Charakterisierung und Löslichkeit von Erdalkaliuranylcarbonaten, $M_2[UO_2(CO_3)_3]\cdot xH_2O$; M: Mg, Ca, Sr, Ba
16.10.2002

Selenska-Pobell, S.
Uranium mining wastes as a reservoir of unusual bacteria, prospective for bioremediation and nanotechnology
12.11.2002

CONFERENCES / WORKSHOPS (organized by Institute of Radiochemistry)

XAFS Training Course
Grenoble, France, 21.-23.01.2002

Reich, T., Hennig, C., Roßberg, A.

XAFS-/XANES-Symposium
Rossendorf, Germany, 12.04.2002

Hennig, C.
FZR, Institut für Radiochemie, ROBL, Grenoble
XAFS-Untersuchungen von Actinidensystemen mittels Synchrotronstrahlung

Mosel, G.
Bundesanstalt für Materialforschung, Berlin
EXAFS- und XANES-Untersuchungen der Nahordnung von Ionen der 3d-Übergangselemente in oxidischen Gläsern

Scheinost, A.C.
ETH Zürich, Institut für Terrestrische Ökologie
Quantitative Speziierung von Schwermetallen in sauren Böden: Kombination von spektroskopischen und nasschemischen Methoden

Workshop: FZR – WISMUT GmbH
Rossendorf, Germany, 07.05.2002

Arnold, T.
Sorption of uranium(VI) on granite: comparison of experimental and predicted U(VI) sorption data

Brendler, V.
Wechselwirkungen zwischen Kontaminanten und Festphasen – Modelle und Datenbasis

Geipel, G.
Komplexbildung von Uran mit organischen Liganden- Untersuchung mittels Ultrakurzzeitspektroskopie

Zänker, H., Richter, W., Brendler, V., Moll, H., Hüttig, G.
Kolloide in Bergwerkswässern und ihr Einfluß auf den Schadstofftransport

Zänker, H, Richter, W., Moll, H., Hüttig, G., Brendler, V.
Colloid Research at the Institute of Radiochemistry (Poster)

German – Japan Workshop: „Metals in environment“
Rossendorf, Germany, 24.09.2002

Ueta, Sh. (Japan)
Introduction of Mitsubishi Materials Corporation

Bernhard, G.
Introduction of the Institute of Radiochemistry

Saito, T. (Japan)
Metal ion binding to heterogeneous geosurfaces

Krawczyck-Bärsch, E.
Formation of iron oxyhydroxide particles during the oxidation of chlorite – effect on uranium sorption

Arnold, T.
Uranium sorption on phyllite and granite rock

Zänker, H.
Topics of colloidal research

Sachs, S.
Synthetic humic acids: a useful tool to study the interaction of humic acids with actinides in the environment

Günther, A.
Determination of the chemical speciation of uranium in plants

Merroun, M.
Characterization of uranium(VI) complexes formed by different bacteria recovered from uranium mining waste piles

Geipel, G.
Laser-induced spectroscopy - Introduction

Ueta, S. (Japan)
Modeling for practical prediction of K_d values on sedimental rocks

Workshop PSI - FZR
Rossendorf, Germany, 21.-22.10.2002

Hadermann, J. (PSI)
Forschungsprofil und aktuelle wissenschaftliche Ergebnisse WML, PSI

Bernhard, G.
Forschungsprofil und aktuelle wissenschaftliche Ergebnisse IRC,FZR

Baeyens, B. (PSI)
Die Sorptionsdatenbank zur neuen Sicherheitsanalyse Opalinuston: Methodik, Resultate

Bradbury, M. (PSI)
Sorption in Bentonit: Die Koexistenz von dynamischen und statischen Untersuchungen

Krawczyk-Bärsch, E.
Bildung von sekundären Eisenphasen während der Verwitterung von Chlorit – Auswirkungen auf den Urantransport

Arnold, T., Walter, M.
Bestimmung von Oberflächenkomplexbildungskonstanten im Uran-Schwertmannit-System unter Berücksichtigung spektroskopisch nachgewiesener Oberflächenspezies

Van Loon, L. (PSI)
Diffusion in dichten Tongesteinen: Experimente, Modellierung

Sachs, S., Schmeide, K.
Weiterentwicklungen bei der Synthese von Huminsäuremodellverbindungen und Untersuchungen zur Komplexierung und Sorption von Neptunium mit Huminsäuren

Brendler, V.
NEA Sorption Projekt, Test Case 1: Neptunium Sorption auf Hämatit

Arnold, T.
NEA Sorption Projekt, Test Case 3: Uran Sorption auf Quarz

Arnold, T., Brendler, V.
NEA Sorption Projekt, Test Case 6 : Uran Sorption auf „weathered schist“ - Probleme bei der Modellierung des Testfalles

Statustreffen „ROBL-Radiochemiemessplatz“
Rossendorf, Germany, 09.12.2002

Günther, A.
EXAFS- Untersuchungen an uranhaltigen Pflanzenproben und ausgewählten Modellkomplexsystemen

Raff, J.
Untersuchung der Uransorption an freien und immobilisierten Biokomponenten von *Bacillus sphaericus* JG-A12 und NCTC 9602 mittels Röntgenabsorptionsspektroskopie

Sachs, S., Schmeide, K.
XANES- und EXAFS-Messungen an Actinid-Humaten

Walter, M.
Uran(VI) Sorption an Albit

TEACHING ACTIVITIES

Bernhard, G.
Umweltchemie (Umwelt-Stoffe-Energie)
Environmental Chemistry (Environment-Substances-Energy)
Technische Universität Dresden
Winterterm 2002/2003

Bernhard, G.
Umweltanalytik (Spurenanalytik)
Environmental Analytics (Trace Analytics)
Technische Universität Dresden
Summerterm 2002

Bernhard, G.
Radiochemie (Radiochemische Methoden)
Radiochemistry (Radiochemical Methods)
Technische Universität Dresden
Summerterm 2002

IV. PERSONNEL

PERSONNEL

Director

Prof. Dr. Th. Fanghänel (until March 31, 2002)
Prof. Dr. F.-P. Weiß (acting, since April 1, 2002)

Administrative Staff

G. Kreusel
H. Pospischil

Scientific Staff

Dr. S. Amayri*
Dr. T. Arnold*
Dr. L. Baraniak*
Dr. N. Baumann*
Prof. Dr. G. Bernhard
DC D. Birnstein
Dr. V. Brendler
Dr. H.-J. Engelmann*
Dr. H. Foerstendorf
Dr. H. Funke
Dr. G. Geipel
Dr. A. Günther*
Dr. K.H. Heise
Dr. C. Hennig
Dr. S. Hübener
Dr. A. Koban+
Dr. E. Krawczyk-Bärsch*
Dr. K. Krogner
Dr. M. Merroun+
Dr. J. Mibus+
Dr. H. Moll*
DC C. Nebelung
Dr. K. Pollmann+
Dr. A. Roßberg
Dr. J. Raff+
Dr. A. Richter*
Dr. W. Richter
Dr. S. Sachs*
Dr. S. Selenska-Pobell
Dr. K. Schmeide*
DB M. Schnorpfeil*
Dr. J. Tutschku*
Dr. H. Zänker

Technical Staff

DI(FH) B. Barz*
DI(FH) C. Eckardt
DBC K. Flemming
J. Falkenberg
DI(FH) H. Friedrich
Ch. Fröhlich
DI(FH) G. Grambole
DI(FH) S. Heller*
DI(FH) K. Henkel
H. Heyne
B. Hiller
DI(FH) G. Hüttig
DI(FH) R. Jander
M. Leckelt*
DI(FH) M. Meyer
Ch. Müller
H. Neubert
DI K. Nicolai*
DI(FH) R. Nicolai*
A. Rumpel
R. Ruske
DI(FH) U. Schaefer

Graduate Students

DB A. Geißler
DB M. Nedelkova
DC K. Opel
DI(FH) D. Vulpius
DM M. Walter

Trainee

J. Bergmann
T. Birk
S. Brockmann
K. Brottka
A. Dillschneider
K. Effenberg
K. Großmann
M. Herber
M. Heymann
A.-M. Hochfeld
B. Hollenbach
C. Jungnickel
U. Koch
T. Ludwig
R. Pechner
J. Scheibke
D. Schröter
R. Schubert
S. Schubert
C. Smidt
M. Thiele
P. Trepte
H. Zimmermann

Former Personnel (who left during the period covered by the report)

Director: Prof. Dr. Th. Fanghänel

Scientific Staff: Dr. T. Reich, Dr. T. Stumpf+

Technical Staff: P. Kluge

+ post doc
* term contract
DC: Dipl.-Chem.
DI: Dipl.-Ing.
DBC: Dipl.-Biochem.
DB: Dipl.-Biol.
DM: Dipl.-Min.

Guest Scientists

S. Tsushima	The University of Tokyo, Department of Quantum Engineering and System Science, Tokyo, Japan
M. Grive	Polytechnical University of Catalonia, Barcelona, Spain
F. Seco	Polytechnical University of Catalonia, Barcelona, Spain
A. Krepelová	Czech Technical University, Prague, Czech
G. Radeva	Institute of Molecular Biology, Sofia, Bulgaria
G. Satchanska	Institute of Molecular Biology, Sofia, Bulgaria
M. Chukalina	Institute of Microelectronics Technology, RAS, Chernogolovka, Russia
I. Kamenzki	Institute of Metal Physics, Ekaterinburg, Russia

V. ACKNOWLEDGMENTS

ACKNOWLEDGMENT OF FINANCIAL SUPPORT

The Institute is part of the Forschungszentrum Rossendorf e.V. which is financed in equal parts by the Federal Republic of Germany and the Free State of Saxony.

Six projects were supported by the Bundesministerium für Bildung und Forschung (BMBF) and by the Bundesministerium für Wirtschaft (BMWi):

- Wechselwirkung von Actiniden mit dominanten Bakterien des Äspö-Grundwasserleiters
  Contract No.: BMWi 02 E 9491

- Integrierter Umweltschutz in der Textilindustrie: Abtrennung von Uranylionen aus Sicker- und Grundwässern mit uranophilen Calixarenen (Verbundprojekt)
  Contract No.: BMBF 0339917/3

- Biocere auf Basis bakterieller Membranproteine für Schwermetall bindende Filter zur Behandlung von industriellen Abwässern und kontaminiertem Grundwasser
  Contract No.: BMBF 03I4004B (InnoRegio)

- Diversity of bacteria in Bulgarian and German uranium waste piles. (Institut für Molekulare Biologie, Sofia)
  Contract No.: BMBF DLR-IB/BGR 99011

- Entwicklung einer mineralspezifischen Sorptions-Datenbank für Oberflächenkomplexierungsmodelle
  Contract No.: BMWA PtWt+E 02 E 9471

- Untersuchungen über die Komplexierung und die Migration von Actiniden und nichtradioaktiven Stoffen mit Huminsäuren unter geogenen Bedingungen – Komplexierung von Huminsäuren mit Actiniden in der Oxidationsstufe IV Th, U, Np (Verbundprojekt)
  Contract No.: BMWA PTE 02 E 9299

The Commission of the European Communities supported six projects:

- Access to Research Infrastructures (5th framework program “Improving Human Research Potential”)
  Contract No.: HPRI-CT-1999-00077

- Aquatic Chemistry and Thermodynamic of Actinides and Fission Products – ACTAF
  Contract No.: FIKW-CT-2000-00035

- Building confidence in deep disposal: the borehole injection sites at KRASNOYARSK-26 and TOMSK-7 (BORIS)
  (SKC/CEN, Belgium; IPSN/DPRE/SERGD, France; FZK; VNIPIPT, Russia; ETSEIB, Spain; Galson Sci Limited, UK; NIREX Limited, UK; AEA, UK)
  Contract No.: FIKW-CT2000-00105

- Humic Substances in Performance Assessment of Nuclear Waste Disposal: Actinide and Iodine Migration in the Far-Field (HUPA)
  Contract No.: FIKW-CT-2001-00128

- Establishment of a Network of Excellence in Actinide Science – ACTINET
  Contract No.: FIR1-CT-2002-20211

- Novel precisious metal-based bionano-catalitics “BIO-CAT”
  (Uni. Birmingham, UK; CNRS Lyon, France; Uni. Leoben, Austria; TUD; Capenhurst Tech. Ltd., UK)
  Contract No.: G1-CT2002-0750

The Sächsisches Staatsministerium für Wissenschaft und Kunst provided support for the following projects:

- Biologische Synthese von Metallclustern an Proteinen und deren technischer Nutzung
  Contract No.: SMWK 4-7531.50-03-370-01/5 (Biotech 2001)

- Mittel- und Osteuropa Gastprogramm (Institut für Molekulare Biologie, Sofia) (20.05. – 20.07.02)
  Contract No.: SMWK 4-7531.50-04-844-02/9

- Mittel- und Osteuropa Gastprogramm (Institut für Molekulare Biologie, Sofia) (03.06.- 03.08.02)
  Contract No.: SMWK 4-7531.50-04-844-02/4

Four projects were supported by Deutsche Forschungsgemeinschaft (DFG):

- Identifizierung und Charakterisierung von Komplexierungsprodukten des U(VI) in Pflanzen
  Contract No.: DFG BE 2234/1-2

- Komplexierung von Uranyl- und Neptunylionen mit phenolischen Monomeren des natürlichen Ligninabbaus als Grundlage für die Beschreibung der Radionuklidausbreitung
  Contract No.: DFG BE 2234/3-1, 3-2

- Heterogene Reaktionsmechanismen und deren Kinetik an Schichtsilikatoberflächen
  Contract No.: DFG BE 2234/4-1, 4-2, 4-3

- BIOCERE mit spezifischer Metallbindungsaktivität
  Contract No.: DFG SE 671/7-1

One project was supported by the BfS:

- Sorptionsexperimente im Deckgebirge des Endlagers für radioaktive Abfälle Morsleben (ERAM)
  BfS-Projekt No.: 9M 212230-62

One project was supported by AMD Saxony Manufacturing GmbH:

- Aufbau, Inbetriebnahme und Erprobung einer Messapparatur zur Low-Level-Alphaspektrometrie